ASSESSMENT OF THE GEOLOGICAL INFORMATION CONTENT OF LEGACY AIRBORNE GEOPHYSICAL DATA SETS OF THE HARZ MOUNTAINS IN GERMANY

JOSHUA JOSEPH CHISAMBI
March, 2015

SUPERVISORS:
Dr. F.J.A. van Ruitenbeek
Mr. W.H. Bakker MSc

ASSESSMENT OF THE GEOLOGICAL INFORMATION CONTENT OF LEGACY AIRBORNE GEOPHYSICAL DATA SETS OF THE HARZ MOUNTAINS IN GERMANY

JOSHUA JOSEPH CHISAMBI
Enschede, The Netherlands, March, 2015

Thesis submitted to the Faculty of Geo-Information Science and Earth Observation of the University of Twente in partial fulfilment of the requirements for the degree of Master of Science in Geo-information Science and Earth Observation.
Specialization: Applied Earth Sciences

SUPERVISORS:
Dr. F.J.A. van Ruitenbeek
Mr.W.H. Bakker MSc

THESIS ASSESSMENT BOARD:
Prof. Dr. F.D. (Freek) van der Meer (Chair)
Dr. Mike Buxton (External Examiner, University of Delft)

ABSTRACT

This research used legacy and lesser quality airborne geophysical data set of the Western Harz Mountains which was acquired in 1985 and originally published in contour map form by Germany Geological Survey (BGR). The contour maps were previously digitized and the new digital dataset had not been tested to determine to what extent it can be used for mapping of lithological units. The research aimed at finding out how to grid the legacy airborne geophysical data and get useful geological information out of it, and to know what kind of information about the geology could be obtained by improving this data set. A remote predictive mapping approach was used to extract information from the data. This involved Supervised and Unsupervised classification methods as well as visual interpretation. Maximum likelihood and isodata classifications were applied.

It was found that isodata unsupervised classification on the legacy airborne gamma ray data, can map low radioelement rocks such as Limestone, Gabbro and Diabase but it cannot differentiate these lithological units. It can also map medium radioelement rocks such as Greywacke and Eckergneiss and again has the limitation that it cannot differentiate these lithologies. Furthermore the classification is able to map high radioelement rocks such as Granite, Shale and Devonian sandstone but cannot differentiate these lithological units because they have similar gamma ray spectral signatures. It was also found out that it is able to map out marsh areas and the lakes. These also have low radioelement content and the classification could not differentiate these water logged areas, lakes and the low radioelement rocks like Limestone, Gabbro and Diabase.

Performing maximum likelihood supervised classification based on both legacy airborne gamma ray and magnetic data can map high magnetic susceptibility and low radioelement content rocks like Gabbro and Diabase but cannot differentiate these rocks. Furthermore it can map low radioelement and low magnetic susceptibility rocks such as Limestone. In addition to this, it can map high gamma ray spectral signature and high magnetic susceptibility rocks like Granite. Also is able to map lithological units with medium radioelement content and low magnetic susceptibility like Greywacke and Eckergneiss but it could not differentiate these units. Similarly it can also map lithological units with high Th and K content and low magnetic susceptibility like Shale and Devonian sandstone but it cannot separate the units. It was also found out that classification accuracy varied from 40% when only gamma ray data was used to 42% when both gamma ray and magnetic data were used. The low accuracy is due to variability within the classes. The research concluded that major lithological units could be identified and mapped with this data set and this shows that though this dataset is very old, it is still very useful.

ACKNOWLEDGEMENTS

I am very grateful to my supervisors Dr. F.J.A. van Ruitenbeek, Mr. Wim Bakker and Drs. Boudewijn de Smeth for their constructive criticism and innovative ideas. Throughout the whole thesis period, they have been very keen to make sure that the arguments made in this work are scientific and critically constructed. Their guidance is highly appreciated.

I wish to express my sincere gratefulness to the government of Malawi for financing my MSc study through the Malawi Governance and Growth Support Project (MGGSP) in the ministry of Mining.

To my fellow classmates (Chikondi Chisenga, Charleson Eliyasi, Denson Makwera, Hassan Mdala and Babatunde Joseph) who were never busy to consider or discuss a question, I am grateful to you all.

TABLE OF CONTENTS

LIST OF FIGURES

LIST OF TABLES

1. INTRODUCTION

1.1. Background to the research

This research assesses the geological information content of legacy airborne geophysical data. A Remote Predictive Mapping (RPM) approach was used to extract geological information from the legacy airborne geophysical data. This approach involves deriving geological information from any available geoscience data (Harris, 2012; Harris, 2008). The methods of information extraction from these datasets involve visual interpretation of enhanced images or computer assisted supervised and unsupervised classification techniques (Schetselaar, Harris, Lynds, and Kemp, 2007). Supervised and unsupervised classifications provides means of extracting geological information in a systematic and unbiased way (Schetselaar et al., 2007). The output is mostly commonly a map showing predicted lithological units which serve as first order source for geological information which to base future mapping or exploration (Harris, Schetselaar, & Behnia, 2004). The predictive maps show areas where the predicted geology agrees or disagrees with the existing geological information.

Remote Predictive Mapping (RPM) has been implemented since 2004 in pilot projects by the Geological Survey of Canada (Harris, Schetselaar, Lynds, and Kemp, 2008). Schetselaar et al., (2007) used this method to map different lithological units and structures in the north of Canada. Using the method they were able to map the area with great detail. Harris, Pilkington, Lynds, and Mcgregor, (2008) used this approach to update the geoscience knowledge of the southwestern Baffin Island region of eastern Nunavut, Canada. In their project, RPM techniques were employed to assist in the geological interpretation of this area in order to expand the possibilities that may be used to identify tectonic features and distinctive structural domains, to target field mapping areas, and to contribute to existing geological map compilations. Harris, et al., (2008) used this technique under the Snowbird Lake mapping project in NW Canada in order to produce a predictive map of bedrock units and geologic structures from available geoscience data in order to assist field mapping and logistical planning within the overall context of developing a better understanding of the geology of the snowbird tectonic zone. They concluded that the RPM process was largely successful, as major lithological domains and major structural trends were identified and mapped. Complex areas requiring more field follow-up were delineated. Also, areas of poor exposure were identified, which facilitated targeted field mapping. Onge & Harris, (2008) used the technique to show the advantages of higher resolution remote sensors, specifically airborne hyper spectral data sensors, for geological mapping in southeastern Baffin Island. Harris and Wickert, (2008) used the method with the aim of demonstrating the value of gamma-ray spectrometry data in conjunction with magnetic and Landsat data for mapping lithology in a mountainous environment of the Sekwi Mountain under a mapping project initiated by the Northwest Territories Geoscience Office in collaboration with, the Geological Survey of Canada (GSC). Their study indicated that airborne data, given the right geological conditions and rock types, can play a significant role in the remote predictive mapping of different lithologies. In the study, a wide range of units, including Granite, Shale, sandstone, and carbonate, were identified based on characteristic radioelement signatures. Based on these findings, this research aims at using Remote Predictive Mapping approach in order to assess the geological information content of legacy airborne geophysical data of the western Harz Mountains.

1.2. Research problem

The Harz is a mountain range in central Germany of Palaeozoic rocks and was formed by uplift during the Cretaceous, which affected the whole area. The area is known for its long history of mining, and contains large and numerous small mineralizations. These include the world-class Rammelsberg massive sulphide deposit(SEDEX) and several vein type deposits (Anderson, 1975). Because the area hosts several types of mineral deposits, and also that on a small area enormous amount of different and important geologic features are found makes it an interesting study area. The area now is densely forested and rock outcrops are mostly covered by vegetation. An old and lesser quality airborne geophysical data set of the western Harz Mountain which was acquired in 1985 and originally published in contour map form by Germany Geological Survey (BGR) is available. The contour maps have been digitized and the new digital dataset has not been tested to determine to what extent it can be used for mapping of lithological units. This research aims at finding out how to processes the legacy airborne geophysical data and get sensible information out of it, and to know what kind of information about the geology could be obtained by improving this data set.

1.3. Objectives and Research questions

1.3.1. Main Objective

The main objective of this research is to determine the best method of gridding of the digitized legacy airborne geophysical data and to extract geological information from it.

1.3.2. Specific objectives

- To characterize geological units in the western Harz Mountains using ground field instruments data in combination with airborne geophysical data
- To determine the extent to which the available legacy geophysical airborne dataset can be used to map geology
- To determine which gridding method can work best in mapping the geology from the geophysical dataset
- To compare field measurements data of the different geological units with those obtained from the airborne geophysical data in order to characterize the geology in terms of chemical and mineralogical composition.

1.4. Research questions

- What is the relationship between the rock composition obtained by ground field measurement data with that obtained by the legacy airborne data

- What is the geological information content of this legacy airborne geophysical dataset

- To what extent can the available legacy geophysical dataset be used to map the lithological units of the western Harz

- Which aspects of the geology (lithologies and structures) of western Harz can be mapped or identified by integrating the geophysical enhancements results with available field datasets.

1.5. Research hypothesis

Using remote predictive mapping approach it is possible to map, interpret and characterize different lithological units and structures from even noisy airborne geophysical datasets.

1.6. General methodology

The study was carried out in three stages. Stage one involved characterization of different lithological units of the study area using ground field data which was collected using a gamma ray spectrometer, EDA Scintillometer, Portable XRF, Analytical Spectral Device (ASD) and magnetic susceptibility meter (kappa meter). Stage two involved the processing of the airborne data in which gridding methods were compared and best and best gridding for this dataset was determined. Stage three involved extraction of geological information from the data sets in which both visual interpretation and computer assisted interpretation which involves supervised and unsupervised classification were applied.

1.7. Thesis structure

This thesis is comprised of seven chapters. Chapter one introduces the background to the research, problem statement, objectives, questions and general methodology. General literature study on geology of the western Harz and dataset used are emphasized in chapter two. Chapter three describes methodology used in this research. Chapter four is comprised of results of data analysis and interpretation of ground field data in characterizing different lithological units. Chapter five deals with results on processing of airborne magnetic and radiometric data. Chapter six deals with extraction of geological information from the airborne geophysical data. Chapter seven gives general conclusion and recommendations of the study.

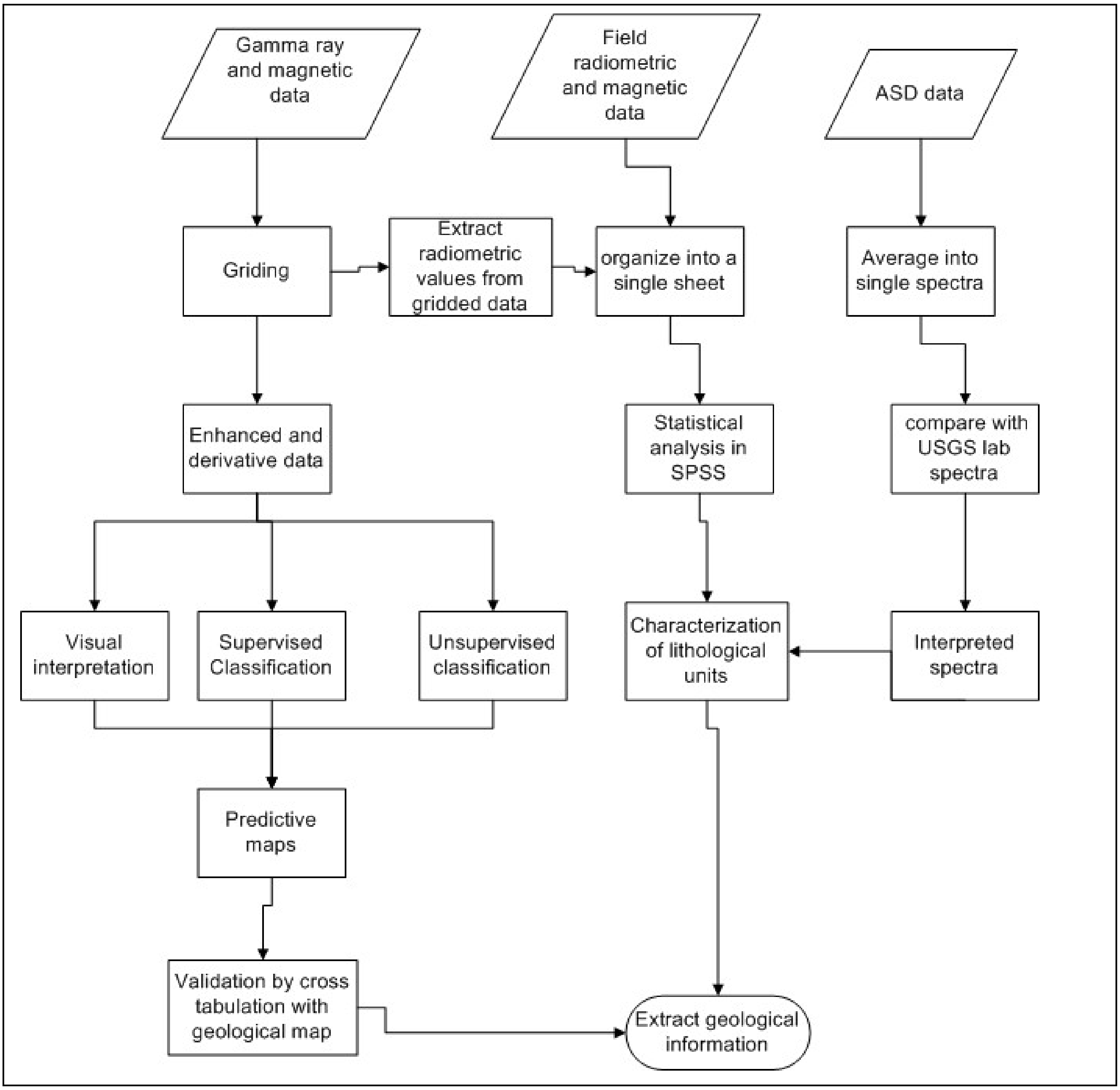

Figure1-1 showing methodological flow chart that was applied in the study

2. STUDY AREA AND DATASETS

2.1. Location

The Harz is a mountain range, 180 km long and 30km wide in Germany. It occupies an area of 2,226 square kilometres. The Harz was formed by uplift, during the lower Cretaceous (140-97Ma) and consists of old, mainly Devonian rocks which are heavily altered and faulted by old orogenies. The area is known for its history in mining. Mining in the Harz has been going on for centuries and was of great economic importance. Secondary copper minerals were mined first, probably around two thousand years ago, in the weathering zone above the Rammelsberg SEDEX deposit. Silver-rich galena was mined from near vertical hydrothermal veins from medieval times till around 1960, iron ore was mined from 10th century AD till 1970. From 1936 till 1988 Pyrite, Copper, Lead and Zinc were mined from the world class Rammelsberg deposit (Mueller, 2008). Other minerals that were mined in the area were barite, Limestone, slate buddingtonite, road metal and peat. Currently only road metal and Limestone are being quarried and there is no base metal mining these days anymore in the Harz Mountains (Scandinavian Highlands, 2009). Because the area hosts several types of mineral deposits, and also that on a small area enormous amount of different and important geologic features are found makes it suitable for this study.

Figure2-1 Location map of western Harz (WorldAtlas, 2013)

2.2. Regional Geology

The Paleozoic (Silurian-Upper Carboniferous) volcano-sedimentary rocks of the Harz mountains were deposited in a rift basin associated with extensional tectonics and form an uplifted block of the variscan structural belt characterized by NE-SW trending fualts and thrust belt (Large & Walcher, 1999). It is fault bounded to the north and west and covered by Paleozoic sediments to the south and east. The Harz massif is divided into three geological zones: upper, middle and lower Harz. The study area is located in the upper Harz and is characterized by a continuous sedimentary succession from the Devonian - carboniferous

2.3. General geology

The Harz Mountain range varies in its geological composition and it is divided into the upper Harz, the middle Harz and the lower Harz. The upper Harz comprises the Oker Granite, the Harzburgite Gabbro, Basalts and the western part of the Brocken Granite complex. The middle Harz consists of Carboniferic intrusions, Devonian Schists, Basalts and Greywacke as well as the eastern part of the Brocken Granite and the Ramberg Granite. Ordovician and Devonian Greywacke formations and molasse basins of the lower Permian form the lower Harz (Zech, Ries, and Faust, 2010). The most important economic mineralization is the Massive Sulphide type deposit, stratiform within the Wissenbach Shale and consisting of pyrite, chalcopyrite, sphalerite, galena as well as some barite (Large and Walcher, 1999). The mineralization was formed during a period of quiet sedimentation in a marine basin, (Large and Walcher, 1999).

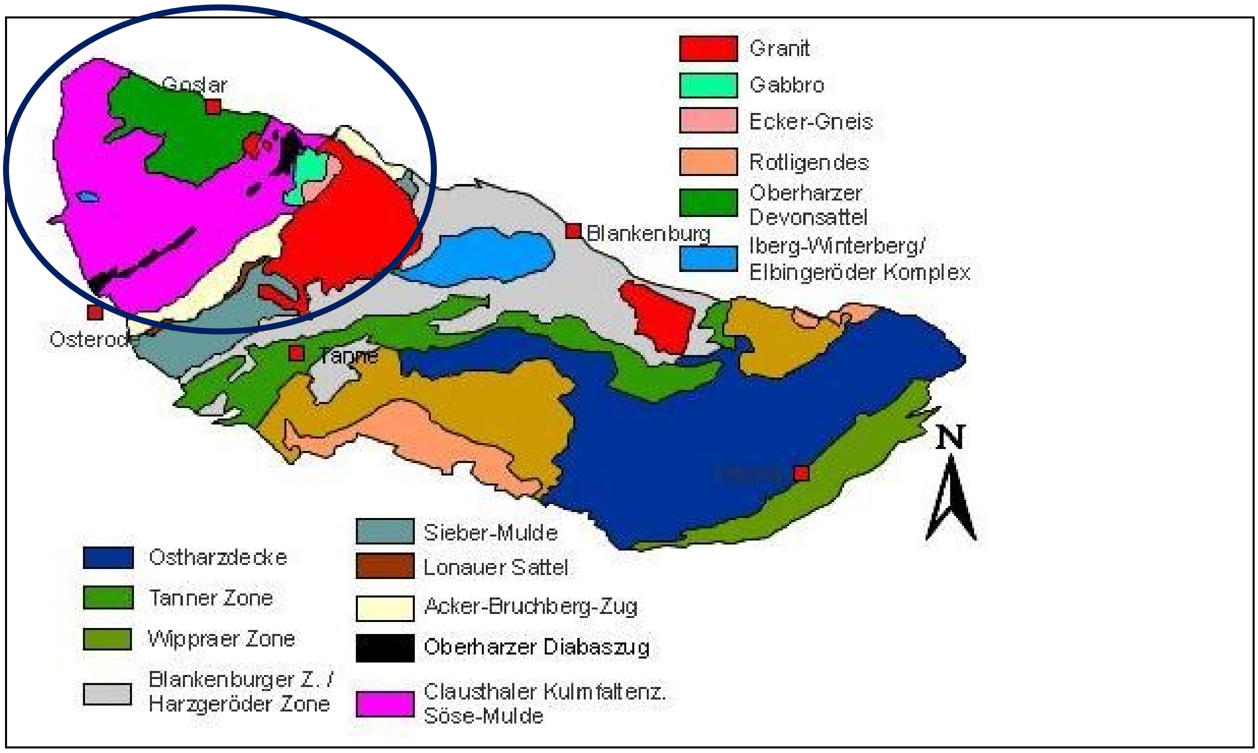

Figure2-2 geological map of the study area (Wikipedia, 2014)

2.4. Sedimentary Sequence

The oldest rocks of the upper Harz (lower Devonian) form the anticlinal hinge of the Devonian carboniferous succession and are characterized by sandstones, siltstones, quartzites probably deposited in high energy oxidizing environment. The transition from the lower to the middle Devonian is very abrupt and marked by a carbonaceous Shale units typical of the deep quiet submarine environment. Large & Walcher, (1999) believe that this phase may mark the transition from initial rift to the sag phases of the basin evolution where differential rates of subsidence during the period of tensional tectonics gave rise to the basin and rise sequence explaining the lateral facies changes and thickness variation. The upper Devonian sequence directly follow on from the Middle Devonian and consists of micritic Limestone and banded Shale in Goslar trough (Anderson, 1975), marked by an absence of volcanic and igneous activity. The upper sequences are dominantly pelitic, gradually becoming more oxidized reflecting a relatively quiet sedimentary basin environment that gradually shallowed during the final phases of thermal subsidence. The lower Carboniferous is characterized by a distinctive pyritic black Shale unit overlying chert sequence. The Shale and cherts are overlain by Greywacke which are considered to represent the onset of the compressive tectonics.

2.5. Generalised tectonic setting

The Harz is part of the Variscan belt (Zech et al., 2010). The Devonian Carboniferous succession in the Harz Massif was deformed during the Variscan orogeny, which reached its climax during the Upper Carboniferous and was accompanied by low-grade regional metamorphism (Mueller, 2008). The dominant fault direction in the Harz is NE-SW and NW-SE direction. The mineralization in the Harz is spatially associated to these faults, which were developed subsequent to the Variscan orogeny, and were active during the generation of vein-type mineralization in the Mesozoic (Large and Walcher, 1999). The Sedimentary Hosted Massive Sulphide mineralization (e.g. Rammelsberg) is associated with tectonic extensional pulses associated with mafic volcanics and syn-sedimentary faulting at specific horizons during the post-rift thermal subsidence phase (Middle Devonian) of the basin evolution (Large and Walcher, 1999)

2.6. Dataset used

2.6.1. Airborne geophysical data

Low resolution legacy airborne geophysical data which was digitized from contour maps that were produced after a helicopter survey in 1985 by the Germany Geological Survey was used in this study. The data was measured at 200m line spacing and at an average height of 60m above ground. It was originally present in hard copy maps and was recently digitized, now is available in database form. These include: Potassium (K), Thorium (Th), Uranium (U) and Total count (TC) channels.

Total Magnetic Intensity (TMI) channel, was measured with Geometric G803 proton magnetometer at an average flying height of 60m above ground and line spacing of 200m. It was corrected for the International Geomagnetic reference Field (IGRF)

The geophysical data is projected to WGS 84 UTM zone 32N which is the projection system for the study area.

2.6.2. Ground Field Data

Ground field data which was collected using portable gamma ray Spectrometer Exploranium GR 320, Scintillometer (GRS-500 Differential Spectrometer), Portable XRF, Analytical Spectral Device (ASD) FieldSpec Pro and Magnetic Susceptibility meter by Earth Resource Exploration ITC students in 2011 till 2014 from Harz was used in characterizing different lithological units. The variables that were measured in the field were K, Th, U and TC using Gamma ray Spectrometer and Scintillometer. Portable XRF measured K, U, Th, Fe, Cu, Pb, Zn, Ba and Ag. Magnetic Susceptibility (Kappa Meter) measured magnetic susceptibility of the rocks. The data was collected on selected outcrops on slate, Greywacke, Wissenbach Shale, Limestone, Granite, Eckergneiss, Gabbro, Diabase, Hornfels, and Harzburgite. Measurements were taken per outcrop per instrument

2.6.3. Geologic and topographical maps

- One sheet of scanned Geological map at 1: 100,000 produced in 1998 by Geological Survey of Germany.
- 7 sheets of Scanned Topographical maps at 1: 50,000.

2.6.4. Remote sensing data

- 1 scene of Landsat TM image with spatial resolution of 30m acquired on 18 June 1986.
- 1 scene of ASTER image acquired on 17 October 2003.
- 1 scene of Alos image with spatial resolution of 2.5m for Prism and 10m AVNIR obtained may 2009.
- SRTM DEM (90m resolution) no date of acquisition given.

2.7. Software used

- ENVI, for processing and analysis of satellite image data.
- ARC GIS, for digitizing, processing and analysis geological and geophysical data
- Oasis Montaj, for processing and analysis of airborne geophysical data.
- SPSS, for statistical analysis.
- ERDAS Imagine for image classification
- Ilwis for cross tabulation

3. RESEARCH METHODOLOGY

3.1. Introduction

In order to achieve the aim and objectives as well as to answer the research questions, the following steps were carried out. The field data was used to characterize the lithological units using gamma ray spectrometry and elemental composition. Gamma ray spectrometry provides a method of measuring individual radioactive elements Potassium, Thorium and Uranium. Naturally all rocks are radioactive and contain K, Th and U in most rock forming minerals. K which is abundant and is a prominent component of most rocks occurs mainly in feldspars, biotite and muscovite. Th and U are generally present in low concentrations in wide range of minerals like zircon and alunite. Distributions of these radioactive elements provide information about mineralogical and geochemical properties of rocks. The digitized legacy airborne data were gridded and then Supervised and unsupervised classification as well as visual interpretation were done on the data.

3.2. Charecterization of lithological units

3.2.1. Field data

The field radiometric and magnetic data from 2011-2014 was combined in order to have an average representation measurements of the area. The average concentration of the elements per lithology was made in Excel. Box plots as well as scatter plots were used in interpretation in order to see the distribution and correlation of various elements in the lithological units. The Box plots were made using SPSS software.

The spectra that were collected from the field were averaged into single spectra in ENVI software using the Spectral math algorithm. This was done because at sample points, three spectral measurements were taken. So the three spectral measurements were averaged into single spectra. The averaged spectra was then interpreted by comparing it with the USGS spectral library in ENVI. The USGS library was resampled to the same wave length as the field spectra for easy comparison, i.e. converted from micrometer to nanometre.

3.2.2. Laboratory data

The laboratory measurements were done in order to validate the field measurements. Rock samples were measured in the laboratory using portable XRF and ASD. First the samples were crushed into powder using Jaw crusher and Ball mill. The rocks were crushed into powder in order to measure a homogenized sample which gives more representative results than measuring the whole uncrushed rock. The powdered rock samples were measured with the pXRF using soil mode. The parameter settings that were used were 30 seconds for main filter, 30 seconds for low filter and 10 seconds for high filter. The variables that were measured were K, U, Th, Cu, Pb, Zn. Box plots as well as scatter plots were used in interpretation in order to see the distribution and correlation of various elements in the lithological units. The Box plots were made using SPSS software.

Mineral spectra were measured using the Analytical Spectra Device (ASD) on the powdered samples. This was done because the powdered rock samples give a more representative and homogenized spectra than the whole rock. The measured spectra were exported as ASCII and its spectral library was made using ENVI software. The measured spectra were interpreted by comparing with USGS spectral library in ENVI.

Magnetic susceptibility was measured on all the rock samples using kappa meter. Magnetic susceptibility is the degree to which a material can be magnetized in an external field.

3.2.3. Comparison between ground field radiometric data and legacy airborne radiometric data

Airborne radiometric values were extracted for K, Th, U and TC from potassium, Thorium, Uranium and Total Count grids using Oasis Montaj software on the same location from where the ground measurements were collected. All these measurements were compared with the field data derived by the gamma ray spectrometer and portable XRF in order to characterize the geology in terms of chemical and mineralogical composition. Box plots and scatter plots were used in order to see the relationship and distribution of the data in different lithologies extracted from the grid and that obtained from the field

3.3. Gridding and geophysical data processing

Gridding refers to the process of interpolating data onto an equally spaced grid of cells in a specified coordinate system, such as X-Y. Minimum Curvature, Kriging and Inverse Distance Weighting (IDW) gridding techniques were applied and their results compared. This was done in order to find the best gridding algorithm for this kind of dataset. Oasis Montaj software was used to grid the data.
The Minimum curvature gridding method fits a minimum curvature surface to the data points. It first estimates grid values at the nodes of a coarse grid (usually 8 times the final grid cell size). This estimate is based upon the inverse distance average of the actual data within a specified search radius. If there is no data within that radius, the average of all data points in the grid is used. An iterative method is then employed to adjust the grid to fit the actual data points nearest the coarse grid nodes (Geosoft, 2013).

Kriging is a statistical gridding technique for random data, non-parallel line data or orthogonal line data. Kriging is usually used when the XYZ data is not sampled along lines that run in roughly the same direction. Such data are often called random, because they give a random appearance when the data locations are plotted. The Kriging statistical gridding method determines a value at each grid node based on the XYZ data. Kriging first calculates a variogram of the data, which shows the correlation of the data as a function of distance (Geosoft, 2013).

The Inverse Distance Weighting (IDW) algorithm is a moving-average interpolation algorithm that is usually applied to highly variable data. It calculates a value for each grid node by examining surrounding data points that lie within a user defined search radius. The node value is calculated by averaging the weighted sum of all the points, where the weighting inversely corresponds to distance from the grid node (Geosoft, 2013).

Grid cell size of 50 m was used. A grid cell size of 50m was used because the data was collected at 200m line spacing so a formula of 1/4*200 i.e. (1/4*line spacing) was applied for optimum grid cell size. The gridded data was exported to ARCGIS in ER Mapper form. ER Mapper was chosen because it preserves grid values. In ARCGIS grid values from the gridded data were extracted using extract values to point tool in order to compare the gridded values with the original values before gridding. The results were then exported to SPSS software for statistical analysis. The gridded values for each method were subtracted from the original values in order to see how close the gridded data differ from the original data. The residuals (differences) were plotted as histograms showing normal distribution. The data was split into two parts, one data set was used for gridding and the other was used for validation. The gridding technique that shows low standard deviation and root mean square error was taken to be the best technique to grid the data set.

3.4. Supervised and Unsupervised Classification

Supervised classification was done on the gridded data in order to extract geologic information in a systematic manner according to Lillesand, Kiefer, & Chipman, (2000). Geological field data where rock samples were taken were used during the training stage of the classification. Maximum likelihood classification was used. Unsupervised classification was done in order to find the natural grouping of the pixels in the data and Isodata clustering algorithm was used. Clustering was done by testing different number of classes and see the pattern.

3.5. Visual Image Interpretation

In addition to the Supervised and unsupervised classification, visual analysis of the legacy airborne geophysical data was done. A number of enhancements were applied to the geophysical data in order to highlight different geological characteristics of the data

3.6. Gamma ray data enhancements

A wide range of processing and enhancements for gamma ray data were used to facilitate extraction of geological information. Geological feature extraction on the enhanced gamma ray images were done by visual interpretation of geologic units based on tone and/or colour, texture, patterns, shape, size, shadow, and association (Drury, 2001).

3.6.1. Single Band

The single band Potassium (K), Thorium (Th), Uranium (U) pseudo color images were used for interpretation because they show areas where a particular radio-element can be directly correlated with the geochemical properties of the surface lithology and regolith (Wilford, 1997).

3.6.2. Ratio images

Radioactive element ratios of U/Th, U/K (ppm/%), and Th/K (ppm/%) were made in Oasis Montaj using grid math algorithm. The Ratio images were made because they enhance subtle features that are not apparent on the original grids. (Tourliere, Perrin, Leberre and Pasquet, 2003)

3.6.3. Ternary image

Gamma-ray channels (bands) were displayed as ternary colour composite image allowing for the interpretation of three channels of data using an additive mix of the primary colors (red-green-blue) of the computer. The ternary map was produced by assigning Th grid to green, K grid to red and U grid to blue in order to qualitatively interpret the various lithologies and compare them with the ground based measurements. This image helped in highlighting different lithological units (Harris, 2008).

3.7. Aeromagnetic enhancements

A wide range of magnetic enhancements were also used to facilitate extraction of geological information. These include:

3.7.1. Reduced to pole (RTP)

A reduction to the pole using the pseudo inclination method developed by MacLeod, Jones, Dai, (1993) and discussed in detail by Li, (2008) was applied to the total magnetic dataset. The reduced to pole image was prepared because it helps in getting rid of the dipolar nature in magnetic field. This facilitated the extraction of geological information. Geological feature extraction on the reduced to pole image was done by Visual interpretation of geologic units based on tone and/or colour, texture, patterns, shape, size, shadow, and association (Drury, 2001).

3.7.2. Shaded relief

This was done by displaying the total magnetic intensity grid RTP as a colour shaded grid in Oasis Montaj. This enhancement was done because it gives more detail on geological information than the raw unenhanced total magnetic intensity. This facilitated extraction of geological information on fine details. Geological feature extraction on the enhanced shaded relief image was done by Visual interpretation of geologic units based on tone and/or colour, texture, patterns, shape, size, shadow, and association (Drury, 2001).

3.7.3. Vertical derivative

Vertical derivative was calculated from the Total Magnetic Intensity RTP grid in Oasis Montaj. This enhancement was done because it highlights geological structures and also anomalies produced by near-surface geological features which are emphasized relative to those associated with deeper features as regional scale anomalies tend to be suppressed (Dobrin and Savit, 1988). Geological feature extraction on the enhanced vertical derivative image was done by Visual interpretation of geologic units and structures based on tone and/or colour, texture, patterns, shape, size, shadow, and association (Drury, 2001)

3.7.4. Tilt derivative

Tilt derivative was calculated from the Total Magnetic Intensity (RTP) in Oasis Montaj. This derivative was used because it enhances linear geological features, such as faults, dykes and provides an excellent base for the structural interpretation (AlSaud, 2008).The tilt derivative gives a better contrast than a normal vertical derivative image. The derivative was displayed as gray scale for good visualization. Geological feature extraction on the enhanced tilt derivative image was done by Visual interpretation of geologic units and structures based on tone and/or colour, texture, patterns, shape, size, shadow, and association (Drury, 2001).

3.7.5. Analytic signal

The analytic signal was calculated in Oasis Montaj software from the total magnetic intensity. This enhancement was made because it provides much improved resolution of prominent magnetic boundaries (Dobrin and Savit, 1988; Harris, 2012) and it was used to delineate the edges of the magnetic anomalies. Geological feature extraction on the enhanced analytic signal image was done by visual interpretation of geologic units based on tone and/or colour, texture, patterns, shape, size, shadow, and association (Drury, 2001)

4. CHARECTERIZATION OF LITHOLOGICAL UNITS USING FIELD DATA

4.1. Introduction

This chapter gives an analysis of the ground field data that was collected in the Harz from 2011-2014. The data was collected using (1) Analytical Spectral Device (ASD) which measures reflectance spectra of the minerals in rocks, (2) Kappa meter, which measures magnetic susceptibility of rocks and (3) Gamma ray spectrometer which was used to measure the concentration gamma ray radiation K, Th, U and TC. The area has a lot of vegetation and this made it not possible to see different lithological units and structures using remote sensing imagery. The figure 4-1 below show locations of the sampling points on the geological map.

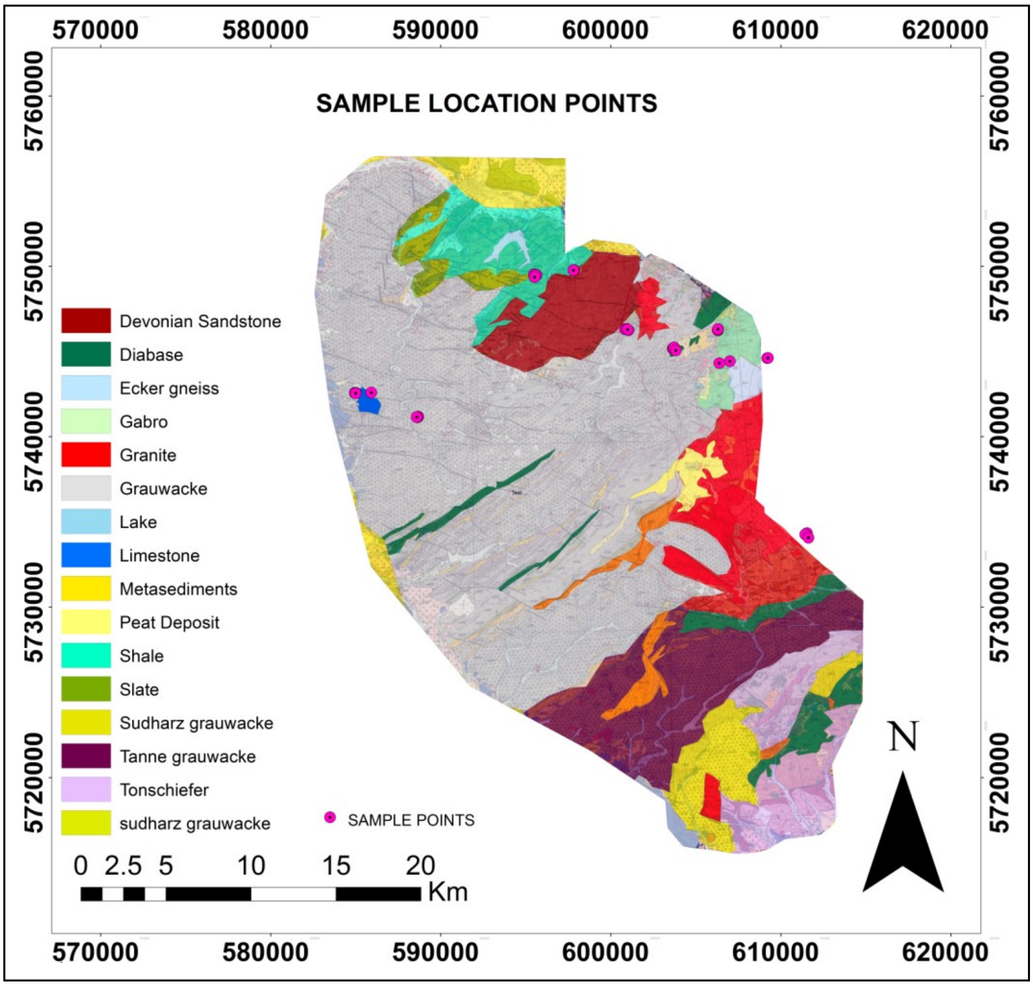

Figure 4-1 Locations of the sampling points on the geological map

4.2. Results on Magnetic Susceptability

The figure 4-2 below show magnetic susceptibility readings for the different types of rocks that were measured. From the figure it shows that Shale Orkertal, Slate, Shale, Hornfels Gneiss and Limestone all are characterized by low magnetic susceptibility which is expected in these rock units. Limestone has the lowest magnetic susceptibility. Harzburgite show the highest magnetic susceptibility. Diabase, Gabbro and Granite also show high magnetic susceptibility but not high as Harzburgite. This high reading is attributed to the presence of Magnetite and iron sulphide mineral Pyrrhotite. Magnetite has the highest susceptibility of all naturally occurring minerals. It contains a combination of ferric and ferrous iron. Low magnetic susceptibilities in the rest of the other units are due to absence of these magnetic minerals in them. Magnetic susceptibility measurements that were made in the laboratory also found similar results (refer to annex 1).

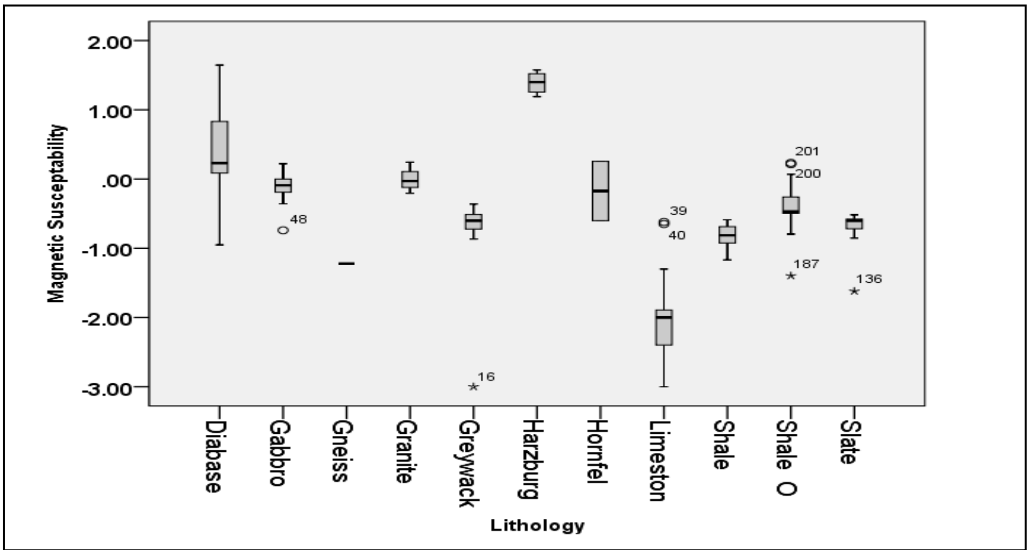

Figure 4-2 Box plot grouped by lithology showing magnetic Susceptibility that were measured in the field.

4.3. K content of rock samples measured by gamma ray spectrometer

Gamma ray spectrometer is an instrument that integrates radiation relatively over a larger area and it normally gives reliable results. Figure 4-3 shows K distribution measured by this instrument which indicates that Shale, Slate, Shale Orkertal and Granite have high K content. Harzburgite Limestone Diabase, Gabbro, Eckergneiss have low K content. Greywacke and Hornfel have medium K content according to the results from the gamma ray spectrometer readings. High K concentration in Shale, Slate and Shale Orkertal is due to the presence of mica and clay minerals that contribute significantly to high K content. Granite has high K content due to the presence of alkali feldspar, biotite, and muscovite. Low K content in the other rocks is due to the absence of these minerals in them. Portable XRF measurements that were made in the laboratory on powdered rock samples also found similar results for K distribution in these lithological units (refer to annex 1).

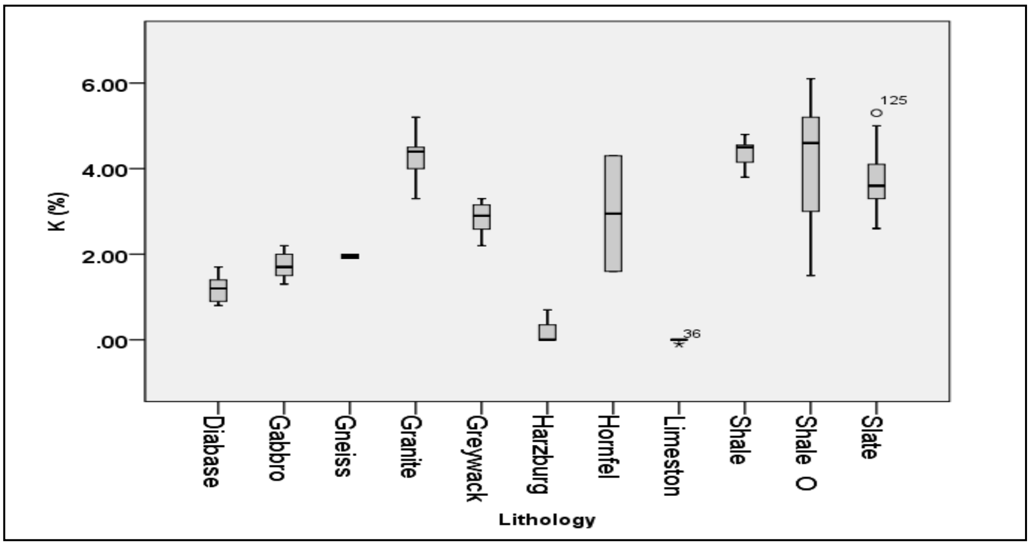

Figure 4-3 K *concentration in all lithological units measured by Gamma ray spectrometer*

4.4. Comparison between K measured by gamma ray spectrometer and pXRF in the lab

Comparison between the K measurements obtained by the gamma ray spectrometer and that obtained by pXRF on the powdered rock samples shows very good positive correlation. This means that the gamma ray spectrometer determinations of K can be reproduced using the pXRF. The scatter plot below shows the correlation between K concentration measured by gamma ray spectrometer and K concentration measured by pXRF in the lab.

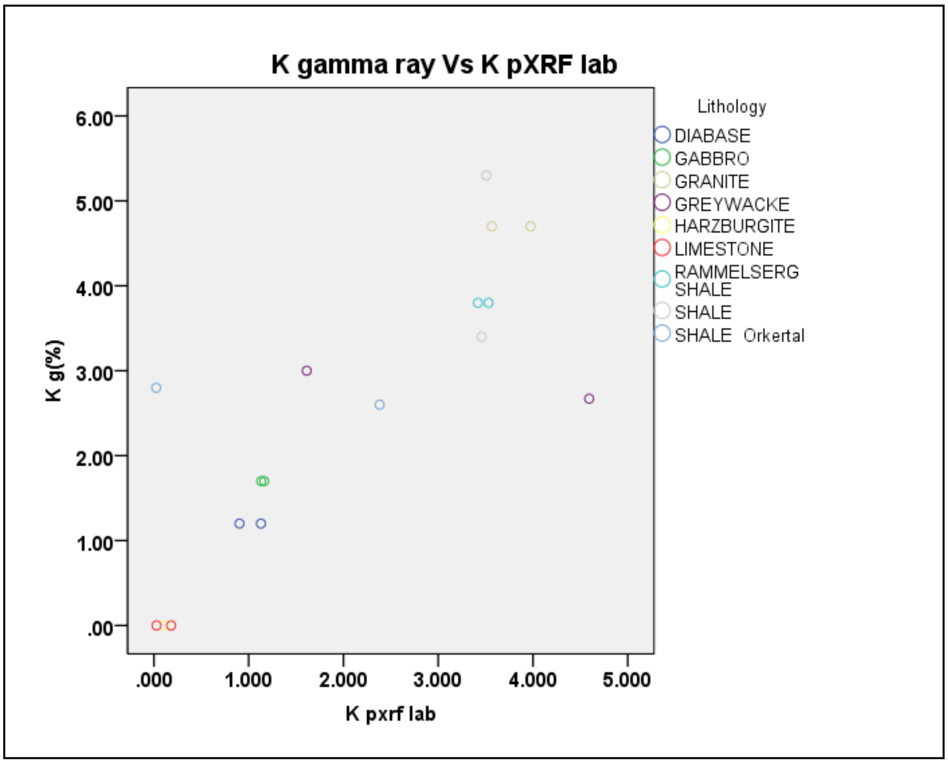

Figure 4-4 Scatter plot showing correlation between potassium measured by gamma ray spectrometer and potassium measured by pXRF in the laboratory

4.5. Th content of rock samples

The gamma ray spectrometer readings in figure 4-5 show that Granite, Shale, Slate and Shale Orkertal have high Th concentration. Harzburgite, Limestone and Diabase have very low Th concentration. Gabbro, Greywacke, Eckergneiss, Hornfels has low-medium Th concentration. High Th concentration in Shale, Slate and Shale Orkertal is due to the presence of monazite and zircon minerals that contribute significantly to high Th content. Granite have high Th content due to the presence of zircon and low Th content in the other rocks is due to the absence of these minerals in them. Portable XRF measurements that were made on powdered rock samples in the laboratory also found similar results (refer to annex 1).

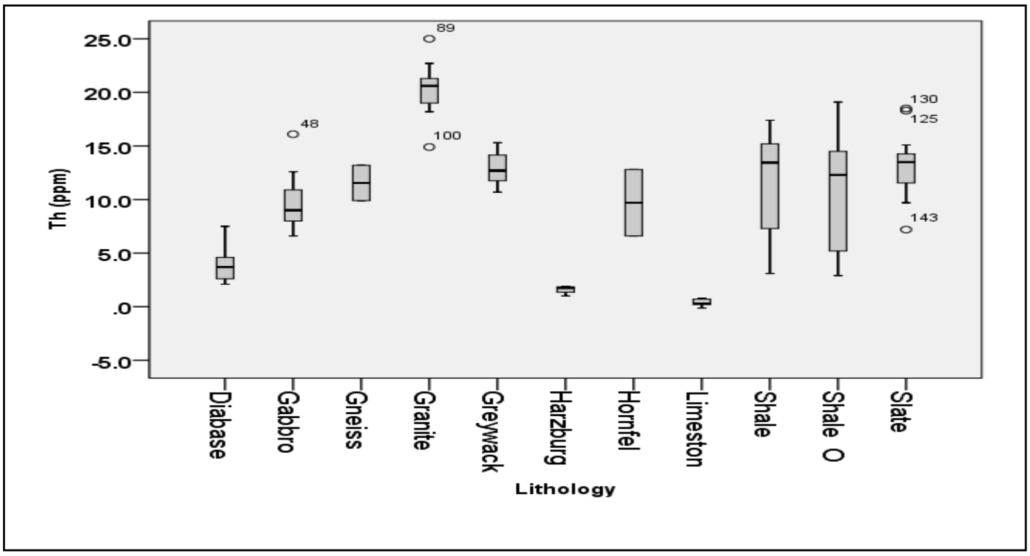

Figure 4-5 Th concentration in all lithological units measured by Gamma ray spectrometer

4.6. Uranium content of rock samples

The gamma ray spectrometer readings for U show that Shale, Shale Orkertal and Greywacke are having relatively high U concentration and Granite has medium concentration of uranium while the rest of the lithological units are characterized by low uranium concentration. Portable XRF measurements that were made in the laboratory on powdered rock samples found that U concentration show high values in Granite and Greywacke (figure4-6b). Limestone, Harzburgite, Gabbro, Shale, Slate and Shale Orkertal and Diabase show low U concentration. High U concentration in Granite is due to presence of zircon and monazite. The other lithological units are characterized by low uranium concentration because of absence of these minerals in them.

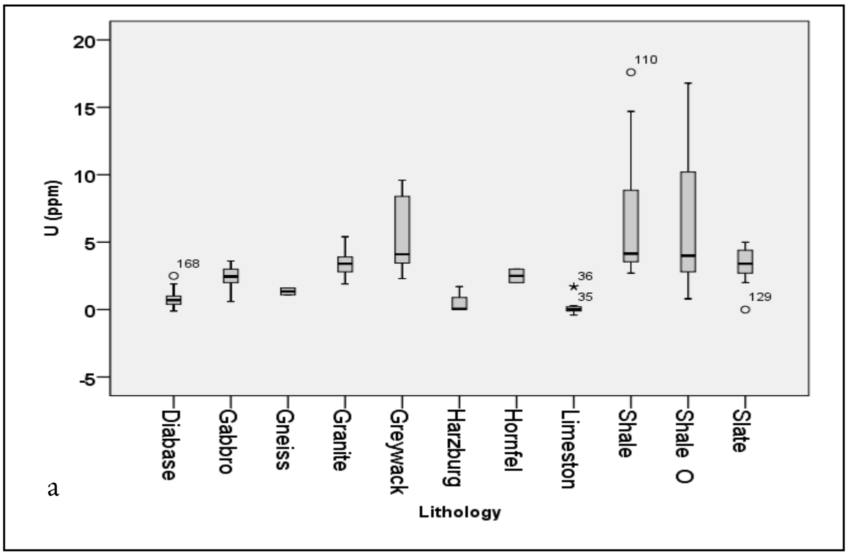

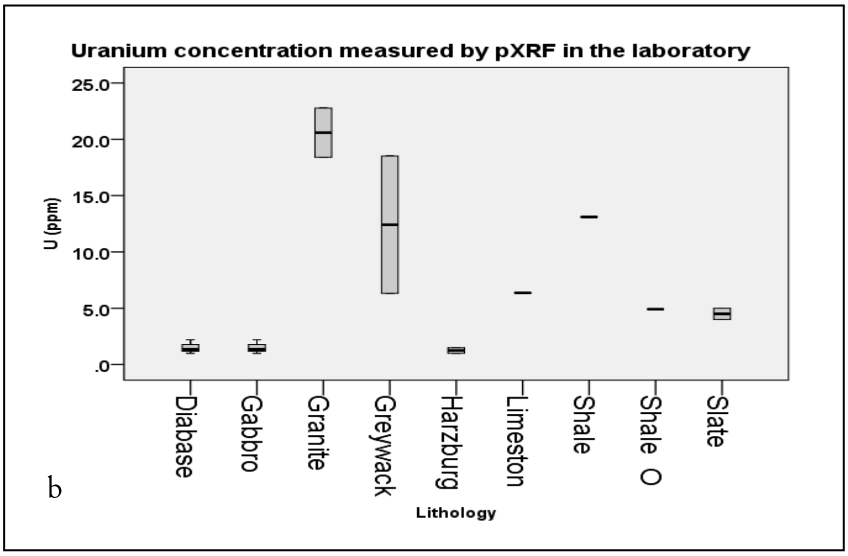

Figure 4-6 U concentration in all lithological units measured by Gamma ray spectrometer and (b) U concentration in all lithological units measured by pXRF.

4.7. Cu-Pb-Zn Distribution

The elements of economic interest minerals Cu-Pb-Zn were also analyzed. The graphs were converted to logarithmic scale in order to see the variation better. Cu-Pb-Zn content in Shale is higher than in all other lithologies as seen in the box plots in figure 4-7 below. There are also elevated values for Pb and Zn in Slate and Shale Orkertal but not as high as the Shale. This is expected because the Shale is the host for the Cu-Pb-Zn Rammelsberg mine in the study area. Portable XRF measurements that were made in the laboratory also found similar results.

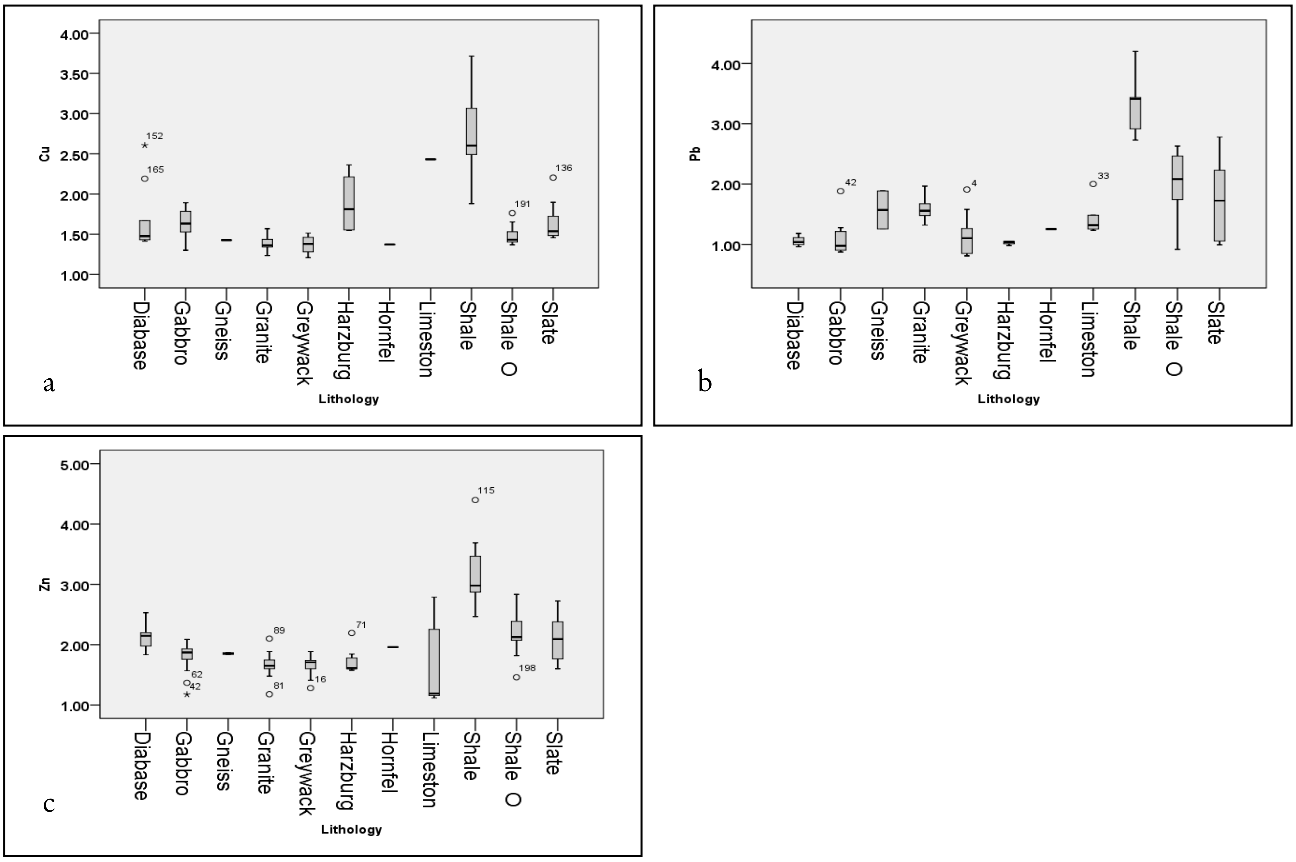

Figure 4-7 Cu-Pb-Zn concentration in all lithological units (a) Cu , (b) Pb and (c) Zn

4.8. Discussion of the results on radioelement and magnetic susceptability distribution

Greywacke is showing low-medium levels of Th and U because heavy minerals such as monazite, sphene and zircon which contribute significantly to Th and U concentration are absent. Similarly the low-medium level of K concentration is due to the low levels of alkali feldspar, hornblend and biotite which contribute significantly to the high levels of K. The distribution of radioelement K,U and Th in sedimentary rocks such as Greywacke is influenced by the composition of the parent rock (Dentith & Mudge, 2014). Greywacke have radioelement concentration similar to their source, but as sediment maturity increases, quartz becomes increasingly dominant with an associated decrease in radioelement content. The magnetic susceptibility is low, this indicates that Greywacke has no strong magnetic properties. Greywacke is characterized by low magnetic susceptibility because of the absence of magnetic minerals such as magnetite, monoclinic pyrrhotite, maghemite and ilmenite.

K, Th and U contents measured using gamma ray spectrometer are low in Limestone. Carbonate rocks have low radioactivity but when they contain organic matter they may have relatively high levels of U. Th content in Limestone is low because it cannot enter the carbonate lattice easily (Dentith & Mudge, 2014). K content is low due to the absence of alkali feldspar, mica and clay minerals which significantly contribute to increased concentration of K. The magnetic susceptibility show low readings in this outcrop because of the absence of magnetic minerals like magnetite and pyrrhotite.

Gabbro is characterized by low radiometric value because of very low levels of alkali feldspar and micas which are responsible for K concentration in rocks. Minerals such as zircon, monazite that are responsible for Th and U concentration are not abundant in maffic rocks like Gabbro. Because of the absence of these minerals Gabbro is being characterized by low radioelement concentration.

Low magnetic susceptibility in Eckergneiss is due to absence of magnetic mineral magnetite. Low levels of K, U and Th in gneiss is due to fluid loss and increased mobility of these elements at high temperature and pressure during metamorphism (Dentith & Mudge, 2014).

Harzburgite is characterized by high magnetic susceptibility because of the presence of magnetite and iron sulphide mineral pyrrhotite. Magnetite has the highest susceptibility of all naturally occurring minerals. It contains a combination of ferric and ferrous iron and has the highest susceptibility of all naturally occurring minerals. The decrease in radioelement concentration in Harzburgite is due to less abundance of alkali feldspars and micas. Concentration of U and Th are extremely low in mafic and ultramafic rocks because accessory minerals like zircon, monazite and allanite, which contributes to increased abundance of U and Th are not present. This is why gamma ray readings show low values for radioelement concentration for K, U and Th.

High K content in Granite is attributed to greater abundance of alkali feldspars, clay minerals and micas which are responsible for increased K concentration. High U and Th are attributed to the presence of zircon and monazite which are common in felsic rocks like Granite. The average magnetic susceptibility measured by the Kappa meter, show low-medium magnetic values as expected for magnetite poor Granite.

Shale, Slate and Shale Orkertal are characterized by low magnetic values because of the absence of magnetic minerals magnetite and pyrhotite which are responsible for high magnetic susceptibility in rocks. The ground data show high Potassium and thorium concentration and low concentration of uranium on the Shale. High K concentration in Shale is due to the presence of muscovite mica and clay minerals. High Th concentration is due to presence of monazite and zircon.

The low radioelement concentration in Diabase is due to low presence of alkali feldspar, muscovite mica and accessory minerals like zircon and monazite which are responsible for K, Th, and U concentration. The high magnetic values may be attributed to presence of magnetic minerals magnetite and pyrhotite in Diabase.

4.9. Results and discussion on ASD Spectrometer (refer to annex 1 for spectra)

ASD field spectrometer allowed the identification of some infrared active minerals for different lithological units. Interpreted minerals can be related with rock forming and alteration processes. In Greywacke muscovite and illite (white Mica) are present in the fine grained facies, muscovite has water absorption feature at 1400 and 1900nm and clay feature at 2205nm and 2208nm. Illite has an absorption feature at 2200nm. In the Limestone lithological unit only calcite was identified. The carbonate absorption feature at 2300nm is conclusive and characterizes the Limestone. In Shale chlorite was recognized with an absorption feature at 2355nm which indicates the presence of Mg-OH bonds. Other minerals identified are muscovite and illite (white Mica) with Al-OH absorption features at 2211-2213nm and 2200nm respectively. White mica consists of minerals like muscovite, illite, phengite and paragonite. Illite is a K-deficient muscovite and can be formed by the alteration of K feldspar, muscovite and phengite minerals or due to smectite to illite transition in low grade metarmophic rocks. Slate has white mica Al-OH absorption feature ranging from 2216 - 2220 nm. Eckergneiss also has muscovite and illite (white mica) with Al-OH absorption features at 2200 - 2201nm. The wave length position of Al-OH feature for white mica (Muscovite and Illite) is not the same in these lithological units for these minerals. The wavelength position of the Al-OH feature is changing due to grade of metamorphism and mineralization process. For example, the mineralized Rammelsberg Shale has an Al-OH absorption feature between 2211 - 2213 nm and slate has Al-OH feature between 2216 - 2220nm. Eckergneiss has a wavelength position for white mica between 2200 - 2201nm. The results show that the high the metamorphic grade the shorter the wavelength positions of AL-OH feature. Dominant spectra detected in the Granite were muscovite with an absorption feature at 2210 nm and halloysite which has the wavelength position at 2205nm. Halloysite is a clay mineral and indicates weathering in the Granite rock unit. Gabbro contains diagnostic features for chlorite, and Prehnite. Prehnite is a secondary Ca-Al phyllosilicate mineral usually found in mafic volcanic and low grade metamorphic rocks. The presence of Prehnite indicates that the rock has been slightly metamorphosed. The main spectral absorption features of Prehnite are found around 1470nm and 2340nm. Harzburgite shows diagnostic features for Chlorite and Serpentine. Chlorite has an absorption feature at 2355 nm and Serpentine with an absorption feature at 2326nm. Chlorite is a group of phyllosilicate minerals containing Al, Mg and Fe end members. Mg and Fe can be identified as Mg-OH and Fe-OH absorption features. The spectral position of Mg-OH and Fe-OH absorption feature depend on iron content as such more or less iron content leads to displacement of the absorption features position to longer or short wavelength respectively. The main diagnostic spectral position of the Mg-OH and Fe-OH absorption features are 2325nm and 2245nm for Mg chlorite respectively and 2355nm and 2261nm for Iron chlorite respectively. The 2355nm chlorite absorption feature show that this lithological unit contains a lot of iron.

4.10. Conclusion

In general Harzburgite, Diabase and Gabbro are characterized with high magnetic susceptibilities and low radiometric signatures. The high magnetic susceptibilities indicate the presence of magnetic minerals such as magnetite in these lithological units. Low radiometric signatures is due to low presence of alkali feldspar, muscovite mica and accessory minerals like zircon and monazite which are responsible for K, Th, and U concentration. Limestone, Slate, Shale, Shale Orkertal, Greywacke, Eckergneiss and Granite are characterized with low magnetic susceptibilities because of the absence of magnetic minerals. Out of these low magnetic susceptibility units, Shale, Slate, Shale Orkertal and Granite are characterised by high K, Th and low U concentration because of the presence of micas, K feldspar while Limestone has low radiometric signatures due to low presence of alkali feldspar, muscovite mica and accessory minerals like zircon and monazite. ASD results have shown that wave length position of Al-OH feature for white mica (muscovite and illite) is not the same in these lithological units. It is changing due to grade of metamorphism and mineralization process. The results have shown that the high the metamorphic grade the shorter the wavelength positions of AL-OH feature. Laboratory measurements measured by pXRF, Kappa meter and ASD give similar results as the field measurements. These results validate the field measurements to be true and are reproducible. The results show that the rock units can potentially be mapped using the legacy airborne magnetic data and radiometric data because there are contrast magnetic susceptibility and radiometric readings among the different rock types.

5. GEOPHYSICAL DATA PROCESSING

5.1. Introduction

The geophysical data consists of Potassium, Thorium, Uranium, Total count and Total Magnetic Intensity. The data was originally published on contour map form as shown in (figure 5-1 a) and was flown in North South direction. It was digitized from the original map form, the actual measurements cannot be recovered, and instead the intersections of the contours with the flight lines were digitized (figure5-1b). The intersections were digitized as points (figure5-1c) and the digitized points were saved as database which was exported into ASCII xyz file that is compatible with Oasis Montaj.

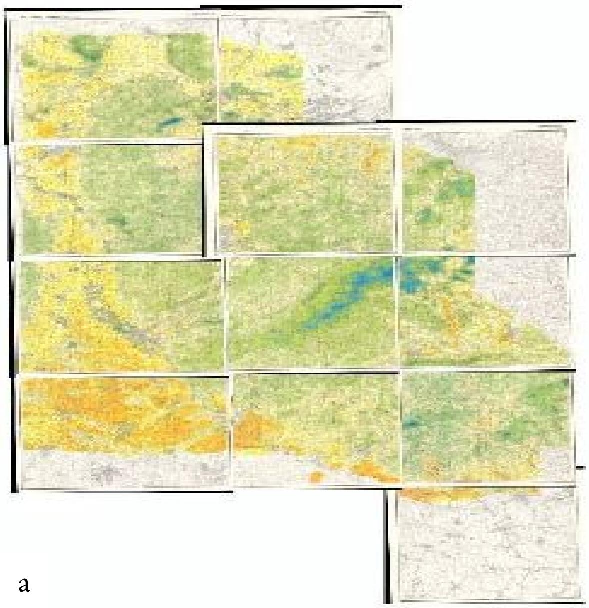

a

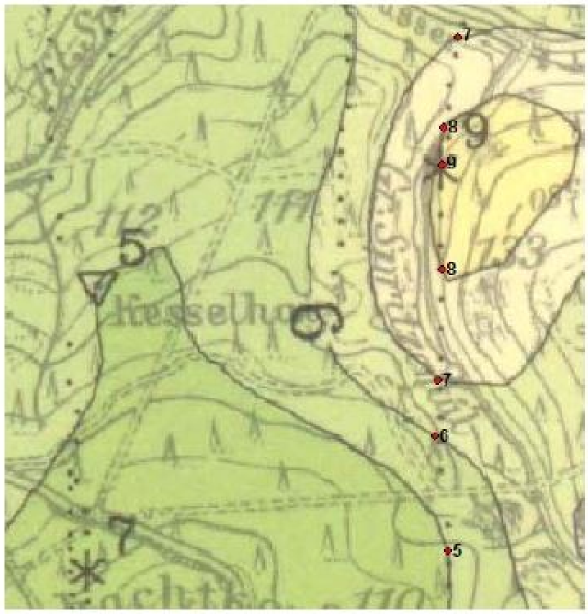

b

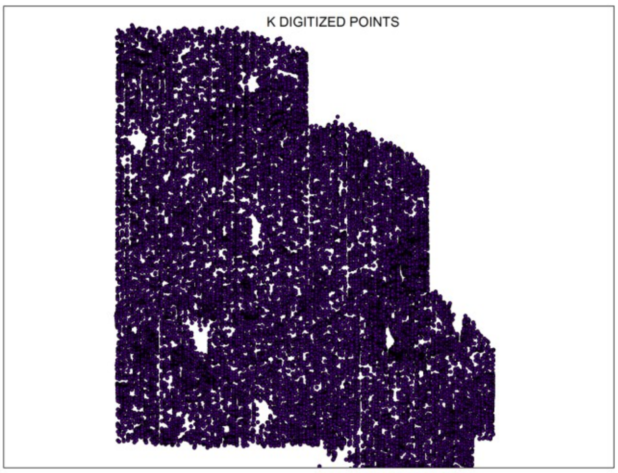

c

Figure5-1 (a) showing the original contour map form for Potassium, (b) showing digitisation of intersection of contours (red dots) and flight lines (black dots), (c) showing digitized points for Potassium as shape file

The data was then gridded using minimum curvature, kriging and IDW as discussed in chapter 3. Figure5-2 shows the results of the three gridding algorithms for potassium.

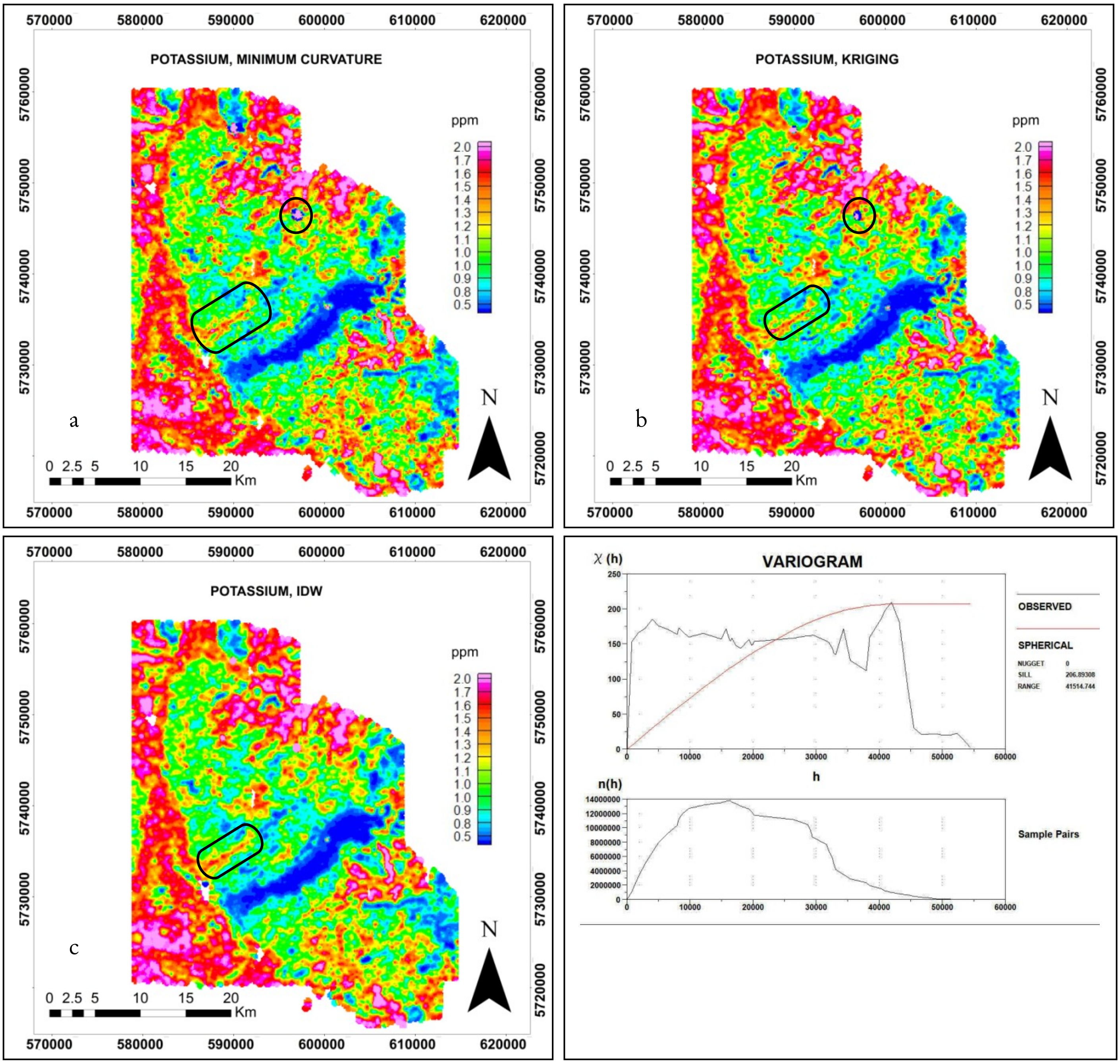

Figure5-2 showing results for gridding for potassium using Minimum curvature, Kriging and IDW and (d) shows a variogram from the Kriging gridding method

5.2. Comparison of gridding algorithms

5.2.1. Visual comparison

All the three gridding algorithms show high K content in the western and north east sides of the grids, medium to low K concentration at the centre and a band of very low K concentration at the centre running SW-NE. Closer comparison of the grids show that there is a strange artefact which is very visible in the minimum curvature gridding method marked in the circle. This anomaly is also visible in the kriging method but it is not sharper as in the minimum curvature. In IDW this strange anomaly is not visible at all. The narrow linear feature marked in ellipse which corresponds to Diabase lithological unit on a geological map shows a sharper/crisp boundary in the kriging method while on the minimum curvature this feature (lithological unit) shows a fuzzy boundary and also in IDW it shows a fuzzy boundary as well. This shows the effects of the gridding algorithms on this legacy airborne data.

5.3. Statistical comparison

The gridded data was exported to ARCGIS in ER Mapper form. ER Mapper was chosen because it preserves grid values. In ARCGIS grid values from the gridded data were extracted using extract values to point tool in order to compare the gridded values with the original values before gridding. The table below shows part of the values that were extracted from the gridded data in the Raster value column and the original potassium values in the K column.

OBJECTID *	Shape *	Comments	Line_No	X	Y	K	RASTERVALU
1	Point		300	602919.563131	5749996.53303	20	19.948126
2	Point		300	602923.286909	5749758.21125	23	21.979452
3	Point		300	602930.734465	5749672.56436	20	19.488846
4	Point	start of line	300	602930.734465	5750115.69391	18	18.22019
5	Point		300	602930.734465	5749577.98041	18	18.591381
6	Point		300	602919.563131	5749481.16219	18	17.72578
7	Point		300	602915.839354	5749231.66908	20	20.043821
8	Point		300	602915.839354	5749216.77397	20	19.730665
9	Point		300	602934.458242	5749060.37531	18	17.60458
10	Point		300	602938.18202	5748989.62353	16	16.230215
11	Point		300	602941.905798	5748926.31931	14	14.360752
12	Point		300	602949.353353	5748866.73887	12	11.311136
13	Point		300	602953.077131	5748779.60247	8	8.896814
14	Point		300	602956.800909	5748254.54981	12	12.168502
15	Point		300	602967.972242	5748146.56025	14	14.031977
16	Point		300	602964.248464	5747997.60915	16	15.839327
17	Point		300	602960.524686	5747908.23848	16	15.761002
18	Point		300	602938.18202	5747595.44115	14	13.960764
19	Point		300	602938.18202	5747185.08085	12	12.02716
20	Point		300	602949.353353	5746961.65418	12	12.27553
21	Point		300	602949.353353	5746831.32196	14	14.001479
22	Point		300	602953.077131	5746648.85686	14	14.055509
23	Point		300	602960.524686	5746414.25886	14	14.122663
24	Point		300	602975.419797	5746224.3462	14	13.528432
25	Point		300	602949.353353	5747069.64374	12	12.087657
26	Point		300	602979.143575	5746084.33215	12	12.147192
27	Point		300	602986.59113	5745860.90549	12	11.985843
28	Point		300	602982.867353	5745652.37394	12	11.826136
29	Point		300	602986.59113	5745509.38087	10	9.800437
30	Point		300	602982.867353	5745271.0591	10	10.073629
31	Point		300	602986.59113	5744760.90155	12	12.355004
32	Point		300	602954.93902	5744394.48183	14	14.02521
33	Point		300	602945.629575	5744159.88383	14	13.841511
34	Point		300	602938.18202	5743958.79983	12	12.026653
35	Point		300	602930.734465	5743902.94317	12	12.142224
36	Point		300	602949.353353	5744297.6636	18	17.972342
37	Point		300	602923.286909	5743742.82072	15	14.540686
38	Point		300	602941.905798	5743395.76464	12	11.996918
39	Point		300	602975.419797	5742967.5302	12	12.648914
40	Point		300	602997.762464	5742684.5231	12	12.02759
41	Point		300	602990.314908	5742874.43576	17	16.364195
42	Point		300	602982.867353	5742559.40417	10	9.981754
43	Point		300	602938.18202	5742257.77817	10	10.040726
44	Point		300	602919.563131	5741777.41084	10	10.603457
45	Point		300	602949.353353	5741550.2604	10	10.018798

Table 1*showing part of the original potassium values K and extracted Gridded values (Raster values)*

The results were then exported to SPSS software for statistical analysis. The gridded values for each method were subtracted from the original values in order to see how close the gridded data differ from the original data. The residuals (differences) were plotted as histograms showing normal distribution. The data was split into two parts, one data set was used for gridding and the other was used for validation. In total there were about 25000 points in which one third of the points which is 17000 points were randomly selected for gridding and the remaining 8000 points were used for validation. These values were chosen because they are representative of the whole dataset. The results below show the histograms of the residuals of each of the three gridding methods.

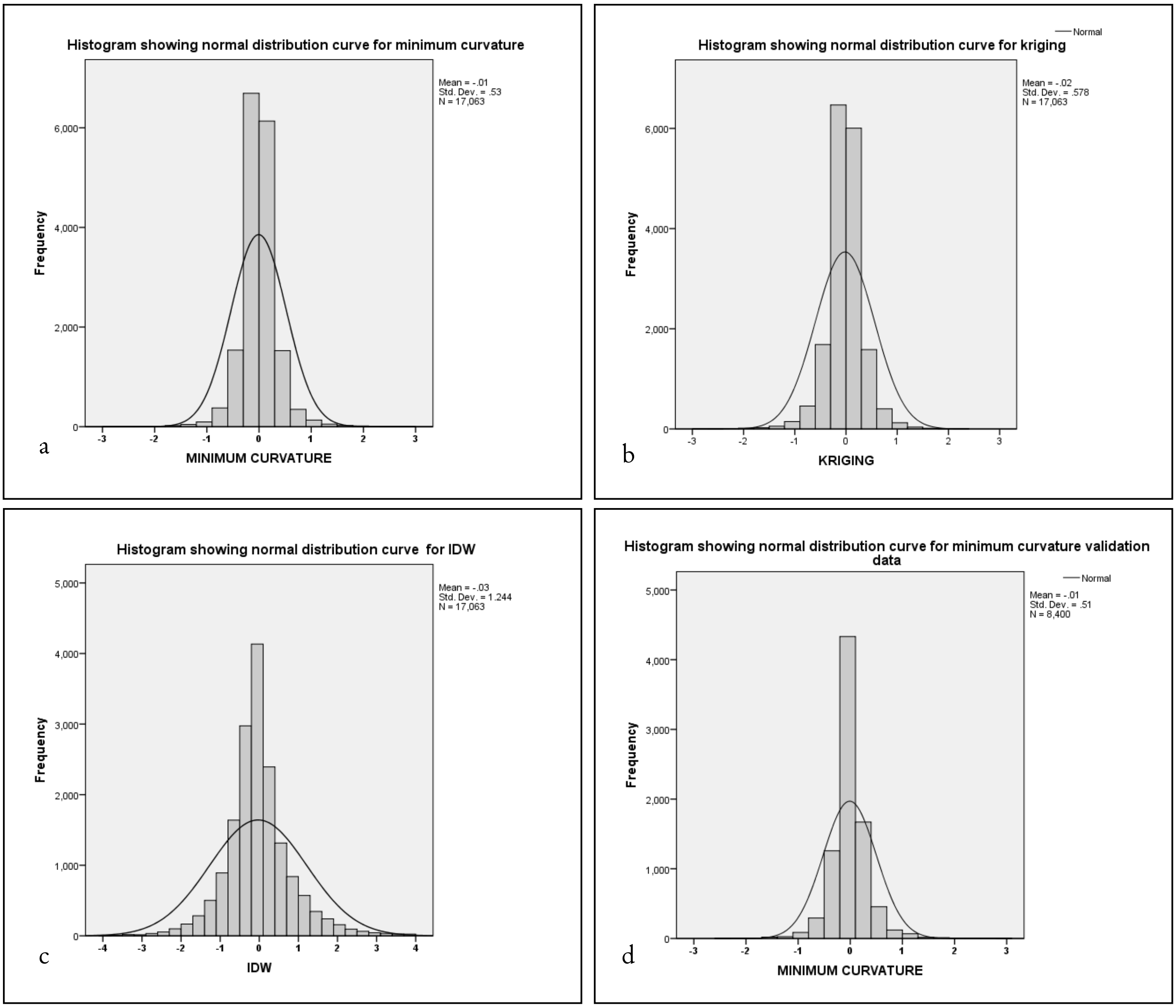

Figure 5-3 showing normal distribution curves for minimum curvature, kriging and IDW gridding methods for potassium and (d) shows validation distribution curve for minimum curvature

The curve of the distribution of minimum curvature shows a standard deviation from the mean of 0.53, kriging shows standard deviation of 0.58 and inverse distance weighting (IDW) shows a standard deviation of 1.2. minimum curvature and kriging show low standard deviation 0.53 and 0.59 respectively which means that these methods have less variability and that the results from these methods are closer to the true original values. The difference between the original and gridded values is not much as compared to IDW. On the other hand IDW shows the highest standard deviation 1.2 which means it has high variability i.e. there is a big difference between the original values and the gridded values. From the results it shows that minimum curvature and kriging gridding methods have values close to the original values evidenced by less variability of their standard deviations. The difference between minimum curvature and kriging is small, this shows that both methods are producing satisfying results.

5.4. Correlation matrix

	K original	Minimum Curvature	Kriging	IDW
K original	1	0.993	0.991	0.77

Table 2 shows correlation matrix among the minimum curvature, kriging and IDW gridding methods

Correlation of original potassium values and potassium values from the minimum curvature show very high positive correlation of 0.993, with kriging method it is 0.991, and with IDW it is 0.77. The high positive correlation of original potassium values and those obtained from minimum curvature and kriging gridding indicates that values of these methods are more close to the original potassium values. These results are also in agreement with the normal distribution curves above. This confirms that the minimum curvature and kriging gridding are the best in this data set.

5.5. Root Mean Square Error (RMSE)

RMSE is used to assess the probability that a particular set of measurements does not deviate too much from true values. It provides an estimate of the spread of a series of measurements around their assumed true values. RMSE was used to assess the quality of the three gridding algorithms and this formula was applied.

$$\text{RMSE} = \sqrt{\frac{\sum_{t=1}^{n}(\hat{y}_t - y_t)^2}{n}}.$$

Minimum curvature gridding has an RMSE of 0.53 kriging has an RMSE of 0.55 and IDW has an RMSE of 1.11. Minimum curvature and kriging are very close all have low RMSE and this shows that their values are close to the original values. On the other hand IDW has an RMSE of 1.11 which is a bit high compared to minimum curvature and kriging and this shows that the values from IDW are not very close to the original values as is the case with minimum curvature and kriging.

5.6. Validation

In order to assess the quality of the above output results the gridded values were compared with the validation data. The original dataset was divided into two parts. One part was used for gridding and the other part was used to compare and validate the output gridded data. The data was divided by generating random values. Two thirds of the data was used for gridding and the other one third was used for validation. In total there were about 25000 points and out of these 17000 points were used for gridding and 8000 points were used for validation. This was done in order to get better representative samples for the whole dataset without bias.

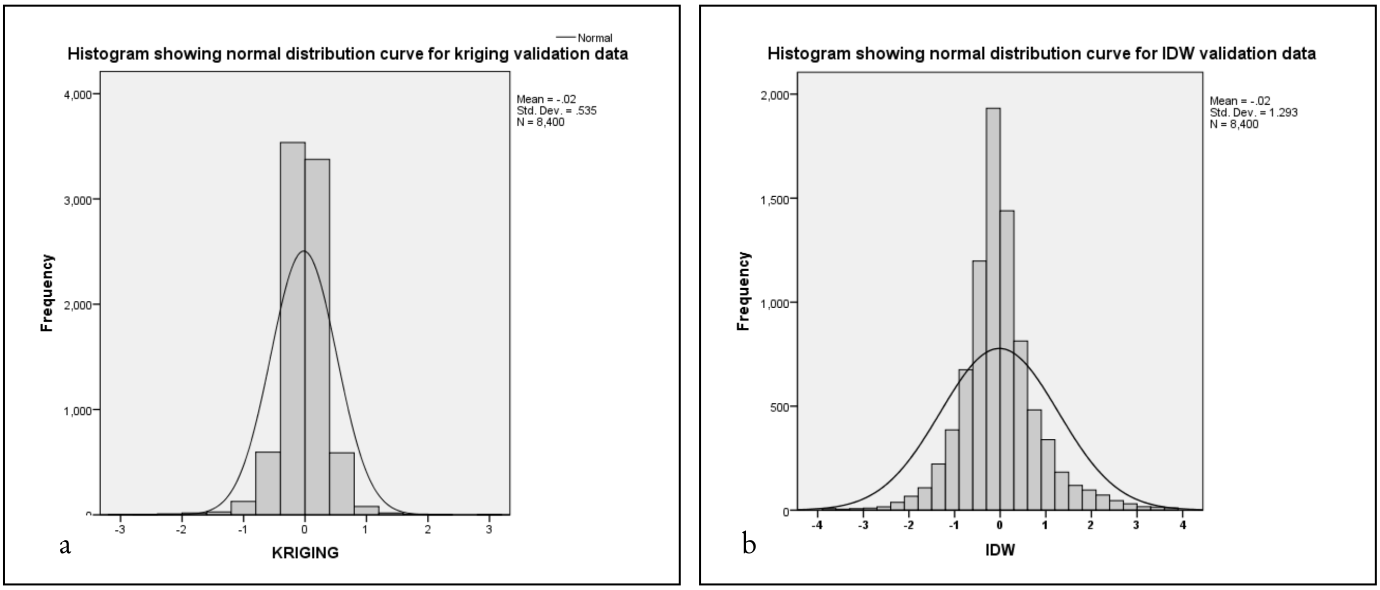

Figure 5-4 shows the results of the histograms for normal distribution curves of the validation dataset for potassium

From the normal distribution curves, minimum curvature (figure 5-3d) shows a standard deviation from the mean of 0.51, kriging has standard deviation of 0.54 and inverse distance weighting (IDW) has a standard deviation of 1.3 (figure 5-4). Minimum curvature and kriging show low standard deviation 0.51 and 0.6 respectively which means that these methods have less variability and that the results from these methods are closer to the true original values. The difference between the original and gridded values is not much as compared to IDW. On the contrary, IDW shows the highest standard deviation 1.3 which means it has high variability i.e. there is a big difference between the original values and the gridded values. From the results it shows that Minimum Curvature and Kriging gridding methods have values close to the original values evidenced by less variability of their standard deviation.
The results from this data set show similar pattern with the dataset used for gridding. This indicates that what was observed in gridding data set is also reflected in the validation data. In order to be more certain of the results, root mean square error was calculated from the validation data set in order to see if similar pattern from the gridding data will be observed.

5.7. Root Mean Square Error (RMSE)

RMSE was used to assess and validate the quality of the three gridding algorithms. Using validation data that was picked randomly, minimum curvature gridding has an RMSE of 0.54 kriging has an RMSE of 0.61 and IDW has an RMSE of 1.11. Minimum curvature and kriging are still very close all have low RMSE and this shows that their values are close to the original values. IDW has an RMSE of 1.11 which is a bit high compared to minimum curvature and kriging and this shows that the values from IDW are not very close to the original values as is the case with minimum curvature and kriging.

These results are similar with the results on the gridding data, what was observed in the gridding data has been reflected on the validation data set and the results can validate the results obtained on gridding data to be true. The same principal has been applied for Thorium, Uranium, Total count and magnetic grids and the results show that minimum curvature and kriging are producing close to true values than IDW, refer to annex 2.

5.8. Conclusion

The precision required in the geophysical data field measurement is irrelevant if we use a grid interpolator that does not represent the reality of the geophysical anomaly spatial variability. The choice of the interpolator is important for estimating the anomaly caused by the sources. Minimum curvature and kriging gridding have shown to be the best gridding algorithm because their values are close to the original values than IDW gridding method. Normal distribution curves for kriging and minimum curvature show low standard deviations and also RMSE for these methods is low than the IDW. Minimum curvature and kriging all have produced very close results as such visual analysis of the individual grids was done in order to find best gridding between them. Visual comparison of kriging and minimum curvature showed that minimum curvature has got pronounced artefacts than kriging and also the boundary for Diabase dyke in minimum curvature is fuzzy while kriging shows crisp/sharp boundary in the potassium grid. Bearing in mind that this can have an impact on interpreting the data later, therefore the grid that has shown less artefacts by visual analysis is taken to be good and in this case Kriging has been chosen. Visual analysis of the magnetic grids for Analytic Signal, (Annex 2) show that kriging is producing good results which are crisp and clear seconded by minimum curvature and in IDW the grids are fuzzy. These results are similar to the results of Arfaoui & Inoubli, (2012) in which they did a comparative study on two interpolator methods for Bouguer anomaly mapping in the El Kef-Ouargha region, Tunisia. They compared the results of minimum curvature gridding and kriging using a geostatistical approach. They found out that kriging closely approximates the measured gravity data than minimum curvature. Hosseini & Marcotte, (2014) also conducted a study to determine interpolation methods that are best suited to map soil salinity. They compared methods of kriging, inverse-distance, and minimum curvature and they found out kriging and minimum curvature were the most precise methods, whereas IDW was the least precise. Similary Schloeder, Zimmerman, & Jacobs, (2001) investigated whether it was appropriate to use spatial interpolation methods with limited coarse-scaled soils data from a vertisol plain. They compared ordinary kriging, inverse-distance weighting, and minimum curvature. Comparison was based on accuracy and effectiveness measures, and analyzed using ANOVA and pair wise comparison *t*-tests. Results indicated that spatial interpolation ordinary kriging was accurate and effective method. Among the spatial interpolation methods compared, kriging appeared to outperform or be more accurate which is also the case with the results obtained in this research.

6. ASSESSMENT OF GEOLOGICAL INFORMATION CONTENT OF THE LEGACY AIRBORNE GEOPHYSICAL DATA

6.1. Introduction

This chapter aims at trying to define the extent to which the legacy airborne geophysical data set can be used to map lithological units and to see the aspects of the lithological units and structures that can be mapped or identified using this dataset. Both visual analysis and computer-assisted techniques which include supervised and unsupervised classification were employed to produce predictive maps. The relationship between ground field data and airborne data was assessed in the last part of this chapter in order to compare the composition of rocks as to what is seen in the airborne geophysical data.

6.2. Unsupervised classification

Unsupervised classification classifies an image based on natural groupings of the spectral properties of the pixels, without the user specifying how to classify any portion of the image (Schetselaar et al., 2007). The user specifies the number of classes to be used in the classification. This classification was used in this research in order to find natural groupings of the spectral properties of the pixels in the data set.

6.2.1. Data preparation

Gamma ray data Potassium, Thorium, Uranium and Total count channels were used as input to the unsupervised classification. All these radioelement channels were layer stacked into one composite image and were used as input into the classification. A subset was made on the data, the left side of the area where it shows the high counts in all the grids was masked out because this area was not covered during field work.

6.2.2. Clustering

The isodata clustering algorithm was applied to the layer stacked image for classification in erdas imagine software. Clustering was done by testing different numbers of classes and see the pattern of the classes. The Iterative Self-Organizing Data Analysis Technique (ISODATA) unsupervised classification calculates class means evenly distributed in the data space then iteratively clusters the remaining pixels using minimum distance techniques. Each iteration recalculates means and reclassifies pixels with respect to the new means. This process continues until the number of pixels in each class changes by less than the selected pixel change threshold or the maximum number of iterations is reached. The figure 6-1 below show the data set used in the unsupervised classification and figure 6-2 show the classified images result.

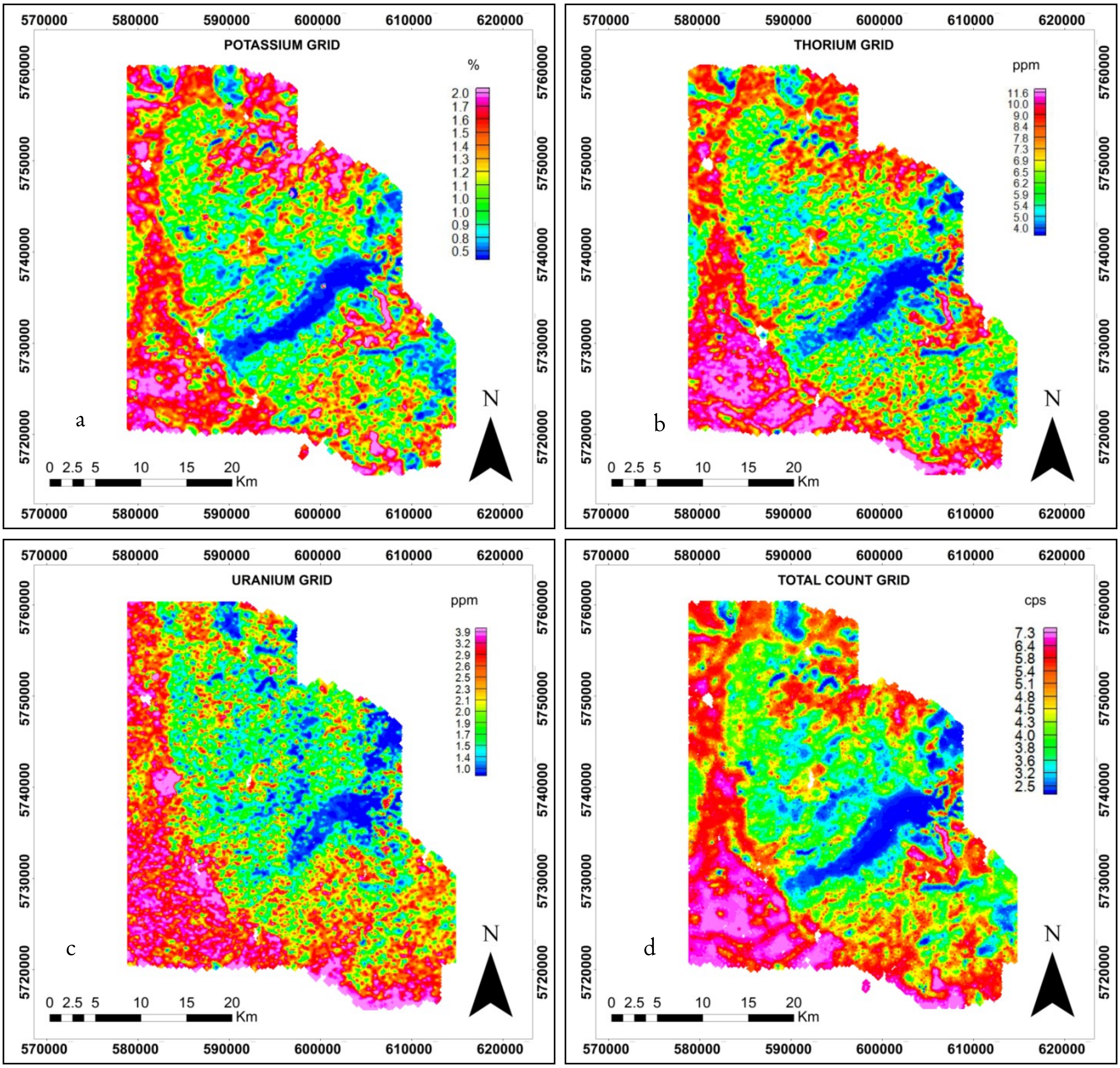

Figure 6-1 showing the data set used in the unsupervised classification (a) Potassium grid, (b) Thorium grid , (c) Uranium grid (d) Total count grid

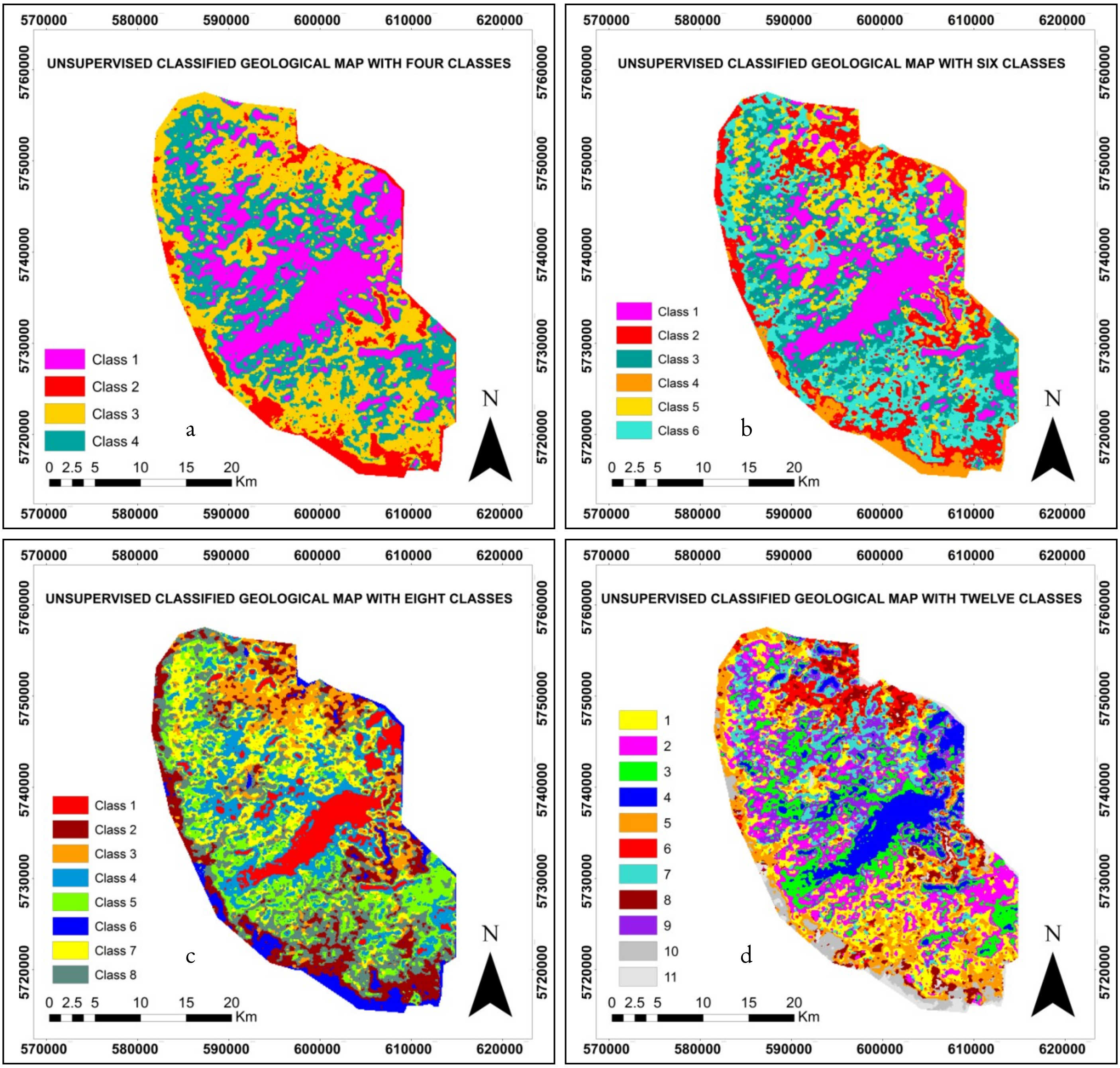

Figure 6-2 results of unsupervised classification obtained by testing different numbers of classes that was done in order to determine optimal number of classes to use. (a) with four classes, (b) with six classes, (c) with eight classes, (d) with twelve classes. The one with four classes was found to be good and was used in the interpretation.

It was observed that increasing the number of classes from four to six and then eight the information content of the data was not really changing only small subclasses are coming in that are not relevant. Increasing the number of classes to twelve a lot of noise was introduced. In order to select the best number of classes from which geological information can be extracted, the classified maps were overlain with the geological map with the aim of trying to understand which classes coincide with the geological map and to qualitatively assess the classification outcome. It was observed that with only four classes, the classified map correlates with certain units in the geological map. Increasing the number of classes from four to six and then eight, it was observed that there is still sensible correlation with the overlaid geological map only that the lithological units are just being split into sub units. Increasing further the classes to twelve the results did not make sense as there was not much correlation with the geological units on the geological map. Sensible correlation with the geological map is seen using four classes because classes in this image are more separable than in the other classified maps and have not been split into sub classes. The image with four classes was used in the interpretation (figure 6-3).

In order to obtain the radiometric statistics of the classes the classified map with four classes was exported to oasis montaj software as geotiff. Point values were extracted for each class on the classified image with all the four layers of Potassium, Thorium, Uranium and Total count grids as background images. After obtaining the statistics for each class, they were exported to SPSS software and box plots for each radioelement per class were plotted (figure6-4).

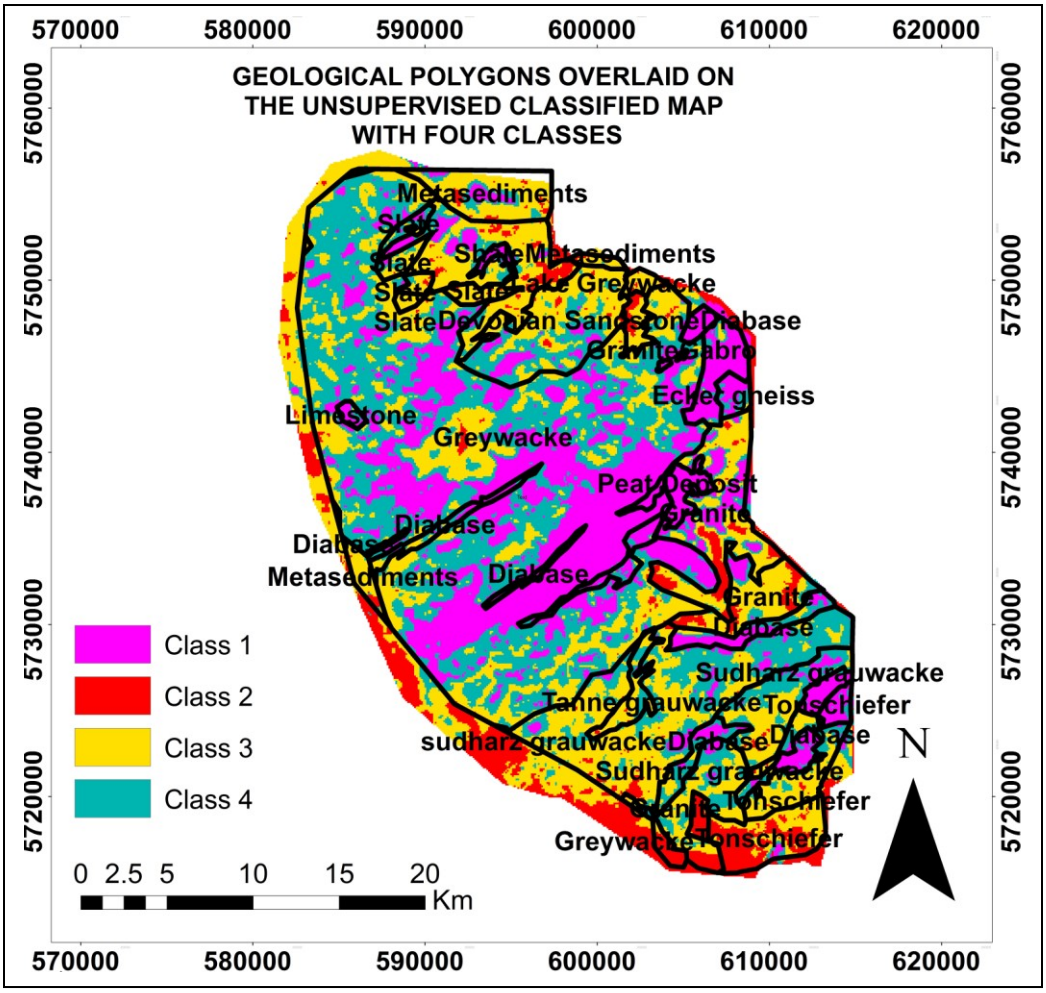

Figure 6-3 geological polygons overlain on the unsupervised classified maps with with four classes..

6.3. Interpretation of the unsupervised classification results (with four classes)

Doing unsupervised classification on the legacy gamma ray data we get a group of pixels that have been classified as class 1 (figure 6-3). These pixels have the lowest radiometric count, (figure6-4). These pixels coincide with the mafic rocks Gabbro and Diabase, Limestone, and the water logged marsh areas on the geological map. The mafic rocks and Limestone are rock units that have the same gamma ray spectral signature and they form one class. This shows that unsupervised classification based on the legacy gamma ray data can map low radioelement rocks but it is not able to differentiate Limestone, the mafic rocks, the water logged areas and the lakes.

Similarly a group of pixels that have been classified as class 2 and 3 are observed in the data (figure 6-3). These pixels have high radiometric content with the class 2 pixels being the highest and followed by the class 3 pixels (figure6-4). These pixels coincide with Granite, Shale and Devonian sandstone on the geological map. These are rock units that have high Th and K contents. This shows that unsupervised classification on the legacy gamma ray data can map high Th and K radioelement rocks but is not able to differentiate between Granite, Shale and Devonian sandstone. Granite can be differentiated from Shale and Devonian sandstone based on uranium because Granite has high uranium content while Shale and Devonian sandstone have low uranium content. In addition it is also observed that there is a group of high radioelement content pixels at the middle that have been classified into the same class. Comparing these pixels with Landsat image (annex 3) they coincide with a town of Claustal. The town is registering high radio element content but this is not related to lithology. This is because building materials do also radiate. This shows that unsupervised classification based on the legacy data can map gamma-ray responses that are not related to bedrock geology.

The other group of pixels observed in the classified map is group of pixels which form class 4. These pixels have medium radioelement signatures (figure6-4). These pixels coincide with the Greywacke and Eckergneiss units on the geological map. These are rocks that contain medium radio element content. This shows that unsupervised classification based on the legacy gamma ray data can map medium radioelement rocks but cannot differentiate Greywacke and Eckergneiss.

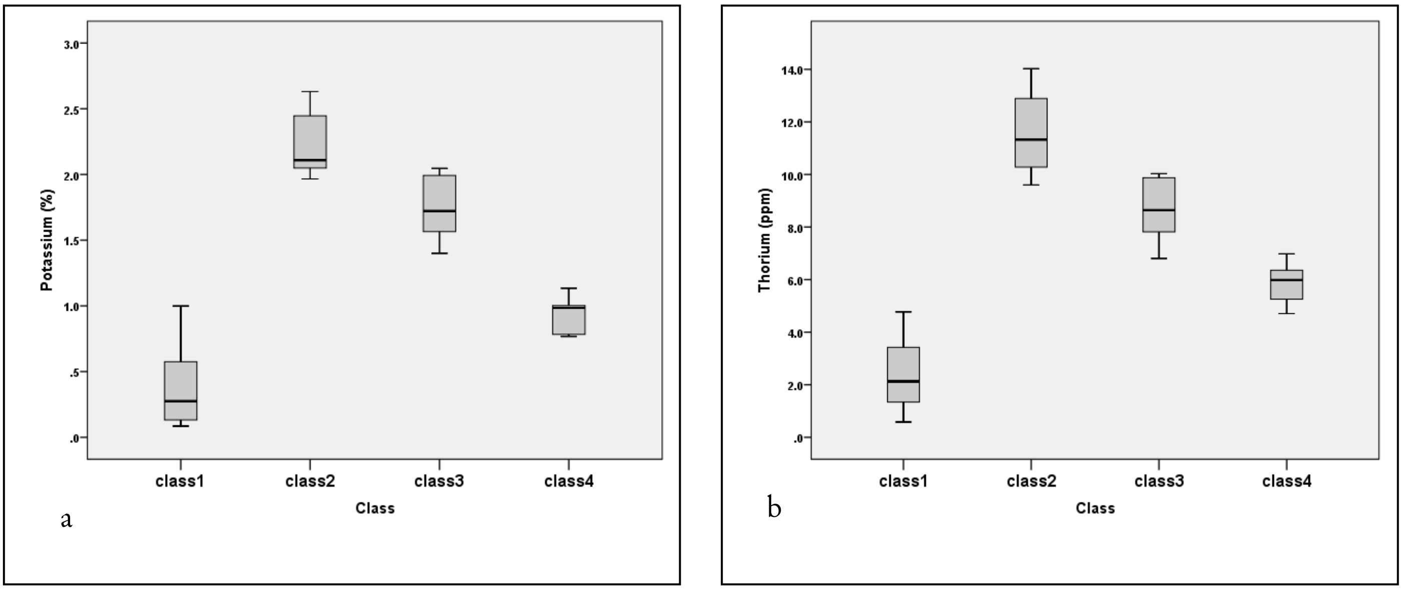

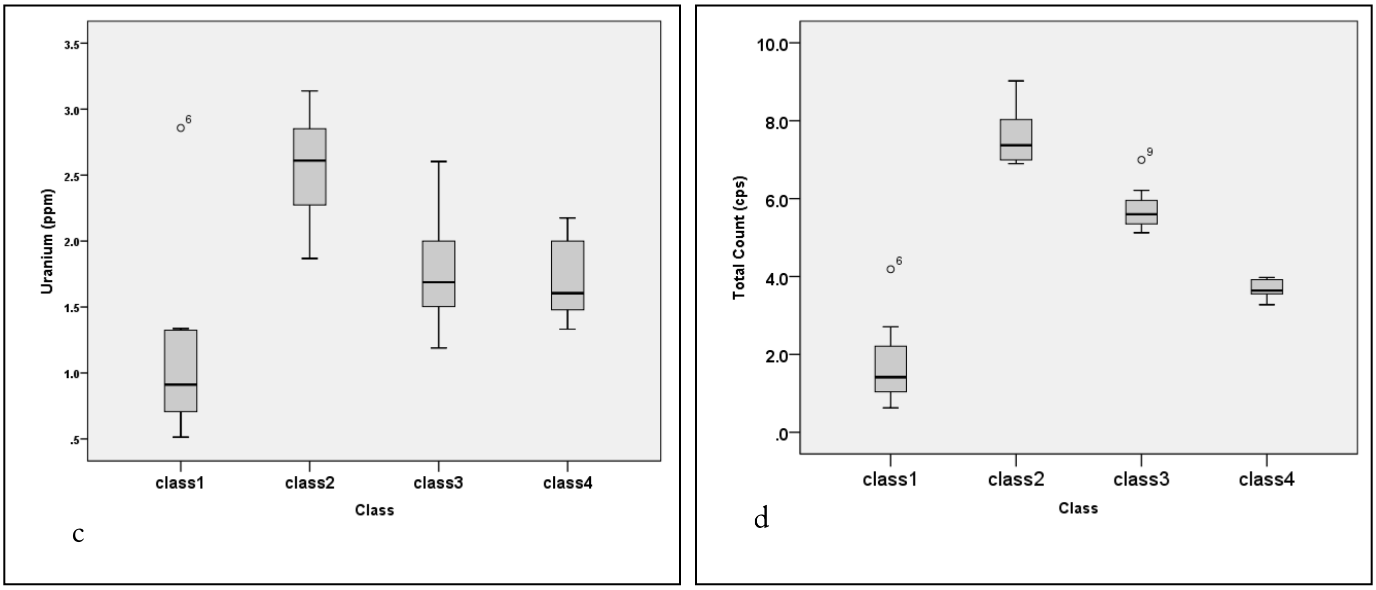

Figure 6-4 box plots showing radioelement content per class (a) Potassium, (b) Thorium, (c) Uranium, (d) Total count

6.4. Area cross tabulation between geological map and the unsupervised classified map with four classes

In order to see the spatial correlation of the geological map and the classified map cross tabulation between the geological map and the unsupervised classified map with four classes was performed. The cross operation performed an overlay of the geological map and the unsupervised classified map by comparing pixels at the same position in both maps. The geological map was rasterised and exported to Ilwis software and also the unsupervised classified map was exported to Ilwis. The two maps were georeferenced to the same georeference using georeference corners in Ilwis. This was done because for maps to be crossed need to have same georeference. Table 2 below shows the output of the cross tabulation between geological map and the unsupervised classified map with four classes, the area units are in m^2.

	GEOLOGICAL MAP LITHOLOGY	UNSUPERVISED CLASSIFIED MAP	Npix	Area
Diabase * Class1	Diabase	Class1	914	15446600
Diabase * Class2	Diabase	Class2	10	169000
Diabase * Class3	Diabase	Class3	251	4241900
Diabase * Class4	Diabase	Class4	495	8365500
Granite * Class1	Granite	Class1	934	15784600
Granite * Class2	Granite	Class2	762	12877800
Granite * Class3	Granite	Class3	1830	30927000
Granite * Class4	Granite	Class4	500	8450000
Shale * Class1	Shale	Class1	382	6455800
Shale * Class2	Shale	Class2	249	4208100
Shale * Class3	Shale	Class3	1410	23829000
Shale * Class4	Shale	Class4	354	5982600
Devonian sandstone * Class1	Devonian sandstone	Class1	224	3785600
Devonian sandstone * Class2	Devonian sandstone	Class2	58	980200
Devonian sandstone * Class3	Devonian sandstone	Class3	1114	18826600
Devonian sandstone * Class4	Devonian sandstone	Class4	824	13925600
Gabbro * Class1	Gabbro	Class1	591	9987900
Gabbro * Class3	Gabbro	Class3	24	405600
Gabbro * Class4	Gabbro	Class4	80	1352000
Ecker gneiss * Class1	Ecker gneiss	Class1	138	2332200
Ecker gneiss * Class2	Ecker gneiss	Class2	2	33800
Ecker gneiss * Class3	Ecker gneiss	Class3	11	185900
Ecker gneiss * Class4	Ecker gneiss	Class4	83	1402700
Greywacke * Class1	Greywacke	Class1	9035	152691500
Greywacke * Class2	Greywacke	Class2	300	5070000
Greywacke * Class3	Greywacke	Class3	5645	95400500
Greywacke * Class4	Greywacke	Class4	11287	190750300
Limestone * Class1	Limestone	Class1	63	1064700
Limestone * Class3	Limestone	Class3	5	84500
Limestone * Class4	Limestone	Class4	22	371800

Table 3 cross tabulation between the geological map and the unsupervised classified map with four classes

The relationship between the geological map units and the unsupervised classified map units are apparent on the cross tabulation. From the table 1 it is observed that Diabase of the geological map and Class 1 of the unsupervised classified map are spatially associated and coincide with 914 pixels in common. This shows that Class 1 corresponds best with Diabase and it means for a large part class 1 represents Diabase. Similarly Gabbro is associated and coincides with class 1 with 591 pixels. This means that class 1 represents Gabbro. Likewise it can be observed that Limestone from geological map is associated with Class 1 with 63 pixels in common. This means that also class 1 is representing Limestone. These results confirm the results obtained from the unsupervised classified image in which Limestone, Gabbro and Diabase have low radioelement signatures and were all classified into same class 1. This shows that unsupervised classification based on the legacy gamma ray data can map these low radioelement rocks but it cannot differentiate them.

Strong association can also be observed on high radioelement content rocks. Granite on the geological map coincides with Class 3 on the unsupervised classified map with a total of 1830 pixels. This means that for a large part class 3 represents Granite. Similarly Shale coincides with class 3 on the unsupervised classified map with 1410 pixels and also Devonian sandstone coincides with class 3 unsupervised classified map with 1114 pixels. This means that class 3 is also represented by Shale and also Devonian Sandstone. These results confirms the one obtained from the classified image in which Granite, Shale and Devonian sandstone were all classified into one class 3. This shows that unsupervised classification on the legacy airborne gamma ray data can map these high radioelement content rocks but it cannot differentiate them.
Greywacke on the geological map show strong correlation and is coinciding with class 4 on the unsupervised classified map with a total of 11287 pixels. This means that for a large part of class 4 represents Greywacke. The Greywacke has medium radioelement content and this show that unsupervised classification on the legacy airborne gamma ray data is able to map medium

radioelement content rocks. However Greywacke is also associated with class 1 with 9035 pixels which indicates that it is being confused with class 1.

6.5. Validation

Based on the cross tabulation data, a confusion matrix was used to assess the accuracy of the unsupervised classified map with four classes as an addition to the qualitative assessment that was made by comparing the unsupervised classified map with the overlain geological polygons. The geological map was used as the reference data. The columns represent the reference data and the rows represent the classified map. In normal circumstances for easy comparison, the geological map and the classified map need to have the same legend. But in this case the legends are different, the classified map has only four classes and the geological map has eight lithological units. Because of this, the normal confusion matrix in which diagonal elements represents areas that are in agreement with the reference data was not possible. To solve this problem, areas that had a lot of pixels in the cross table (table 3 above) were considered to be the class that make up that particular lithological unit on the geological map. For example Diabase has a lot of pixels in class 1 so class 1 is considered that one lithological unit in it is Diabase. Similarly Gabbro has many pixels in class 1 and it was considered that class1 also contains Gabbro as another lithological unit in this class and so on. Greywacke has many pixels in class 4 so class 4 contains Greywacke as lithological unit.
To calculate the overall accuracy, the highlighted pixels were added and divided by the total number of pixels and this shows an overall accuracy of 46.1%.

	Devonia	Diabase	Ecker g	Gabbro	Granite	Greywa	Limestone	Shale	TOTAL	Error of commission%	User Acuracy %
Class1	224	914	138	591	934	9035	63	382	12281	87.23	12.77
Class2	58	10	2	0	762	300	0	249	1381	44.82	55.18
Class3	1114	251	11	24	1830	5645	5	1410	10290	57.69	42.31
Class4	824	495	83	80	500	11287	22	354	13645	16.67	83.33
Total	**2220**	**1670**	**234**	**695**	**4026**	**26267**	**90**	**2395**	**37597**		
Error of Ommission %	49.82	**45.27**	**64.53**	**14.96**	**54.55**	57.03	**30.00**	**41.13**			
Producer Accuracy %	**50.18**	**54.73**	**35.47**	**85.04**	**45.45**	42.97	**70.00**	**58.87**			
Overall accuracy %			**46.1**								

Table 4 Confusion matrix between geological map and the unsupervised classified map with four classes. The reference data pixels (geological map) are listed in columns and the classification results are listed in rows. The highlighted pixels represent the pixels that are in agreement with the geological map.

The matrix shows that class 1 is confused with Diabase, Gabbro and Limestone as most pixels of these lithological units were classified into this class. This is so because these lithological units have same gamma ray spectral signatures. Similarly class 3 is mostly confused with Devonian sandstone, Granite and Shale because most pixels of these lithological units were classified into this class. These units have all high potassium and thorium content and this explains for the confusion. Overall accuracy is low 46.1% because there is a lot of variability and overlap within the classes which is confusing the classification.

6.6. Conclusion

From this analysis it has been observed that performing isodata unsupervised classification on the legacy airborne gamma ray data, it can map low radioelement rocks such as Limestone, Gabbro and Diabase but cannot differentiate these lithological units. It can also map medium radioelement rocks such as Greywacke and Eckergneiss and again has the limitation that it cannot differentiate these lithologies. Furthermore the classification is able to map high radioelement rocks such as Granite, Shale and Devonian sandstone but cannot differentiate these lithological units because they have similar gamma ray spectral signatures. It has also been found out that it is able to map out marsh areas and the lakes. These also have low radioelement content and the classification could not differentiate these water logged areas, lakes from the low radioelement rocks like Limestone, Gabbro and Diabase. The southern part of the classified map does not correlate very well with the overlain geological map while the rest of the map apart from the southern part does correlate. This is because there is a lot of variability and overlap within the classes which is confusing the classification. These results are similar to the results of Schetselaar et al., (2007) in which they used unsupervised classification on gamma ray data K, Th and U channels in the Melville Penisula, Nanavut and they found that there were places that distinct radioelement domains correlated with mapped units and also there were areas that differ appreciably from the geological map.

6.7. Supervised classification

In addition to the unsupervised classification discussed above, supervised classification was also used to further understand the information content of this legacy airborne data. Supervised classification is done by an operator who defines spectral characteristics of the classes by identifying training areas. It requires that the operator is familiar with the area of interest, needs to know where to find the classes of interest in the scene (Richards, 2013). In this research this information was derived from general knowledge of the scene and field observations. The same layer stacked image that was used in the unsupervised classification was also used in the supervised classification.

6.7.1. Training of samples

The selection of training sites was based on the geological map and the lithological code was based on the name of the unit on the map. The number of pixels that were used for training ranged from 14-25 and areas that were homogeneous were selected for sampling. A total of 8 training areas were used. Refer to annex 3 for areas where training samples were taken.

6.7.2. Seperability analysis

Seperability is a statistical measure of distance between two classes. This distance is used to determine how distinct the classes are from each other. Assessment of the statistical separation of each class was done to determine whether classification would be feasible. In order to get radioelement statistics per lithological unit the geological polygons were overlain on the input grids and point value extraction tool was used to extract radioelement contents for each lithology. To assess the statistical seperability of the different lithological unit classes, box and whisker plots were used. Granite, Shale, and Devonian sandstone are not separable. Similarly Diabase, Gabbro and Limestone are overlapping and this show that they are not well separable. The statistical separation indicates that reasonable results can still be expected from supervised classification even though the seperability is not very good (figure 6-5).

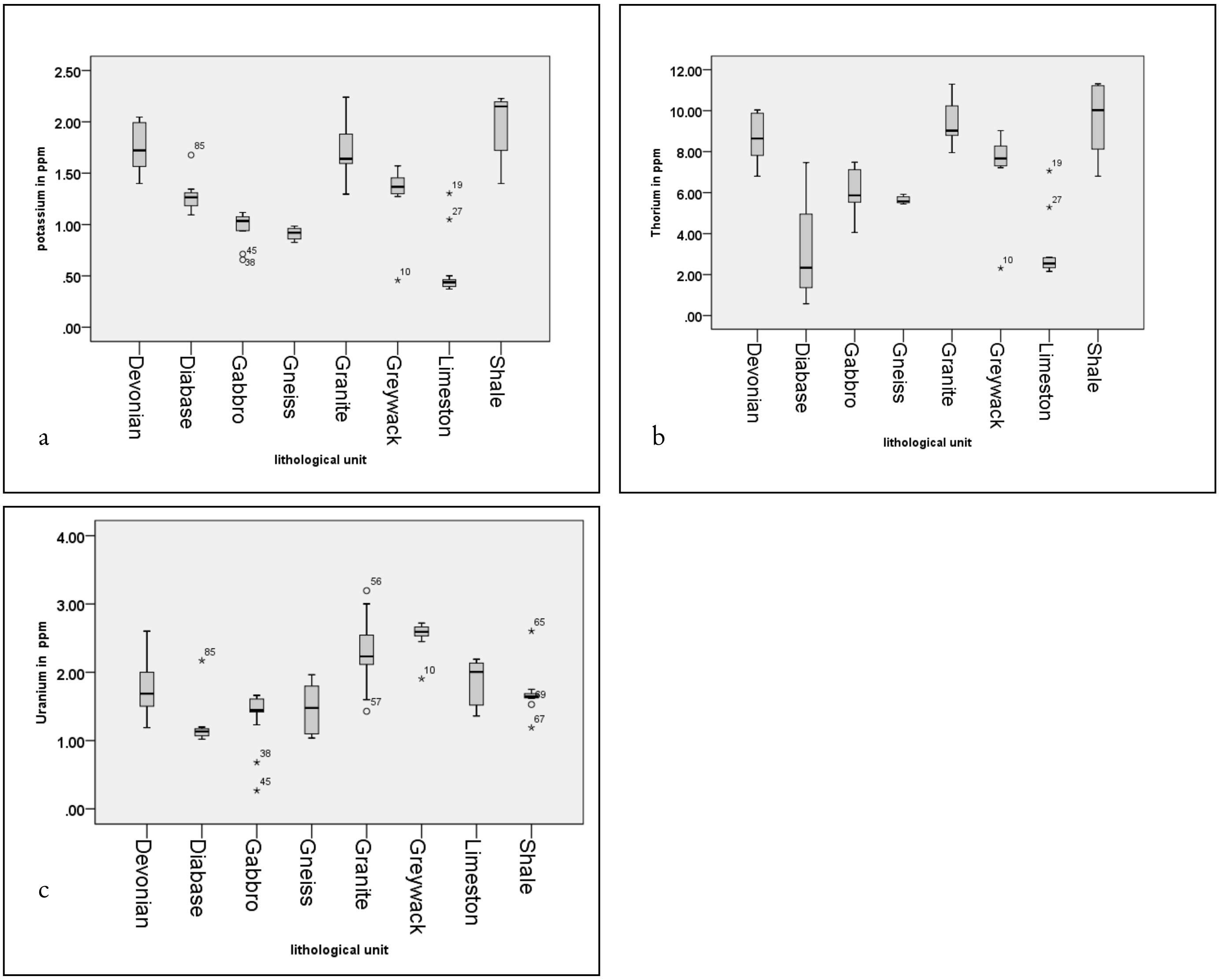

Figure 6-5 Showing seperability analysis results by lithological class (a) Potassium, (b) Thorium, (c) Uranium

6.7.3. Clustering

The image was classified using maximum likelihood algorithm in Erdas Imagine software. This algorithm was chosen because research has shown that it gives more accurate results (Schetselaar, 2000). The way this algorithm works is that it calculates statistical distance based on the mean values of the clusters. This statistical distance is a probability value and a cell is assigned to the class to which it has the highest probability (Schetselaar, 2000).

6.8. Results of supervised classification

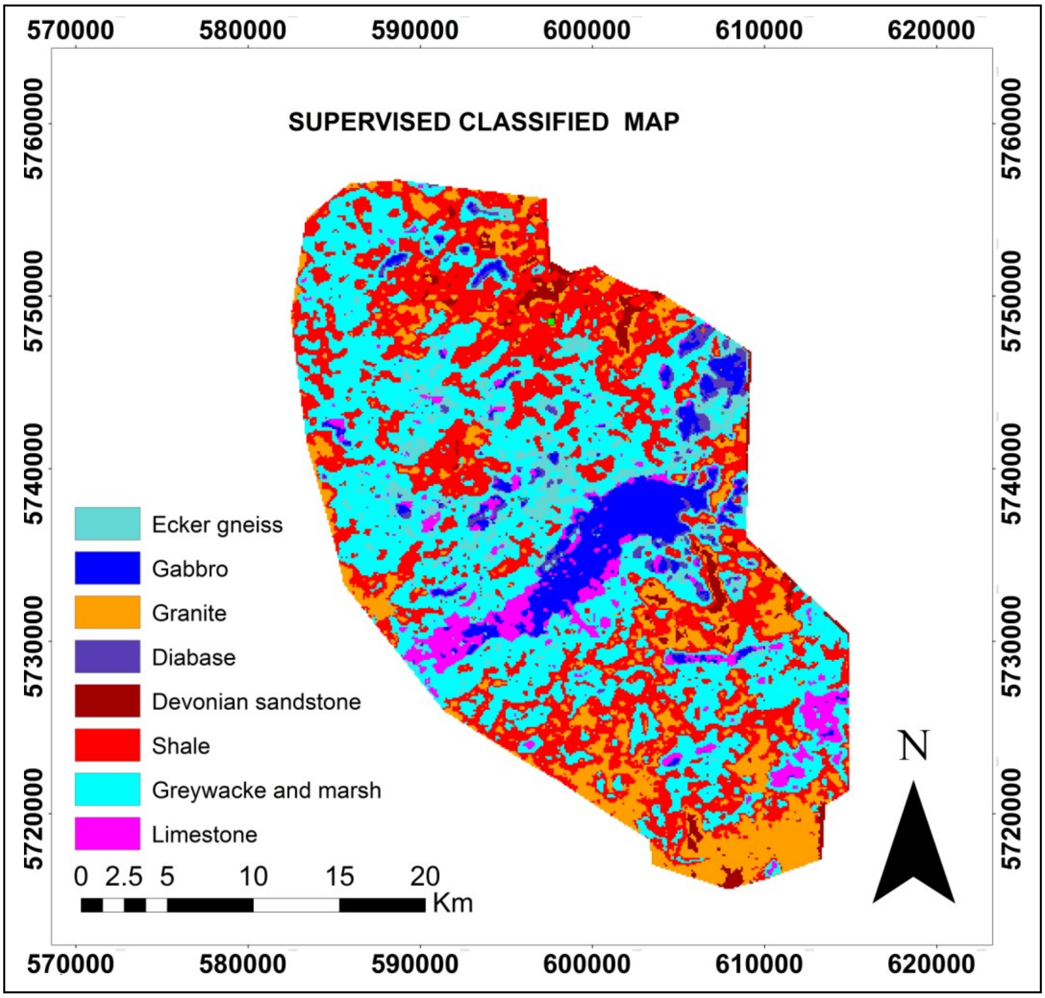

Figure 6-6 showing results of supervised classification based on legacy gamma ray data only

The classified map was overlain with the geological map with the aim of trying to understand which classes coincide with the geological map as shown in the figure 6-7. In order to get radioelement statistics per lithological unit the geological polygons were overlain on the input grids and point value extraction tool was used to extract radioelement contents for each lithology according to the geological polygons. Box plots were plotted indicating the content of radioelement per lithological unit (figure 6-8).

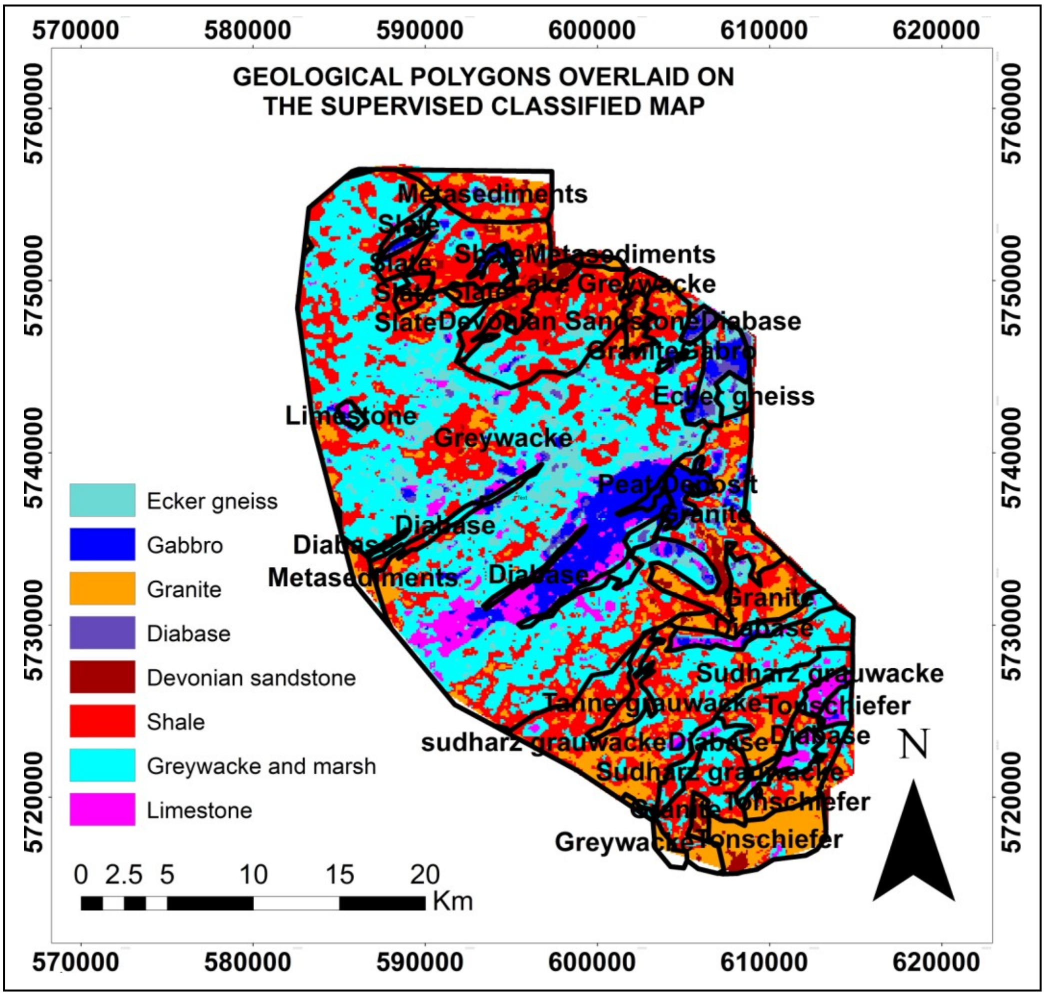

Figure 6-7 geological polygons overlain on the supervised classified map

6.9. Interpretation of supervised classification results

In the supervised classification, there are pixels that have been classified as Granite, Shale and Devonian sandstone (figure 6-7). These pixels have high radiometric content (figure 6-8). On the eastern side of the map they coincide with Granite on the overlaid geological map and in the north they coincide with Shale and Devonian sandstone. These are rock units that have same gamma ray spectral signature and the algorithm could not differentiate them. This shows that supervised classification based on the legacy airborne gamma ray data can map high radioelement rocks but it is not able to differentiate Granite, Shale and Devonian sandstone since all have high K and Th content.

Similarly there are pixels that have been classified as Limestone, Gabbro and Diabase in the supervised classified map. These pixels have low radioelement content (figure 6-8). On the north western side of the map, they coincide with Limestone lithological unit on the overlaid geological map and on the eastern they coincide with Gabbro and Diabase on the overlaid geological map (figure 6-7). These are rock units that have on average low gamma ray spectral signature (figure 6-8). The marsh area at the middle (blue band running SW-NE at the middle of the classified map in figure 6-7) are being confused with Limestone and the mafic rocks, Gabbro and Diabase because these water areas also have low radioelement signatures. This shows that supervised classification on the legacy airborne gamma ray data is able to map low radioelement content rocks but cannot differentiate Limestone, Gabbro and Diabase. It also shows that it can map the water logged areas and the lakes but it cannot differentiate them from the mafic rocks and Limestone.

Also there are pixels that have been classified as Greywacke and Eckergneiss. The pixels of these rocks have medium gamma ray spectral signature. The classified Greywacke and Eckergneiss pixels coincide with Greywacke unit on the overlaid geological map and also on the east coincide with Eckergneiss lithological unit on the overlain geological map. These are lithological units that have medium radioelement content. This shows that supervised classification based on the legacy airborne gamma ray data is able to map lithological units with medium radioelement content but cannot differentiate Greywacke and Eckergneiss lithologies.

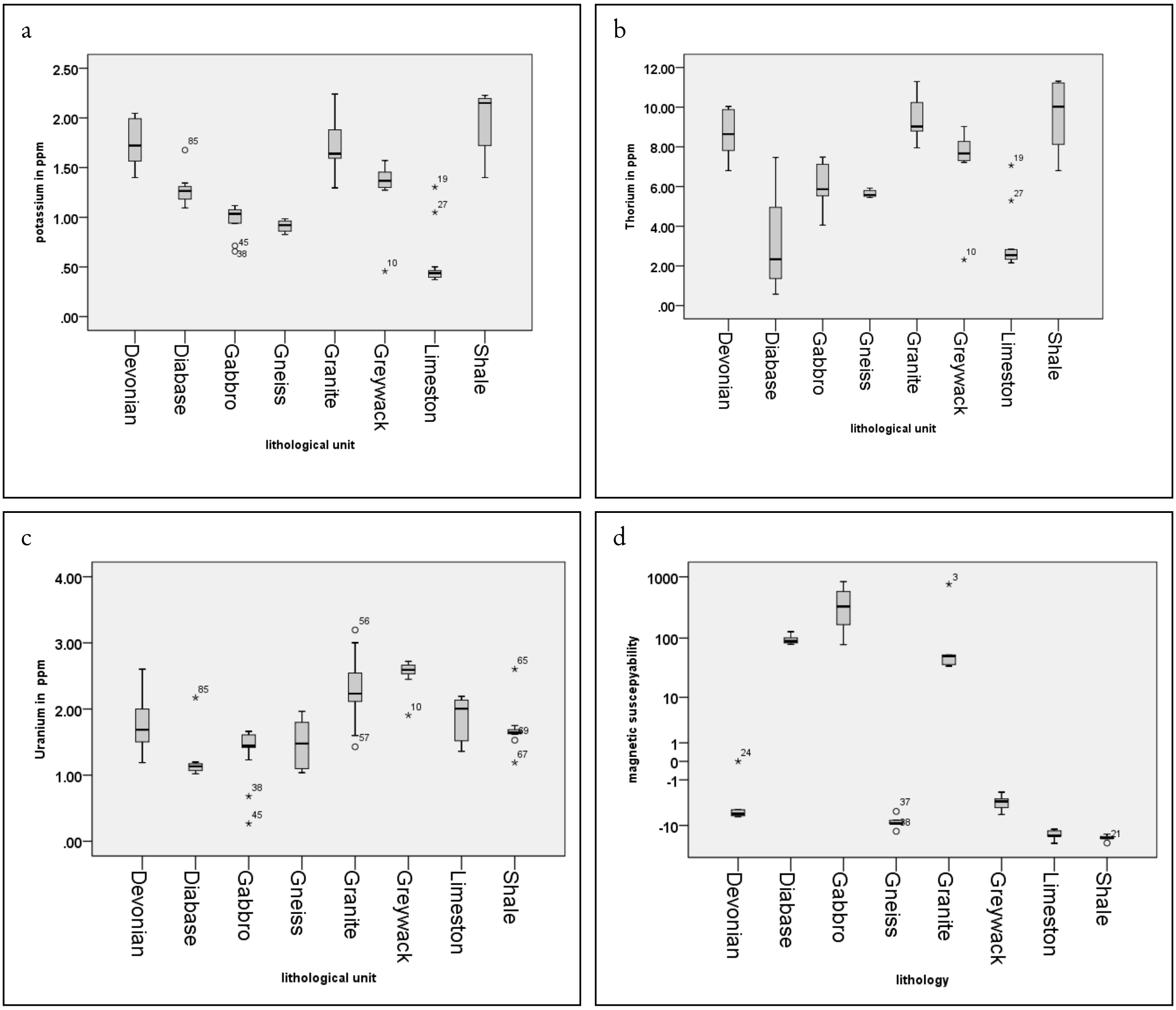

Figure 6-8 radioelement content for the lithological units (a) Potassium, (b) Thorium, (c) Uranium (d) Magnetic susceptibility

6.10. Accuracy Assessment

An error matrix was calculated to assess the quality of the supervised classification results. It shows the relationship between the known reference data and the corresponding cluster/classes of the clustering results. An existing lithological map (figure 4-1) was used as the reference data for this research. From the error matrix the overall accuracy was calculated to assess the classification outcome. Overall accuracy is a ratio of total number of correctly classified pixel to the total pixel number. As was done in section 6.4 and 6.5, area cross tabulation of the geological map and the supervised classified map was performed in order to come up with the error matrix shown in table 5 below.

	Devonian sandstone	Diabase	Eckergneiss	Gabbro	Granite	Greywacke	Limeston	Shale	**Total**	**Error of ommission%**	**ucer Acuracy %**
Devonian sandstone	53	7	176	13	128	576	13	1254	2220	97.61	2.39
Diabase	2	123	62	115	64	665	360	279	1670	92.63	7.37
Ecker gneiss	1	18	109	5	2	86	0	13	234	53.42	46.58
Gabbro	0	170	165	240	2	77	6	35	695	65.47	34.53
Granite	409	159	241	415	996	444	52	1310	4026	75.26	24.74
Greywacke	76	356	2177	2066	1155	12252	1540	6458	26080	53.02	46.98
Limestone	0	0	6	15	0	41	23	5	90	74.44	25.56
Shale	249	77	63	96	266	373	14	1257	2395	47.52	52.48
Total	**790**	**910**	**2999**	**2965**	**2613**	**14514**	**2008**	**10611**	**37410**		
Error of commission %	93.29	86.48	96.37	91.91	61.88	15.58	98.85	88.15			
user Accuracy %	6.71	13.52	3.63	8.09	38.12	84.42	1.15	11.85			
Overall Acuracy %					**40.24**						

Table 5 *Confusion matrix between the geological map and the supervised classified map obtained by cross tabulation. The elements on the diagonal marked in grey represents areas of agreement between the classified map and the geological map. The off diagonal elements represent or show where the maps are in conflict. The columns represent classes of the classified map and the rows represents ground truth geological map pixels. The matrix show an overall accuracy of 40%*

From the matrix in table 5, it can be observed that Devonian sandstone is mainly confused with Granite and Shale. This is because these lithological units have the same gamma ray spectral signatures. Diabase is confused with Gabbro and Greywacke. The marsh area on the reference geological map is part of the Greywacke unit and most pixels of Diabase were falling on this part. This marsh area has low radioelement gamma ray signature and Diabase has also low gamma ray spectral signature. This is the reason why Diabase is confusing with Gabbro and Greywacke. Similarly Eckergneiss is mostly being confused with Greywacke as most pixels of Eckergneiss were classified as Greywacke. This happened because Greywacke has almost similar gamma ray radiometric content as Eckergneiss. Limestone is being confused with Diabase and Greywacke especially at the marsh region because they both have a low radioelement gamma ray spectral signature which is the same as Limestone. Overall accuracy is low 40% because there is a lot of variability and overlap within the classes which is confusing the classification.

6.11. Classification based on gamma ray data and magnetic data

In order to get more detail regarding the information content the legacy airborne data can provide, another classification was done using gamma ray data and magnetic data. The gamma ray channels K, Th, U and Apparent Magnetic Susceptibility were used. The Total Magnetic Intensity grid was converted to Apparent Magnetic Susceptibility. The same training areas as shown in annex 3 were used. The figure below show the result of classification using maximum likelihood.

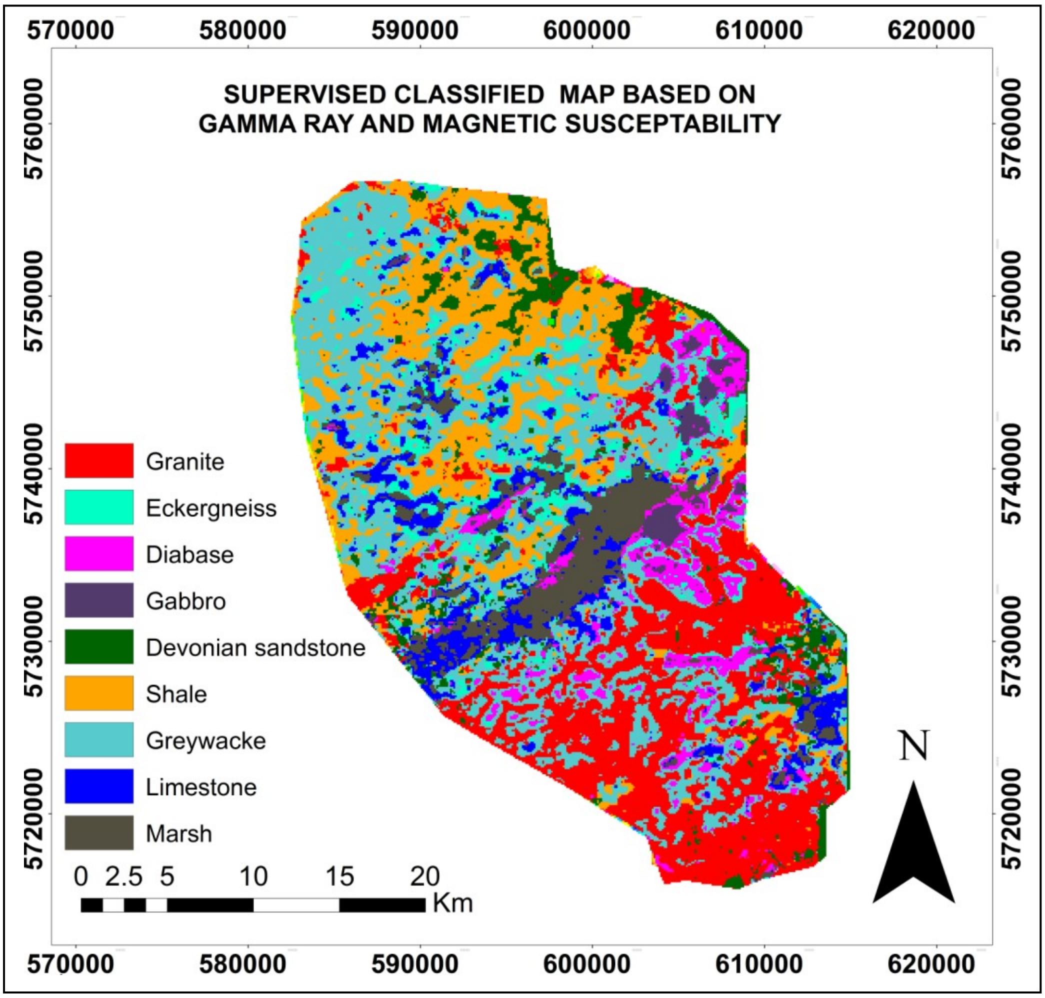

Figure 6-9 results of supervised classification using gamma ray data and magnetic susceptibility

6.12. Interpretation

The classified map was overlain with the geological map with the aim of trying to understand which classes coincides with the geological map as shown in the figure 6-10. In order to get radioelement statistics per lithological unit the geological polygons were overlain on the input grids and point value extraction tool was used to extract radioelement contents for each lithology according to the geological polygons. Box plots were plotted indicating the content of radioelement per lithological unit (figure 6-8)

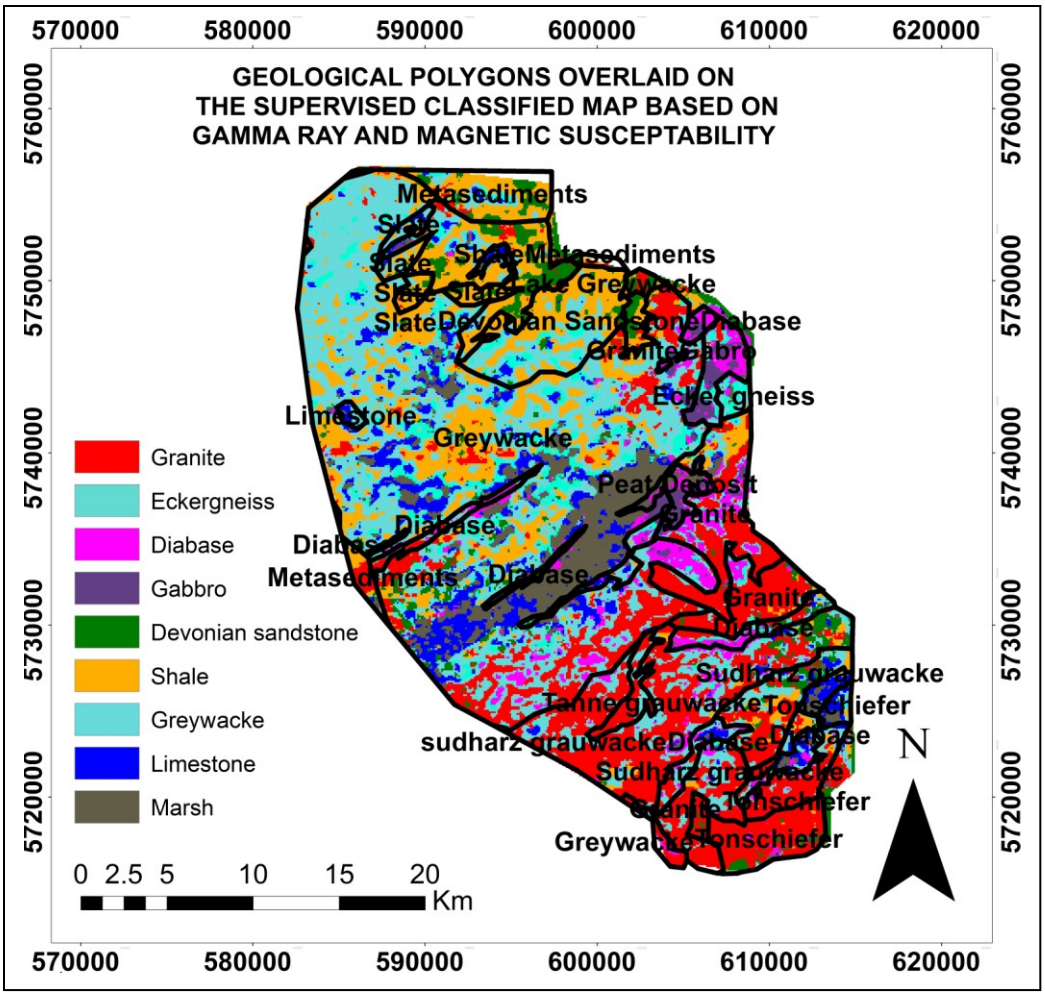

Figure 6-10 geological polygons overlain on the supervised classified map using gamma ray and magnetic susceptibility

There are group of pixels that have been classified as Diabase and Gabbro on the supervised classified map. The pixels of these units have high magnetic susceptibility and low radiometric content (figure 6-8). These pixels coincide with Diabase and Gabbro on the overlaid geological units. This shows that supervised classification based on legacy airborne gamma ray and magnetic susceptibility data can map high magnetic susceptibility and low gamma ray spectral signature rocks but cannot differentiate Gabbro and Diabase.

Limestone can also be identified in the supervised classified map. Classified Limestone pixels coincide with the Limestone lithological unit on the overlaid geological map. Limestone has low gamma ray spectral signature and also low magnetic susceptibility (figure 6-8). Limestone has been separated from the mafic rocks because it has low magnetic susceptibility. This shows that supervised classification on the legacy airborne gamma ray and magnetic data can map low radioelement and low magnetic susceptibility rocks like Limestone. Again it shows that using both magnetic susceptibility and gamma ray channels it is possible to separate Limestone from the mafic rocks which was not possible when only gamma ray data was used.

There are also pixels that have been classified as Granite on the supervised classified map. Classified Granite pixels coincide with Granite from the overlaid geological polygons. This lithological unit has high gamma ray radioelement content and also high magnetic susceptibility (figure 6-8). Granite has been separated from Shale and Devonian sandstone because it has high radioelement content and also high magnetic susceptibility. This shows that supervised classification on the legacy airborne gamma ray and magnetic data can map high gamma ray spectral signature and high magnetic susceptibility rocks such as Granite. Using both gamma ray and magnetic susceptibility Granite can be separated from Shale and Devonian sandstone which was not possible when only gamma ray data was used.

Group of pixels that have been classified as Greywacke and Eckergneiss can be identified on the classified map. These pixels coincide with Greywacke unit and Eckergneiss on the overlaid geological map. These are lithological unit that have medium radioelement content and low magnetic susceptibility (figure6-8). This show that supervised classification based on the legacy airborne gamma ray and magnetic data is able to map lithological units with medium radioelement content and low magnetic susceptibility such as Greywacke and Eckergneiss but it cannot differentiate these lithologies.

Group of pixels that have been classified as Shale and Devonian sandstone can also be observed in the classified map. The classified Shale and Devonian sandstone pixels coincide with Shale and Devonian sandstone on the overlaid geological map. These are lithological units that have high potassium and thorium content and low magnetic susceptibility (figure 6-8). This shows that supervised classification on the legacy airborne gamma ray and magnetic data can map lithological units with high Th and K content and low magnetic susceptibility like Shale and Devonian sandstone but cannot separate them.

Pixels for the marsh area can also be observed in the classified map. This area has low magnetic susceptibility and low gamma ray spectral signature just like Limestone. This area is being confused with Limestone since they all have same low magnetic susceptibility and gamma ray spectral signatures.

6.13. Accuracy assessment

Error matrix was calculated to assess the quality of the classification results. This was done by cross tabulating the classified map and the geological map which was used as the reference. Table 6 shows overall accuracy of 42 %. Overall accuracy is low 42% because there is a lot of variability and overlap within the classes which is confusing the classification.

	Devonian sandst	Diabase	Ecker gneiss	Gabbro	Granite	Greywacke	Limesto	Shale	TOTAL!	Error of ommission%	Producer Acuracy %
Devonian sandstone	136	59	3	0	190	633	0	525	1546	91.2	8.8
Diabase	0	358	24	231	519	991	1	9	2133	83.2	16.8
Eckergneiss	195	40	93	97	123	1708	11	61	2328	96.0	4.0
Gabbro	0	57	2	263	206	265	0	13	806	67.4	32.6
Granite	13	322	0	32	2122	2911	0	89	5489	61.3	38.7
Greywacke	711	381	85	60	377	10056	28	396	12094	16.9	83.1
Limestone	55	241	0	2	25	2482	42	142	2989	98.6	1.4
Shale	1109	62	8	1	320	3917	4	1111	6532	83.0	17.0
Total	**2219**	**1520**	**215**	**686**	**3882**	**22963**	**86**	**2346**	**33917**		
Error of commission %	93.87	76.45	56.74	61.66	45.34	56.21	51.16	52.64			
User Accuracy %	6.13	23.55	43.26	38.34	54.66	43.79	48.84	47.36			
Overall acuracy %				**41.81**							

Table 6 Confusion matrix between the geological map and the supervised classified map using both gamma ray and magnetic data obtained by cross tabulation. The elements on the diagonal marked in grey represents areas of agreement between the classified map and the geological map. The off diagonal elements represent or show where the maps are in conflict. The columns represent classes of the classified

map and the rows represents ground truth geological map pixels. The matrix show an overall accuracy of 42%

From the matrix it can be observed that Devonian sandstone is mainly confused with Shale. This is because these lithological units have the same gamma ray spectral signatures and magnetic susceptibility. Diabase is confused with Gabbro, Granite and Greywacke. The marsh area on the reference geological map is part of the Greywacke unit and some pixels of Diabase were also falling on this part. This marsh area has low radioelement gamma ray signature and Diabase has also low gamma ray spectral signature. It is confused with Gabbro and Granite because all have high magnetic susceptibilities. Similarly Eckergneiss is mostly being confused with Greywacke as most pixels of Eckergneiss were classified as Greywacke. This happened because Greywacke has almost similar gamma ray radiometric signature and magnetic susceptibility as Eckergneiss. Limestone is being confused with Greywacke especially of the marsh region. This is so because they have both low radioelement gamma ray spectral signatures and low magnetic susceptibility. The low accuracy is due to the overlap of classes causing the classification to be confused.

6.14. Conclusion

Performing maximum likelihood supervised classification on the legacy gamma ray data is able to map low radioelement rocks such as Limestone, Gabbro and Diabase but it cannot differentiate these lithological units. It can also map medium radioelement rocks such as Greywacke and Eckergneiss and again has the limitation that it cannot differentiate these lithological units. Furthermore the classification is able to map high radioelement rocks such as Granite, Shale and Devonian sandstone but cannot differentiate these lithological units because they have similar gamma ray spectral signatures. It was also found out that it is able to map out marsh areas and the lakes. These also have low radioelement content and the classification could not differentiate these water logged areas, lakes and the low radioelement rocks like Limestone, Gabbro and Diabase.

Performing maximum likelihood supervised classification based on both legacy airborne gamma ray and magnetic data has shown that it can map high magnetic susceptibility and low radioelement content rocks like Gabbro and Diabase but it cannot differentiate these lithological units. Furthermore it can map low radioelement and low magnetic susceptibility rocks such as Limestone. Again it showed that using both magnetic susceptibility and gamma ray data it is possible to separate Limestone from the mafic rocks which was not possible when only gamma ray data was used. In addition to this, the classification can map high gamma ray spectral signature and high magnetic susceptibility rocks like Granite. Using both gamma ray and magnetic susceptibility Granite can be separated from Shale and Devonian sandstone which was not possible when gamma ray data only was used. Also based the gamma ray and magnetic data the classification can map lithological units with medium radioelement content and low magnetic susceptibility but could not differentiate Greywacke and Eckergneiss. It can also map lithological units with high Th and K content and low magnetic susceptibility such as Shale and Devonian sandstone but cannot separate these units. Using both gamma ray and magnetic susceptibility, Shale and Devonian sandstone can be separated from Granite which was not possible with gamma ray data only.

The classified maps do not correspond very well with the overlaid geological map on the southern part, but on the other hand apart from this part the rest do corresponds. This is because of noise factor in the data. There is a lot of variability and overlap within the classes which is confusing the classification. Classification accuracy varied from 40% when only gamma ray data was used to 42% when both gamma ray and magnetic data were used. The low accuracy is due to a lot of variability within the classes which is confusing the classification. These results are similar to the results of

Schetselaar et al., (2007) in which they did supervised classification on gamma ray data using maximum likelihood over Melville Peninsula with the aim of determining whether geological units could be successfully mapped using gamma ray data in combination with magnetic data. Their results found out that there were areas that show good correspondence with the geological map and other areas that differed from the mapped geology and also observed that classification accuracy increased when both gamma ray and magnetic data were used in the classification. Similarly Harris et al., (2008) used gamma ray and magnetic data and did supervised classification using maximum likelihood to map different lithologies in Sekwi region of Canada with the aim of demonstrating the value of gamma ray data in conjunction with magnetic data . They found that best map was produced from using both gamma ray data and magnetic data than only using gamma ray data.

6.15. Visual Image Interpretation

In addition to the Supervised and unsupervised classification, visual analysis of the airborne data was done. In order to get insight of the data to see if different lithologies can be differentiated, statistical analysis was carried out to depict the concentration of each radioelement per lithological unit. To get values per lithological unit, a point value extraction tool in Oasis Montaj was used to extract values from each lithological unit. Mean values were calculated and the results were plotted as box plots. The mean values per lithological unit suggest that it is possible to discriminate lithological units based on their contrast radiometric and magnetic signatures (figure 6-11).

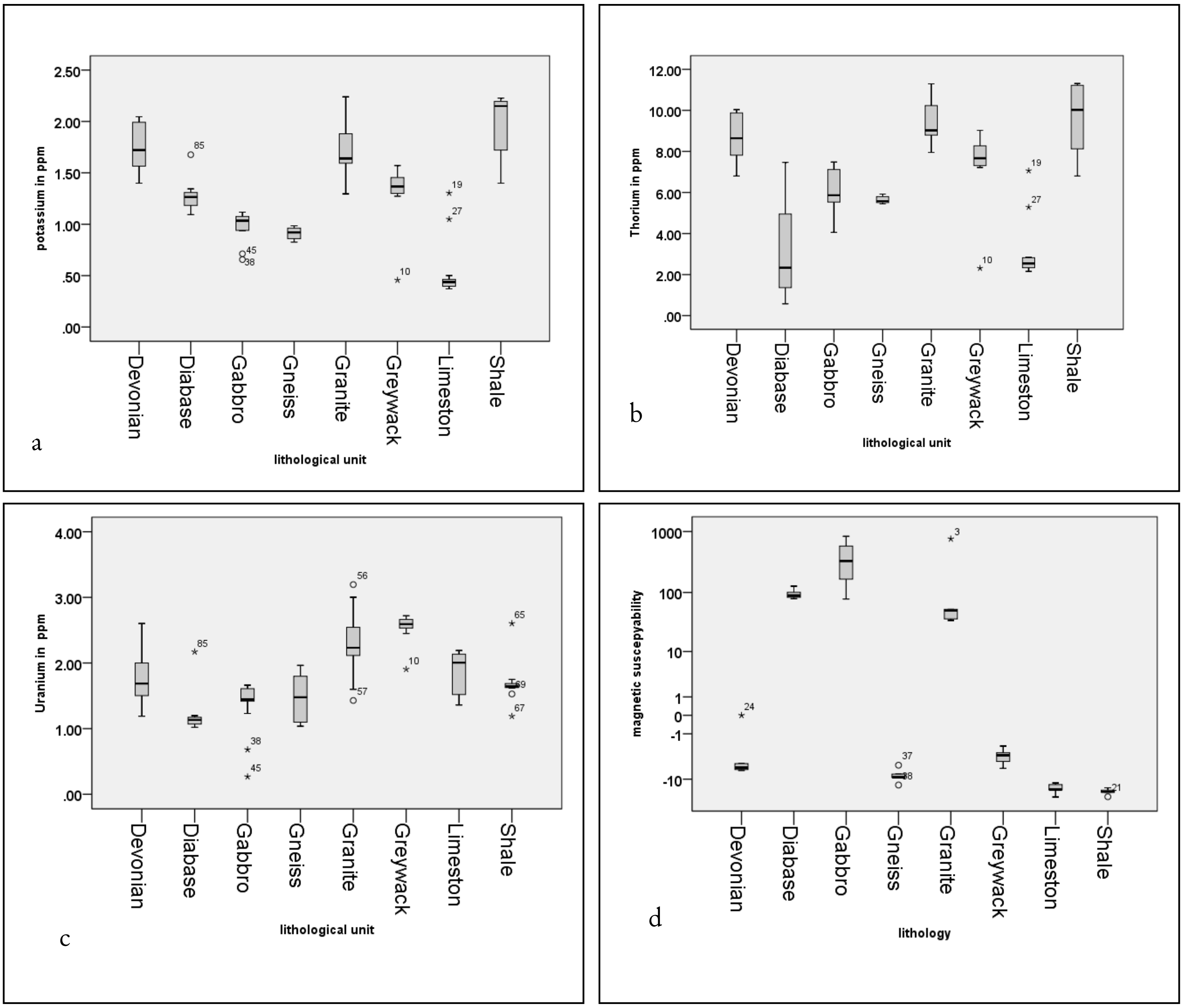

Figure 6-11 Box plots showing the distribution of radioelement per lithological unit

A number of enhancements were applied to the geophysical data in order to highlight to facilitate extraction of geological information from the data.

6.16. Gamma ray image enhancements

The gamma ray data was enhanced in various ways in order to increase interpretation for geological information extraction. The data was presented in pseudo colour single band images, ratio images and Ternary colour composite image. These provided good enhancements possibilities to discriminate different surface lithologies. The single band pseudo colour images show areas where a particular radioelement has relatively higher concentration which can be directly correlated with the geochemical properties of the surface lithology and regolith (Wilford, 1997). Ratio image of the individual radioelement (Th/K) helped in enhancing subtle features that were not apparent in the original images. The ternary colour composite image provided an overall pattern of radioelement distribution over the study area. The radiometric data were also integrated with the STRM DEM data to add topographic information. The ternary image was pan sharpened with the SRTM DEM in ARC GIS using pan sharpening tool. This resulted in a better enhanced image in comparison to the original ternary image.

6.17. Visual Interpretation on gamma ray data

Qualitative photo geological interpretations were applied in order to get geological information from the data. Lithological units were discriminated based on their tonal/ colour, texture, shape, size and association. Close inspection was made on the K image and revealed that there are distinct lithologies which can easily be discerned. Greywacke covering most of the central part of the study area is discriminated by its medium K concentration. Limestone lithological unit in the north western area of the Greywacke unit is discriminated by its very low K content. Similarly Gabbro and Diabase in the eastern part of the study area are discriminated by their low K content. Shale and Devonian sandstone in the north eastern part are discriminated by their high K content. Similarly Granite in the central eastern part of the study area is discriminated by its high K content (figure 6-12a). In addition, interesting radiometric distributions were obtained from the ratio images mainly Th/K. The Greywacke lithology covering the central part of the area (figure 6-12b) including the Limestone in the western part of Greywacke and Eckergneiss covering the eastern part can be discriminated by their relatively high Th/K ratio values. Shale in the north eastern part can be delineated due to its very low Th/K values. Gabbro and Diabase in the east and the central (linear feature) are discriminated by their low Th/K ratio values; similarly Granite in the east can be delineated by its medium Th/K ratio values (figure 6-12b).

Interpretations were also made on the ternary (figure6-12c) image. Ternary image discriminate best the different lithological units of the area. Shale covering the north east part is discriminated by its higher Th and K content displaying yellow colour on the image. Granite and Devonian sandstone are also discriminated from other lithologies by their elevated Th and K concentration also appearing yellow in the image. Greywacke covering the central part is clearly identified having black-greenish colour which indicates medium concentration of K, Th and U. The boundary of this unit is also clearly outlined in the K image. Gabbro covering the eastern part is delineated by its low levels of K, U and Th and on the ternary image is shown having dark colour which indicates low levels of these elements. Eckergneiss is discriminated from Gabbro by its medium level of Th and K concentration appearing green to bluish green in the image. Diabase which appears as dyke in the geological map is discriminated on the ternary image by elevated levels of K (appearing red) and elongated on the central part and in the eastern part close to Gabbro. The pan sharpened image (figure 6-12d) has confirmed most of the above interpretations extracted from the radiometric data. It has provided clearer and sharp lithology contact. Lithological units are apparent and easily identified on the ternary image pan-sharpened by SRTM hill shade DEM.

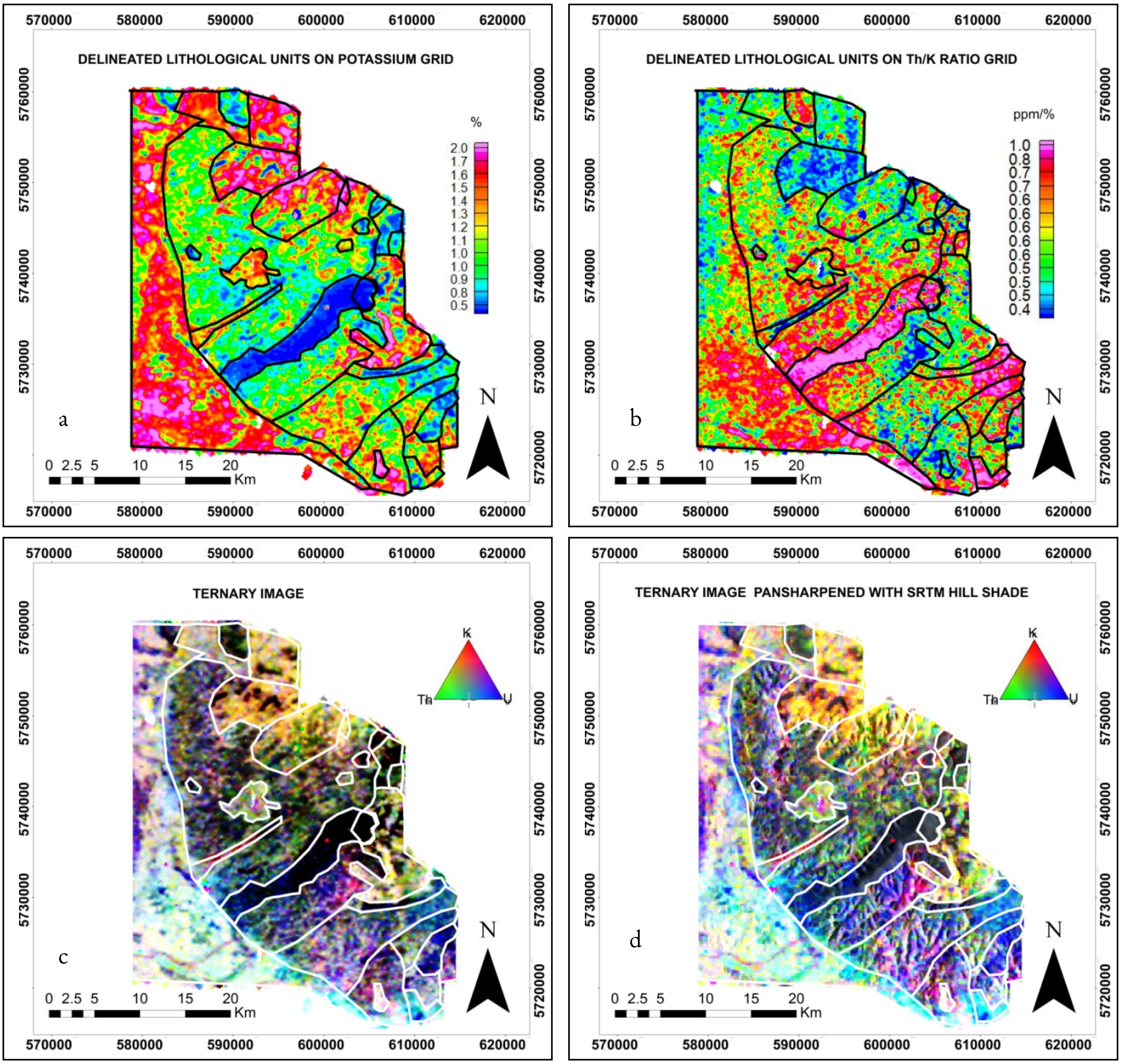

Figure 6-12 delineated lithological units on K grid and Th/K ratio grid, black lines indicate lithological boundaries (c and d) delineated lithological units on ternary image, white lines indicate lithological boundaries

6.18. Aeromagnetic data enhancements

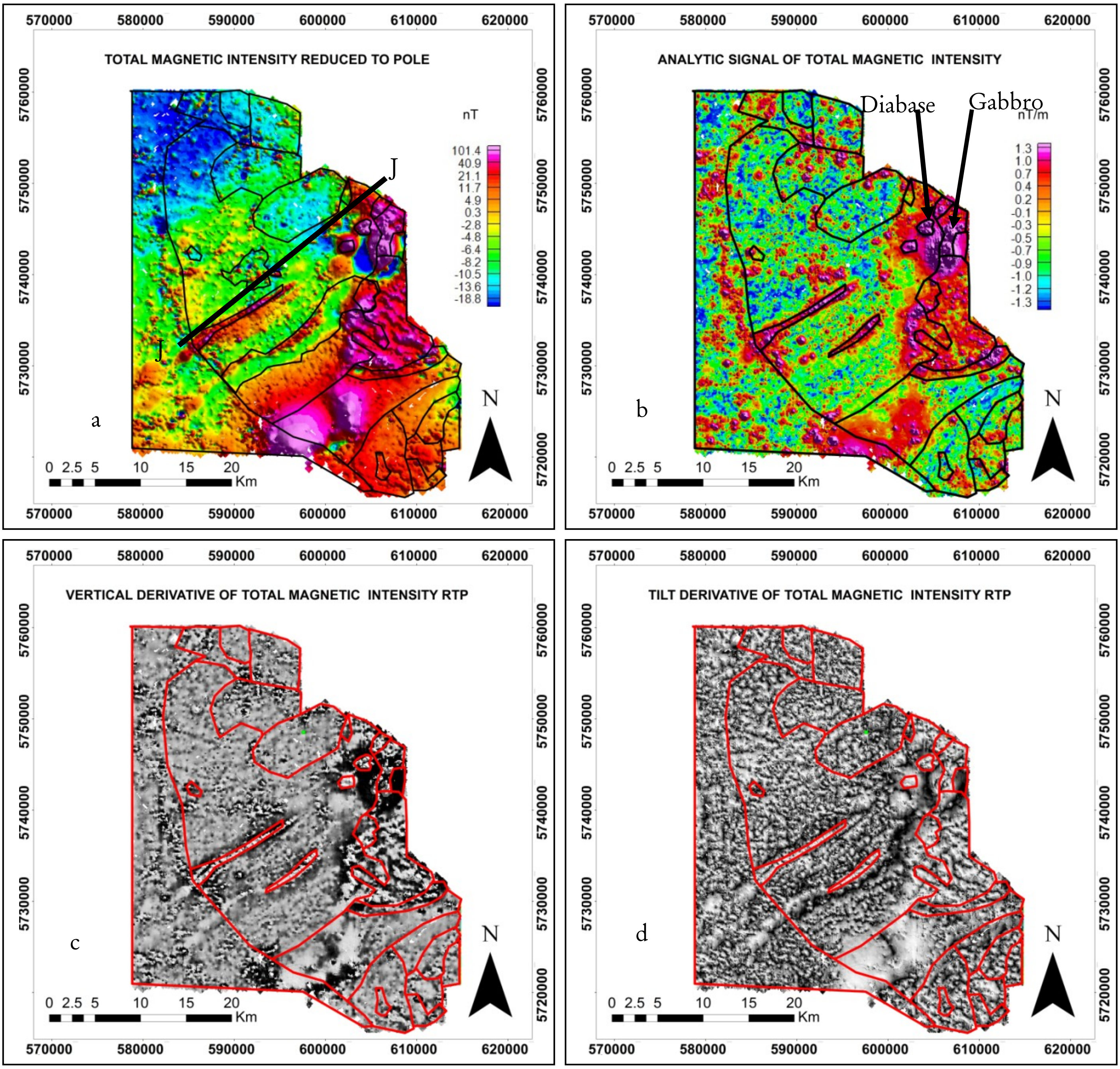

Figure 6-13 enhanced Aeromagnetic images of the study area, (a) Reduced to pole (RTP) of Total Magnetic Intensity, (b) Analytic Signal, (c) Vertical derivative and (d) Tilt derivative

6.19. Interpretation Aeromagnetic data

The reduced to pole image in figure 6-13a; show that the study area can be divided into two sections and this has been done using line JJ. Western part of this line is characterised by low magnetic signatures and the eastern part is characterised by high magnetic signatures. The low magnetic signatures in the western part of the study area are mainly underlain by Greywacke, Limestone, Shale, Devonian sandstone and Slate. The localised high magnetic signatures in that area can be attributed to variation in amounts of magnetite bearing minerals in the respective lithological units.

Gabbro and Diabase can be delineated in the east due to their high magnetic signatures. The presence of high magnetic signature is due to the presence of magnetite in these lithological units. These high magnetic signatures are related to the Brocken intrusive complex which consists of Brocken and Oker Granite and the Gabbro that occurred after the variscan orogeny (Large & Walcher, 1999).

Another high magnetic signature from south east to central eastern part is observed in the data. This area is mainly characterized by post tectonic granitic intrusion which occurred in the Harz after the variscan orogeny. The lithological units identified under this area are Granite, Diabase and Tannegreywacke. The high magnetic signature is attributed to the presence of iron mineral such as magnetite.

The south eastern corner shows medium magnetic signature. This area is underlain by sudharz Greywacke lithological unit. Similarly this moderate magnetic signature indicates the presence of magnetite in this unit.

The elongated linear feature on the centre trending NE-SW which shows high magnetic signature is associated with Diabase on the geological map. The high magnetic susceptibility is due to presence of magnetic minerals such as magnetite in the Diabase. This lithological unit is also related to the Brocken intrusive complex that occurred in the study area after the variscan orogeny (Large & Walcher, 1999).

Analysis of the analytic signal revealed the existence of various anomaly peaks and boundaries of the mafic intrusive rocks Diabase and Gabbro can be clearly delineated using the analytic signal. Anomalies with high magnitude in the eastern part of the study area which is underlain by mafic rocks Gabbro, Diabase and their boundaries are clearly outlined. Two prominent Diabase dykes on the centre trending NE-SW can be clearly seen from the analytic signal (figure 6-13 b).

Granite is well delineated in the vertical and Tilt derivatives due to its course texture, Diabase dykes on the centre are well delineated on both vertical and Tilt derivatives as elongated linear features trending NE-SW. Tannegreywacke in the south eastern part is delineated due to its smooth texture Intrusive mafic rocks Gabbro and Diabase are recognised by their circular shapes on both vertical and tilt derivatives (figure 6-13 c & d).

6.20. Visual Intepreted geological map

The interpretations made on gamma ray data and the aeromagnetic data has resulted in extraction of valuable information regarding lithology. The information has been integrated to form the geological map in the figure 6-14 below.

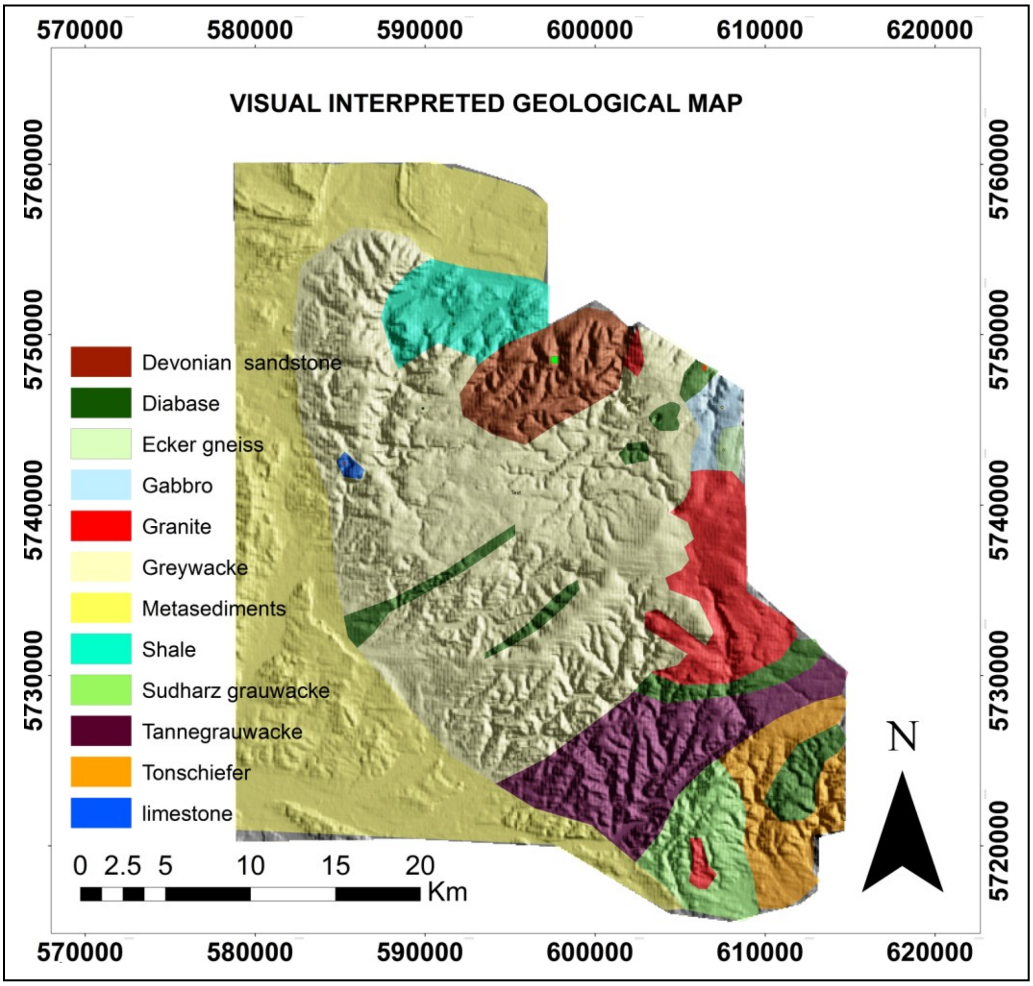

Figure 6-14 Geological map made from visual interpretation of the legacy airborne gamma ray and magnetic data

6.21. Conclusion

Visual interpretation, based on the legacy airborne gamma ray and magnetic data has shown that can map high magnetic susceptible and low radioelement content rocks like Gabbro and Diabase. The boundaries of these units can be clearly delineated using the analytic signal image and also the vertical and tilt derivative images. Furthermore is able to map low radioelement and low magnetic susceptibility rocks such as Limestone. Limestone can be well delineated on the K grid due to its very low radioelement content. It can also map high radioelement and high magnetic susceptible rocks like Granite. In the tilt and vertical derivative Granite has course texture which makes it to be easily differentiated from other units. It is also able to map lithological units with medium radioelement content and low magnetic susceptibility like Greywacke and Eckergneiss. These units can be easily delineated on the K grid as well as the Ternary image. Similarly visual interpretation on the legacy data can also map lithological units with high Th and K content and low magnetic susceptibility like Shale and Devonian sandstone. Shale can be differentiated from Devonian sandstone using Th/K ratio image. Shale has very low Th/k than Devonian sandstone. This shows that this data is very useful as all major lithological units could be identified using this legacy dataset.

6.22. Comparison between field data and legacy airborne geophysical data

In order to see relationship between the ground field data and the airborne data, comparison was made between these data sets. This was done in order find out if the rock signatures depicted using ground instruments can be observed in the airborne data and vice versa.

Ground magnetic readings shows that Intrusive rocks Harzburgite, Diabase and Gabbro show the highest magnetic susceptibility due to the presence of magnetite and iron sulphide mineral pyrrhotite. Shale Orkertal, Slate, Shale, Hornfels gneiss and Limestone all are characterized by low magnetic susceptibilities. These results compared with the Magnetic map on figure 6-13b also show that the intrusive rocks Harzburgite, Diabase and Gabbro have high magnetic susceptibilities and all other rocks indicate low magnetic susceptibilities which is in agreement with the ground field measurements. This shows that what is measured in the airborne data is reflected in the rocks themselves and shows that the legacy airborne magnetic data is very useful for mapping.

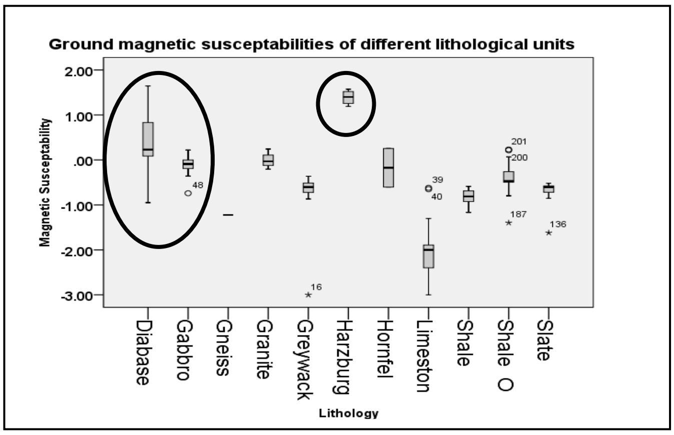

Figure 6-15 Comparison between ground field magnetic data and airborne magnetic data refer to figure 6-13b for airborne magnetic data

Similarly K and Th ground measurements show that Shale, Slate, Shale Orkertal and Granite in black circles have high K and Th content while Harzburgite Limestone, Diabase, Gabbro, Eckergneiss have low levels of K, and Th. Greywacke has medium K and Th content. The same trend is also seen in the airborne data. The airborne data also show high K and Th content for Shale, Slate, Shale Orkertal and Granite. Intrusive rocks Gabbro, Diabase and Harzburgite as well as Limestone, and Eckergneiss have low content of K and Th radioelements. These results show correlation and are in agreement with the ground field measurements and it shows that what is seen in airborne data is also reflected in rocks themselves.

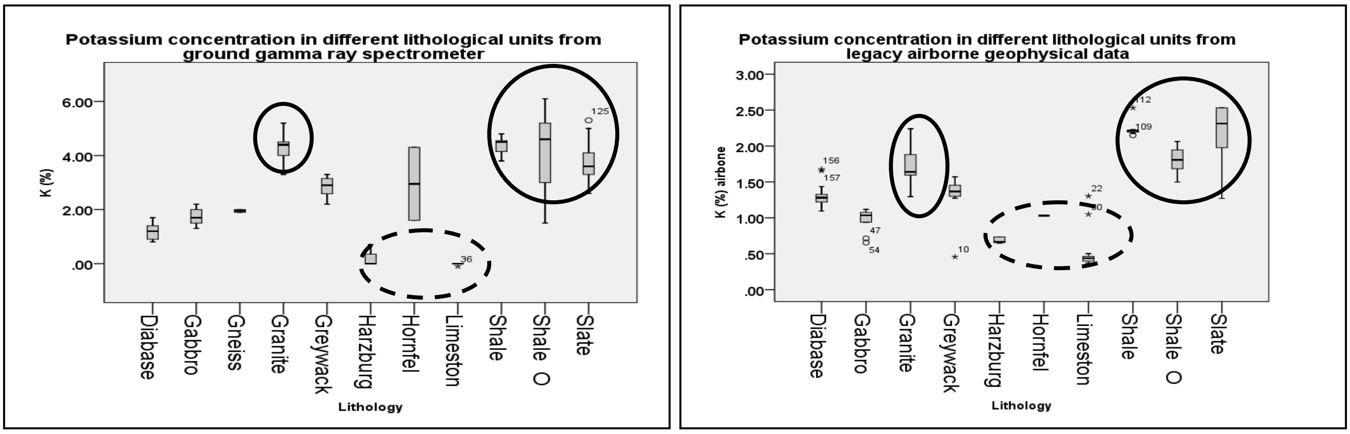

Figure 6-16 comparison between ground potassium data and airborne potassium data, black circle indicates high concentration, dashed circle indicates low concentration.

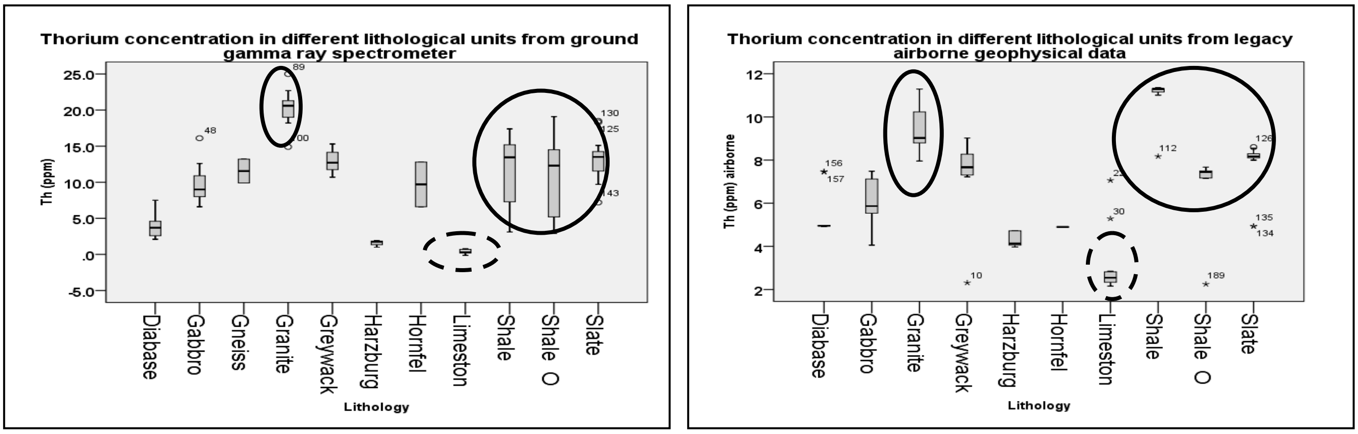

Figure 6-17 comparison between ground Thorium data and airborne Thorium data black circle indicates high concentration, dashed circle indicates low concentration.

6.23. Conclusion

The radioelement and magnetic signatures derived from the ground measurements show correlation with the airborne signatures. This shows that what is seen in the airborne data is also reflected in the rocks. This again shows that the airborne geophysical data is very useful as the composition of the rocks obtained by ground field instruments is the same with the legacy airborne data. Harris, Ford, Charbonneau, & Buckle, (2008) did similar comparison on ground gamma ray data measurements obtained by gamma ray spectrometer in Sekwi region, Canada (which they used to characterize signatures of major lithologies) and the airborne data and found that there was also a correlation.

From this chapter it can be concluded that performing isodata unsupervised classification on the legacy airborne gamma ray data, it can map low radioelement rocks such as Limestone, Gabbro and Diabase but it cannot differentiate these lithological units. It can also map medium radioelement rocks such as Greywacke and Eckergneiss and again has the limitation that it cannot differentiate these lithologies. Furthermore the classification is able to map high radioelement rocks such as Granite, Shale and Devonian sandstone but cannot differentiate them because they have similar gamma ray spectral signatures. Maximum likelihood and Isodata classifications based on gamma ray data give similar results. When both magnetic and gamma ray data are used in the supervised classification, more classes can be separated but however the classification accuracy does not improve much. It only changed by 2% i.e. from 40% to 42%, this low accuracy is due to overlap within the classes and this is confusing the classification. Visual interpretation worked better than classification because we see a lot more than the classifier. The classifier only look at distance from the signature in feature space while in visual interpretation we see a lot more like texture, colour, tone, association, these things the classifier does not see as it only looks at pixel level. As a result the overlap within the classes confused the classification. However the results have shown that the legacy airborne geophysical data is still very useful.

7. CONCLUSION AND RECOMMENDATIONS

This research used legacy airborne geophysical data set which was digitised from contour maps. The research aimed at finding out how to grid the legacy airborne geophysical data and get useful geological information out of it, and to know what kind of information about the geology could be obtained by improving this data set.

Minimum curvature, IDW and kriging gridding algorithms were compared and kriging was found to be the best gridding algorithm for this legacy airborne geophysical dataset. It was found out that normal distribution curves for Kriging had low standard deviations and RMSE. In addition visual analysis of the output grids showed that kriging has sharp and crisp boundaries and less artefacts which were not the same with minimum curvature and IDW.

Maximum likelihood supervised classification and isodata unsupervised classification were used to extract geological information content from this legacy airborne geophysical dataset. Visual interpretation was also used to support the classification.

This research has found out that performing isodata unsupervised classification on the legacy airborne gamma ray data, it can map low radioelement rocks such as Limestone, Gabbro and Diabase but cannot differentiate them because they have same radiometric signatures. It can also map medium radioelement rocks such as Greywacke and Eckergneiss and again has the limitation that it cannot differentiate these lithologies. Furthermore the classification is able to map high radioelement rocks such as Granite, Shale and Devonian sandstone but cannot differentiate these lithologies because they have similar gamma ray spectral signatures. It was also found out that it is able to map out marsh areas and the lakes. These also have low radioelement content and the classification could not distinguish these water logged areas, lakes from the low radioelement rocks, Limestone, Gabbro and Diabase.

Similarly performing maximum likelihood supervised classification on the legacy airborne gamma ray data, the results were the same with the isodata classification. Maximum likelihood can map low radioelement rocks such as Limestone, Gabbro and Diabase but also it cannot differentiate them because they have similar gamma ray radiometric signatures. It can also map medium radioelement rocks such as Greywacke and Eckergneiss and again has the limitation that it cannot differentiate these lithologies. Furthermore the classification is able to map high radioelement rocks such as Granite, Shale and Devonian sandstone but cannot differentiate these lithological units because they have similar gamma ray spectral signatures. It was also found out that it is able to map out marsh areas and the lakes. These also have low radioelement content and the classification could not differentiate these water logged areas, lakes from the low radioelement rocks Limestone, Gabbro and Diabase.

Performing maximum likelihood Supervised classification based on both legacy airborne gamma ray and magnetic data has shown that it can map high magnetic susceptibility and low radioelement content rocks like Gabbro and Diabase but it cannot differentiate these lithological units because they all have high magnetic susceptibilities and low radioelement content. Furthermore it can map low radioelement and low magnetic susceptibility rocks such as Limestone. Again it showed that using both magnetic susceptibility and gamma ray data it is possible to separate Limestone from the mafic rocks which was not possible when only gamma ray data was used. In addition to this, the classification can map high gamma ray spectral signature and high magnetic susceptibility rocks like Granite. Using both gamma ray and magnetic susceptibility Granite can be separated from Shale and Devonian sandstone which was not possible when gamma ray data only was used. Also based the gamma ray and magnetic data the classification is able to map lithological units with medium radioelement content and low magnetic susceptibility like Greywacke and Eckergneiss but again could not differentiate these lithological units. It can also map lithological units with high Th and K content and low magnetic susceptibility like Shale and Devonian sandstone but it cannot separate them. Using both gamma ray and magnetic susceptibility, Shale and Devonian sandstone can be separated from Granite which was not possible with gamma ray data only

Classification accuracy varied from 40% when only gamma ray data was used to 42% when both gamma ray and magnetic data were used. This low accuracy is due to variability within the classes. There is a lot of overlap within the classes and this confused the classification. (For instance looking at the Ternary image, there is a lot of variability within the classes). There are areas that are dark (low radioelement content) and also bright areas within the dark lithologies. This confuses the classification and explains why classification is not good.

Visual interpretation, based on the legacy airborne gamma ray and magnetic data has shown that can map high magnetic susceptible and low radioelement content rocks like Gabbro and Diabase. The boundaries of these units can be clearly delineated using the analytic signal image and also the vertical and tilt derivative images. Furthermore is able to map low radioelement and low magnetic susceptibility rocks such as Limestone. Limestone can be well delineated on the K grid due to its very low radioelement content. It can also map high radioelement and high magnetic susceptible rocks like Granite. In the tilt and vertical derivative Granite has course texture which makes it to be easily differentiated from other units. It is also able to map lithological units with medium radioelement content and low magnetic susceptibility like Greywacke and Eckergneiss. These units can be easily delineated on the K grid as well as the Ternary image. Similarly visual interpretation on the legacy data can also map lithological units with high Th and K content and low magnetic susceptibility like Shale and Devonian sandstone. Shale can be differentiated from Devonian sandstone using Th/K ratio image. Shale has very low Th/K than Devonian sandstone.

Comparison of the ground field data and airborne data has shown that there is correlation between the datasets. The radioelement and magnetic signatures derived from the ground measurements show good correlation with the airborne signatures sampled at the same geographic locations as the ground measurements. This shows that what is seen in the airborne data is also reflected in the rocks.

The research has found that major lithological units could be identified using this data set and this shows that though this dataset is very old (1985), it is still very useful. Performing supervised and unsupervised classification on the gamma ray data gives similar kind of geological information. More information is obtained when both gamma ray data and magnetic data are used.

7.1. Recommendation

- Other processing steps useful in obtaining more information about the study area such as correcting for the effect of vegetation on gamma ray data should be considered as this could help to have more insight into the data.

LIST OF REFERENCES

AlSaud, M. M. (2008). Structural mapping from high resolution aeromagnetic data in west central Arabian Shield, Saudi Arabia using normalized derivatives. *Arabian Journal of Geosciences*, *1*(2), 129–136. doi:10.1007/s12517-008-0012-2

Anderson, T. A. (1975). Carboniferous subduction Complex in the Harz Mountain, Germany. *Geological Society of America Bulletin*. doi:50110

Arfaoui, M., & Inoubli, M. H. (2012). Advantages of using the kriging interpolator to estimate the gravity surface, comparison and spatial variability of gravity data in the El Kef-Ouargha region (northern Tunisia). *Arabian Journal of Geosciences*, *6*(8), 3139–3147. doi:10.1007/s12517-012-0549-y

Dentith, M., & Mudge, S. (2014). Geophysics for Exploration Geoscientist (1st ed.). University Printing house,Cambridge University Press, UK. doi:978-0-521-80951-1

Dobrin, M., & Savit, C. H. (1988). Introduction to Geophysical Prospecting. Retrieved August 19, 2014, from http://www.amazon.com/Introduction-Geophysical-Prospecting-Milton-Dobrin/dp/0070171963

Drury, S. (2001). Image interpretation in geology. Malden; Cheltenham: Blackwell science; Nelson Thornes.

Geosoft. (2013). Geosoft Oasis montaj tutorials 7.1. Geosoft. Retrieved November 27, 2014, from www.geosoft.com

Harris, J. R. (Ed.). (2008). Remote Pridictive Mapping: An Aid for Northern Mapping. Geological Survey of Canada Open File 5643.

Harris, J. R. (2012). Remote Predictive mapping. In *Kidney international supplements* (Vol. 2, pp. 343–346). Ottawa, Ontario K1A 0E9: Geological Survey of Canada. doi:10.1038/kisup.2012.51

Harris, J. R., Ford, K., Charbonneau, B., & Buckle, J. (2008). Application of Gamma-Ray Spectrometer Data for Lithological Mapping in a Cordilleran Environment, Sekwi Region, Northwest Territories. *Journal of the Geological Association of Canada*.

Harris, J. R., Pilkington, M., Lynds, T., & Mcgregor, R. (2008). The Application of Remotely Sensed Data for Structural Mapping, Southwest Baffin Island. In J. R. Harris (Ed.), Remote Predictive Mapping: An aid for Northern mapping (pp. 191–202). Geological Survey of Canada open file 5643.

Harris, J. R., Schetselaar, E. M., Lynds, T., & Kemp, E. A. (2008). Remote Predictive Mapping: A Strategy for Geological Mapping of Canada' s North. *Journal of the Geological Association of Canada*, *34*(3 and 4).

Harris, J. R., Schetselaar, E.M, & Behnia, P. (2012). Remote Predictive Mapping: An Approach for the Geological Mapping of Canada' s Arctic. *Intech Journals*. doi:10.5772/25475

Harris, J. R., & Wickert, L. (2011). Optical Remote Sensing – A Review for Remote Predictive Geological Mapping in Northern Canada. *Journal of the Geological Association of Canada*, *38*(2). doi:268601375

Harris, J.R., Martel, E., Currie, M., Pierce, K., Pilkington, M., & Keating, P. (2008). Snowbird Lake (NTS 65D) Remote Predictive Mapping and Geoscience Data Compilation; Northwest Territories Geoscience Office, NWT Open File 2005-08. Digital files.

Hosseini, E., & Marcotte, D. (2014). Theoretical and Experimental Performance of spatial Interpolation Methods for Soil Salinity analysis. *American Society of Agicultural Engineers ASAE*, *37*(6), 1799–1807.

Large, D., & Walcher, E. (1999). The Rammelsberg massive sulphide Cu-Zn-Pb-Ba-Deposit, Germany: an example of sediment-hosted, massive sulphide mineralisation. *Springer*, *34*(5-6), 522–538. doi:10.1007/s001260050218

Li, X. (2008). Magnetic reduction-to-the-pole at low latitudes: Observations and considerations. *The Leading Edge*, *27*(8), 990–1002. doi:10.1190/1.2967550

Lillesand, T., Kiefer, R. W., & Chipman, J. (2004). Remote Sensing and Image Interpretation. Hoboken, USA: John Wiley and Sons Inc. Retrieved August 22, 2014, from http://www.amazon.com/Remote-Sensing-Interpretation-Thomas-Lillesand/dp/0470052457

MacLeod, I., Jones, K., Dai, T. F. (1993). 3-D Analytic signal in the interpretation of total magnetic field data at low magnetic latitudes. *Exploration Geophysics*.

Mueller, A. G. (2008). The Rammelsberg shale-hosted Cu-Zn-Pb sulfide and barite deposit, Germany: Linking SEDEX and Kuroko-type massive sulfides - Slide presentation and explanatory notes. Retrieved October 16, 2014, from http://www.e-sga.org/fileadmin/sga/Mineral_Deposit_Archive/Rammelsberg/RB-SGAslides1.pdf

Onge, M., & Harris, J.R. (2008). The Advantages of High-Resolution Spectral and Spatial Hyperspectral Data for Lithological Mapping: An Example from Southeast Baffin Island. In J. R. Harris (Ed.), Remote Predictive Mapping: An aid for Northern mapping (pp. 183–189). Geological Survey of Canada, open file 5643.

Richards, A. J. (2013). Remote Sensing Digital Image Analysis (5th ed., p. 503). Heidelberg New york Dordrecht London: Springer. doi:10.1007/978-3-642-30062-2

Scandinavian Highlands. (2009). Harz SEDEX Project - Base metals, Silver and Gold. Retrieved July 29, 2014, from http://www.scandinavian-highlands.com/projects/harz-sedex-project.aspx

Scandinavian Highlands. (2010). Exploration for Base Metals in the Harz Mountains, central Germany, un published report. Retrieved July 29, 2014, from http://www.scandinavian-highlands.com/projects/harz-sedex-project.aspx

Schetselaar, E. M. (2000). Integration of Landsat TM, Gamma-Ray, Magnetic, and Field Data to Discriminate Lithological Units in Vegetated Granite-Gneiss Terrain. *Remote Sensing of Environment*, *71*(1), 89–105. doi:10.1016/S0034-4257(99)00069-3

Schetselaar, E. M., Harris, J. R., Lynds, T., & Kemp, E. A. De. (2007). Remote Predictive Mapping (RPM): A Strategy for Geological Mapping of Canada North. *Journal of Geoscience, Canada*, *34* (December), 93–111.

Schloeder, C. A., Zimmerman, N. E., & Jacobs, M. J. (2001). Comparison of Methods for Interpolating Soil Properties Using Limited Data. *Soil Science Society of America Journal*, *65*(2), 470. doi:10.2136/sssaj2001.652470x

Tourliere, B., Perrin, J., Leberre, P., & Pasquet, J. (2003). Use of airborne gamma-ray spectrometry for kaolin exploration. *Journal of Applied Geophysics*, *53*(2-3), 91–102. doi:10.1016/S0926-9851(03)00040-5

Wikipedia. (2014). Geological map of Harz. Retrieved August 27, 2014, from http://de.wikipedia.org/wiki/Datei:Geologie_Harz.JPG

Wilford, J. (1997). Airborne Gamma Ray Spectrometry: Cooperative Research Centre for Landscape Environments and Mineral Exploration, Geoscience Australia, 46–52.

WorldAtlas. (2013). Germany large color map. Retrieved August 26, 2014, from http://www.worldatlas.com/webimage/countrys/europe/lgcolor/decolorlf.htm

Zech, J., Ries, T. J., & Faust, D. (2010). U/Pb-dating and geochemical characterization of the Brocken and the Ramberg Pluton, Harz Mountains, Germany. *Journal of Central European Geology*, *1*, 9–24.

7.2. Annex1 Boxplots showing portable XRF laboratory measurements for K and Th , magnetic susceptibility measured by the kappa meter and ASD field spectra

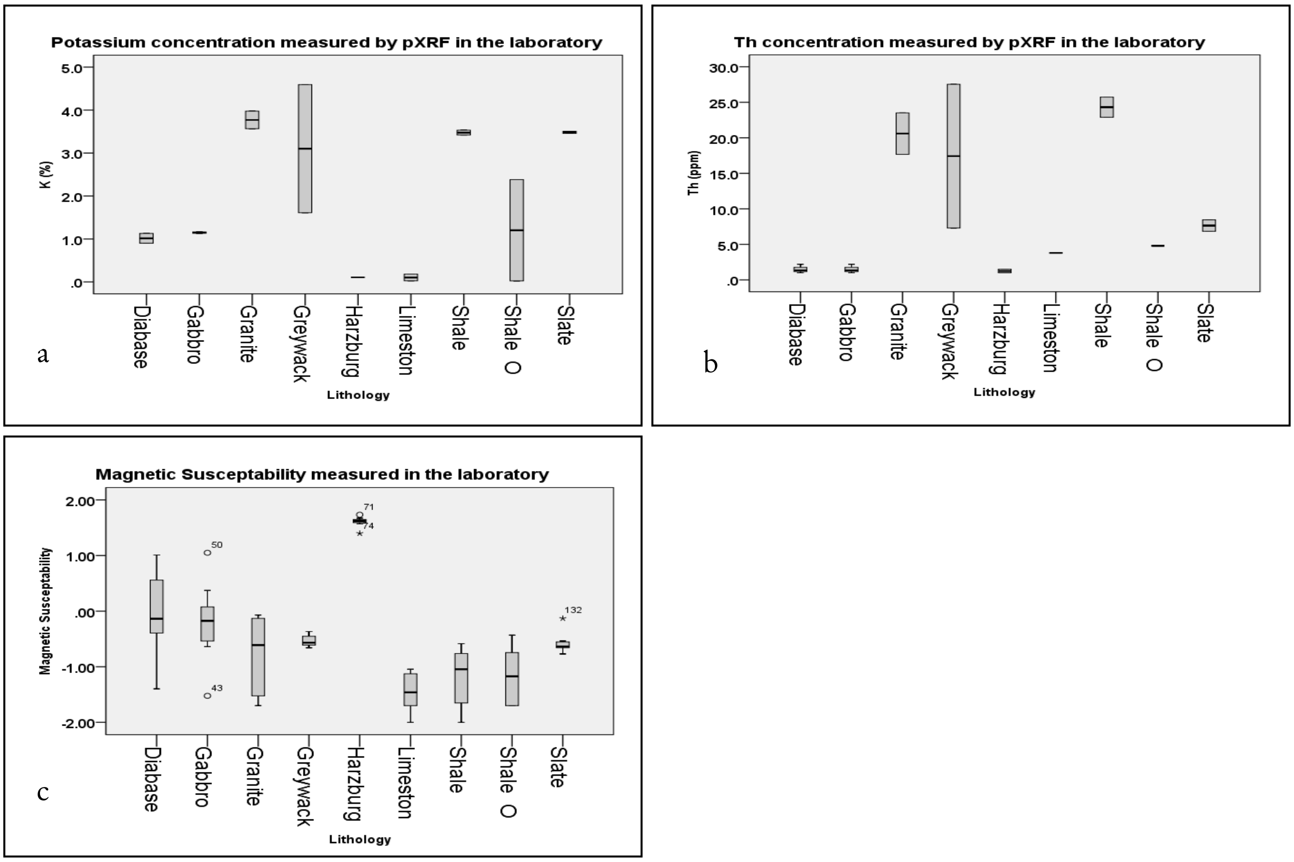

Figure 7-1 K, Th , Concentration and magnetic susceptibility measured in the laboratory (a) Potassium, (b) Thorium, (c) magnetic susceptibility

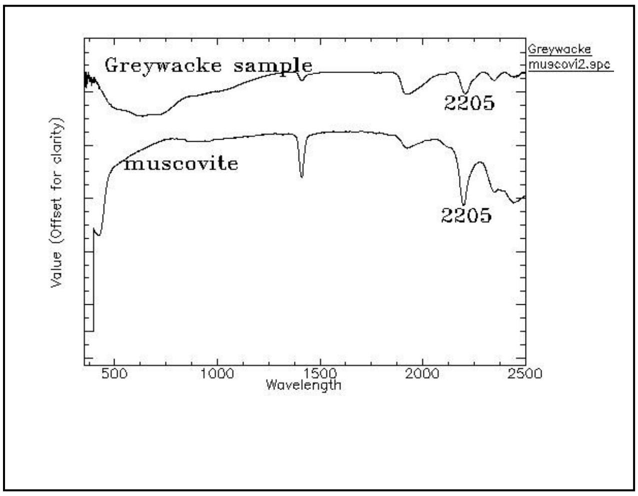

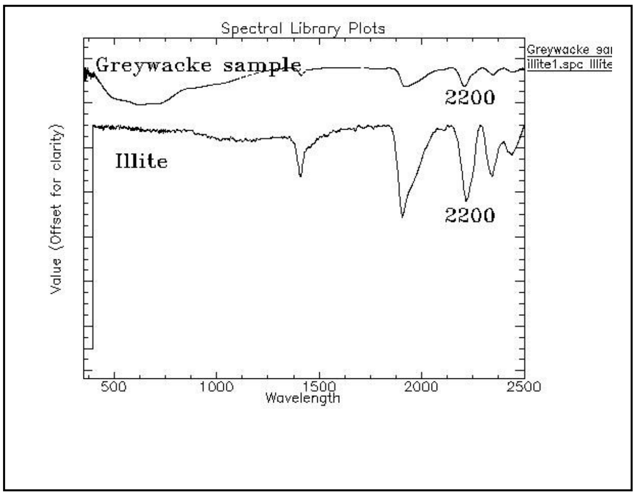

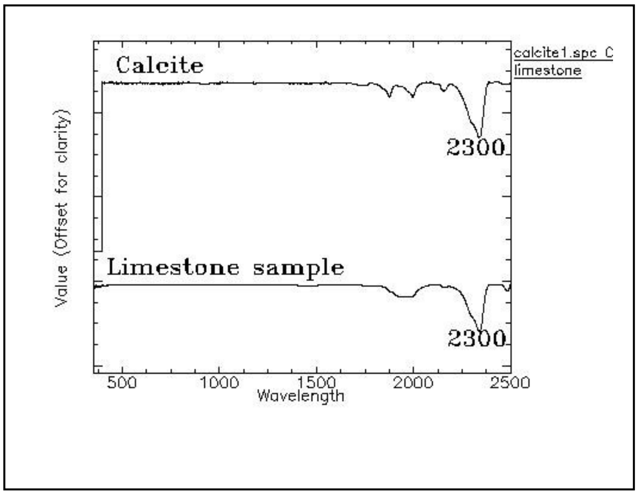
Calcite
calcite1.spc C
limestone
2300
Limestone sample
2300
Value (Offset for clarity)
500
1000
1500
2000
2500
Wavelength

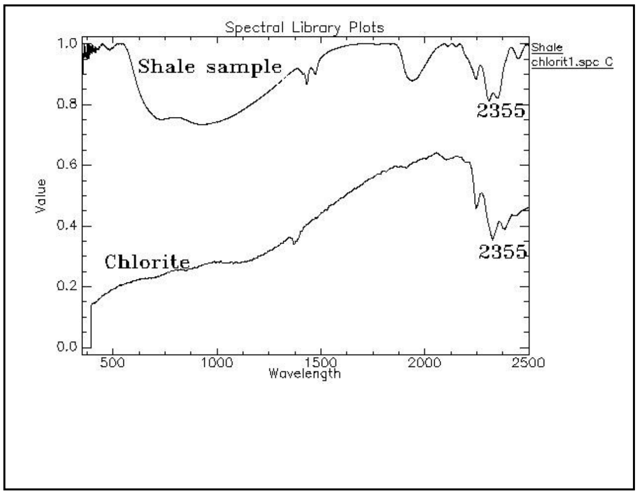
Spectral Library Plots
Shale sample
Shale
chlorit1.spc C
2355
Chlorite
2355
Value
1.0
0.8
0.6
0.4
0.2
0.0
500
1000
1500
2000
2500
Wavelength

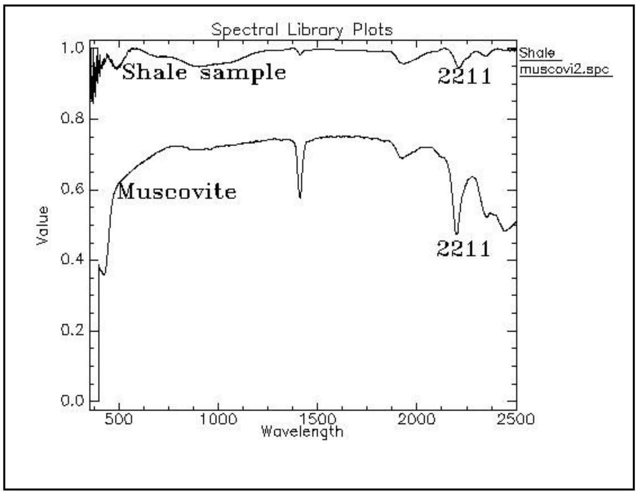
Spectral Library Plots
Shale sample
Shale
muscovi2.spc
2211
Muscovite
2211
Value
1.0
0.8
0.6
0.4
0.2
0.0
500
1000
1500
2000
2500
Wavelength

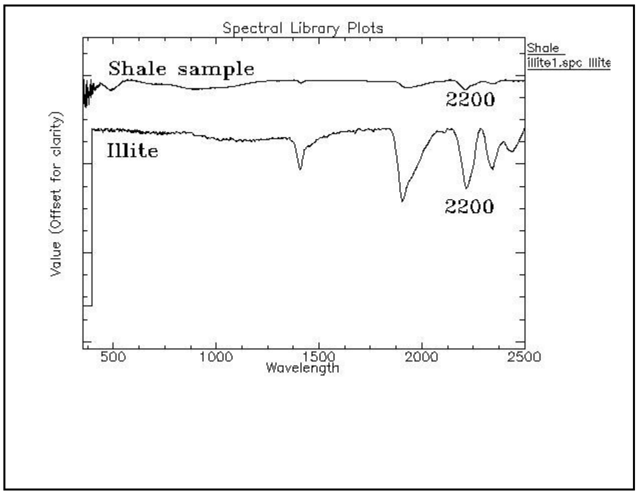
Spectral Library Plots
Shale sample
Shale
illite1.spc Illite
2200
Illite
2200
Value (Offset for clarity)
500
1000
1500
2000
2500
Wavelength

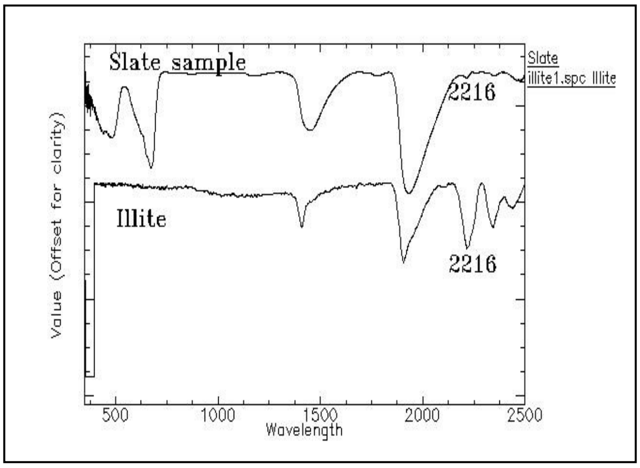
Slate sample
Slate
illite1.spc Illite
2216
Illite
2216
Value (Offset for clarity)
500
1000
1500
2000
2500
Wavelength

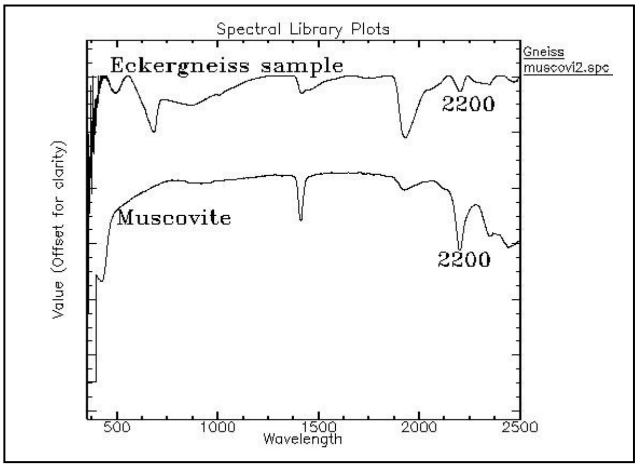
Spectral Library Plots
Eckergneiss sample
Gneiss
muscovi2.spc
2200
Muscovite
2200
Value (Offset for clarity)
500
1000
1500
2000
2500
Wavelength

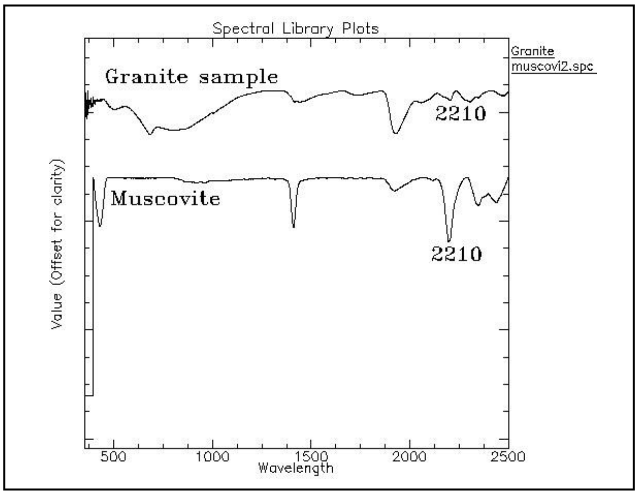
Spectral Library Plots
Granite
muscovi2.spc
Granite sample
2210
Muscovite
2210
Value (Offset for clarity)
500
1000
1500
2000
2500
Wavelength

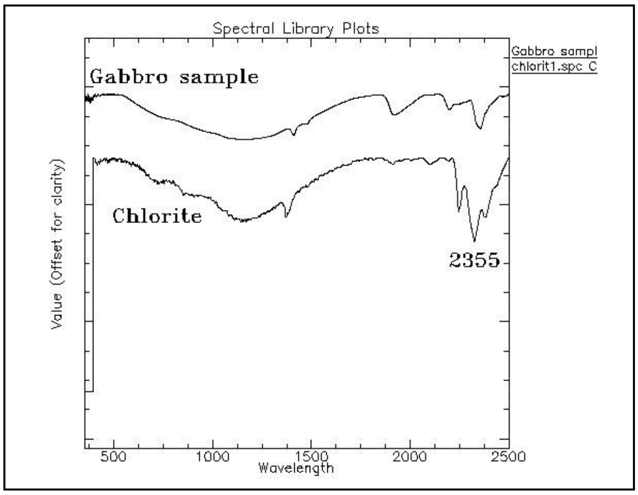
Spectral Library Plots
Gabbro sampl
chlorit1.spc C
Gabbro sample
Chlorite
2355
Value (Offset for clarity)
500
1000
1500
2000
2500
Wavelength

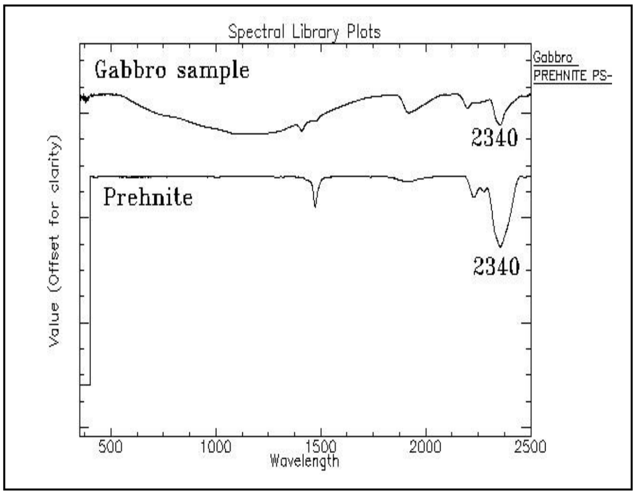
Spectral Library Plots
Gabbro
PREHNITE PS-
Gabbro sample
2340
Prehnite
2340
Value (Offset for clarity)
500
1000
1500
2000
2500
Wavelength

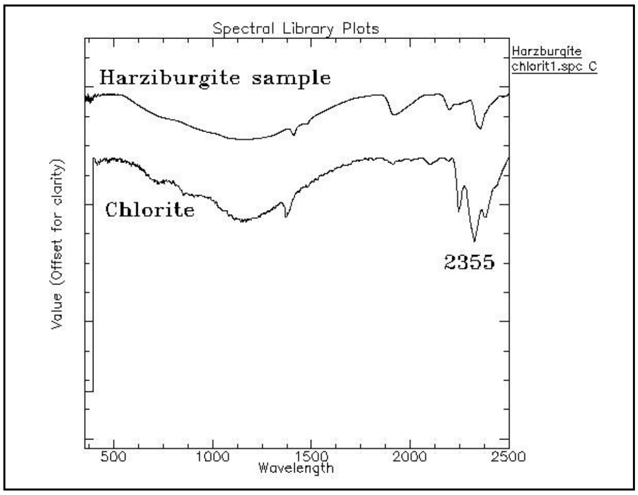
Spectral Library Plots
Harzburgite
chlorit1.spc C
Harziburgite sample
Chlorite
2355
Value (Offset for clarity)
500
1000
1500
2000
2500
Wavelength

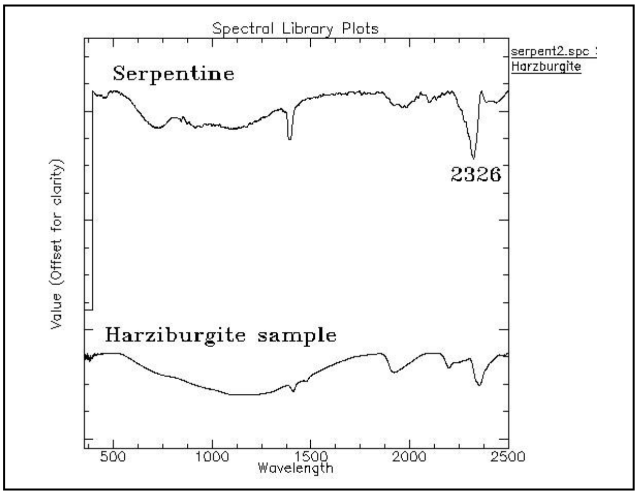
Spectral Library Plots
serpent2.spc :
Harzburgite
Serpentine
2326
Harziburgite sample
Value (Offset for clarity)
500
1000
1500
2000
2500
Wavelength

7.3. Annex 2 showing results of geophysical data processing , this annex is linked to chapter 5

Thorium

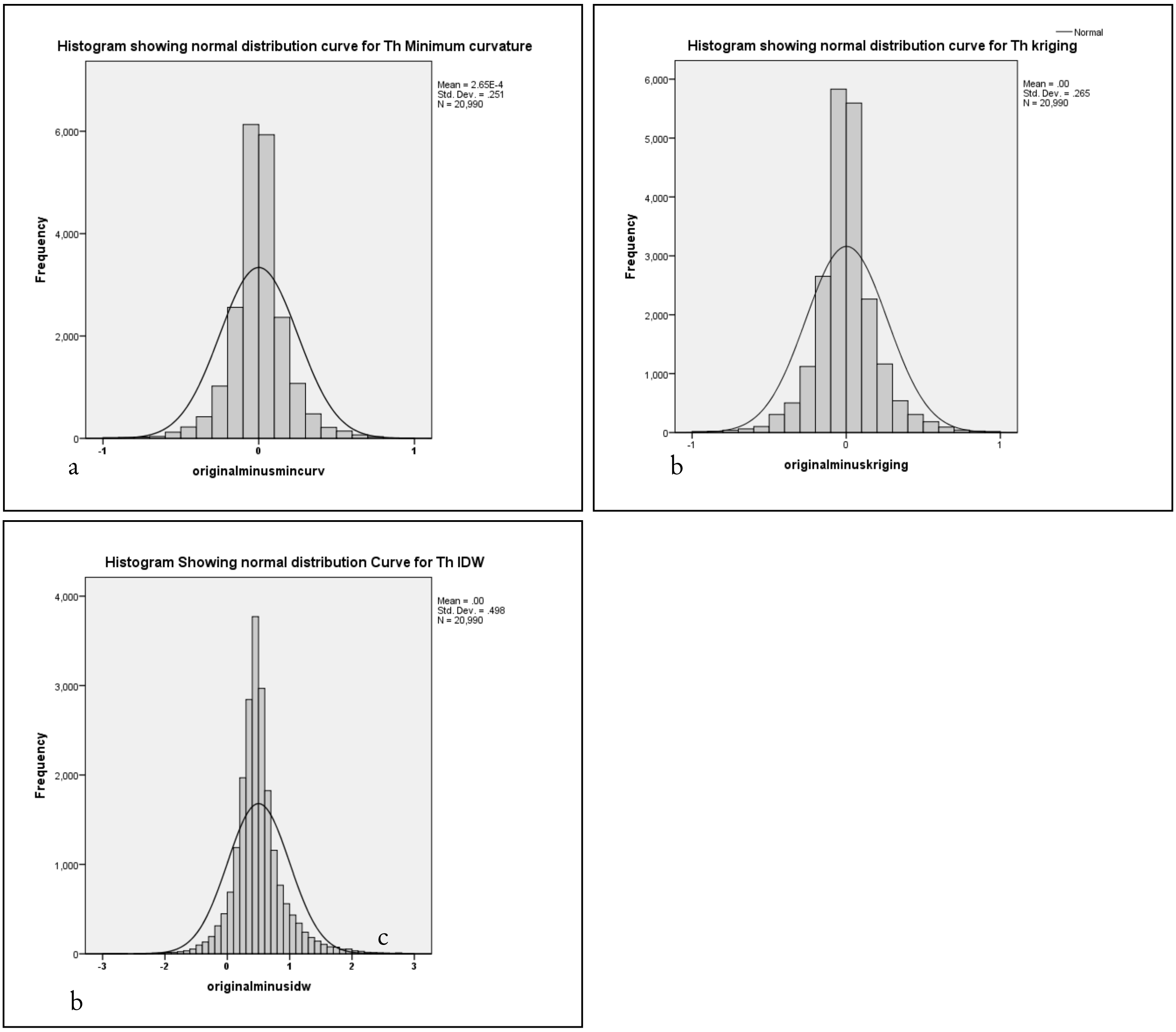

Figure 7-2 shows the results of the histograms for normal distribution curves for thorium gridding data (a) Minimum Curvature, (b) Kriging and (c) IDW

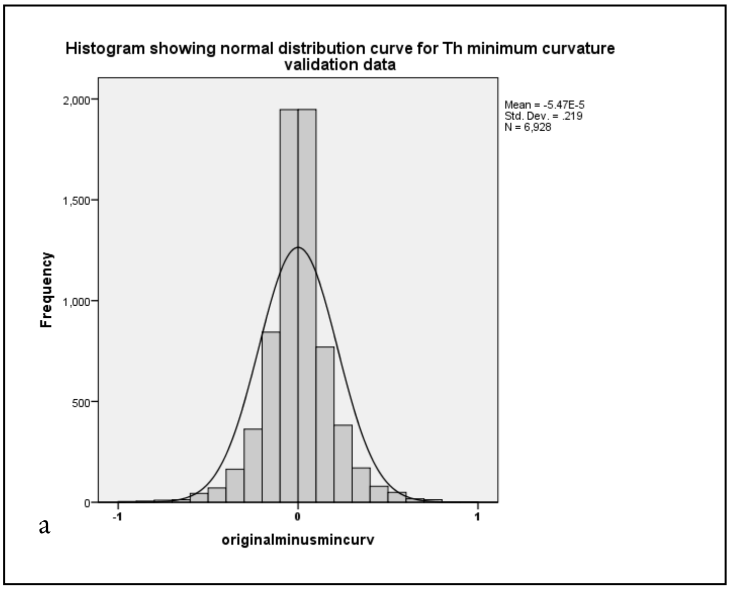

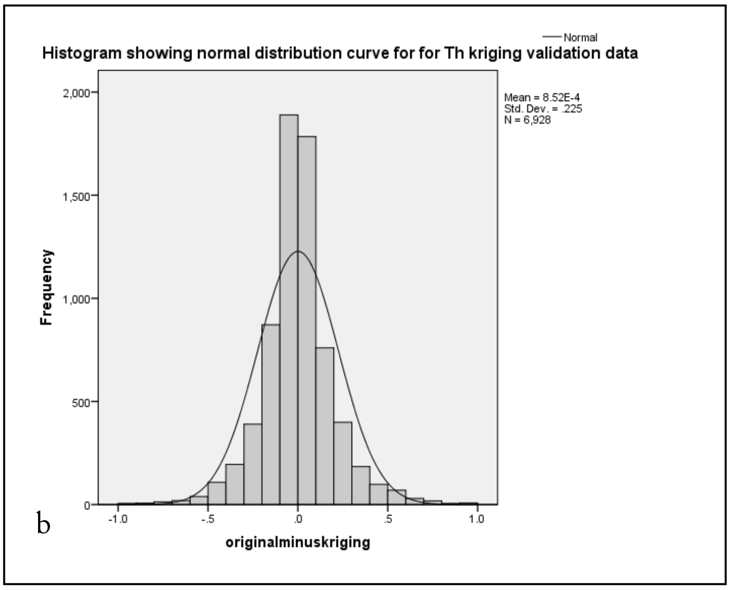

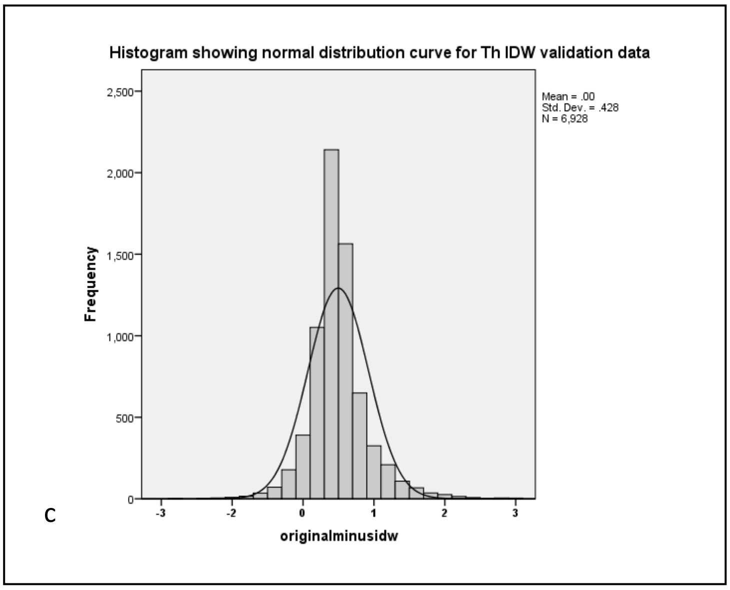

Validation data for Th

rmse minimum curvature = 0.21

rmse kriging = 0.22

rmse idw = 0.42

Figure 7-3 shows the results of the histograms for normal distribution curves for thorium validation data (a) Minimum Curvature, (b) Kriging and (c) IDW

Uranium

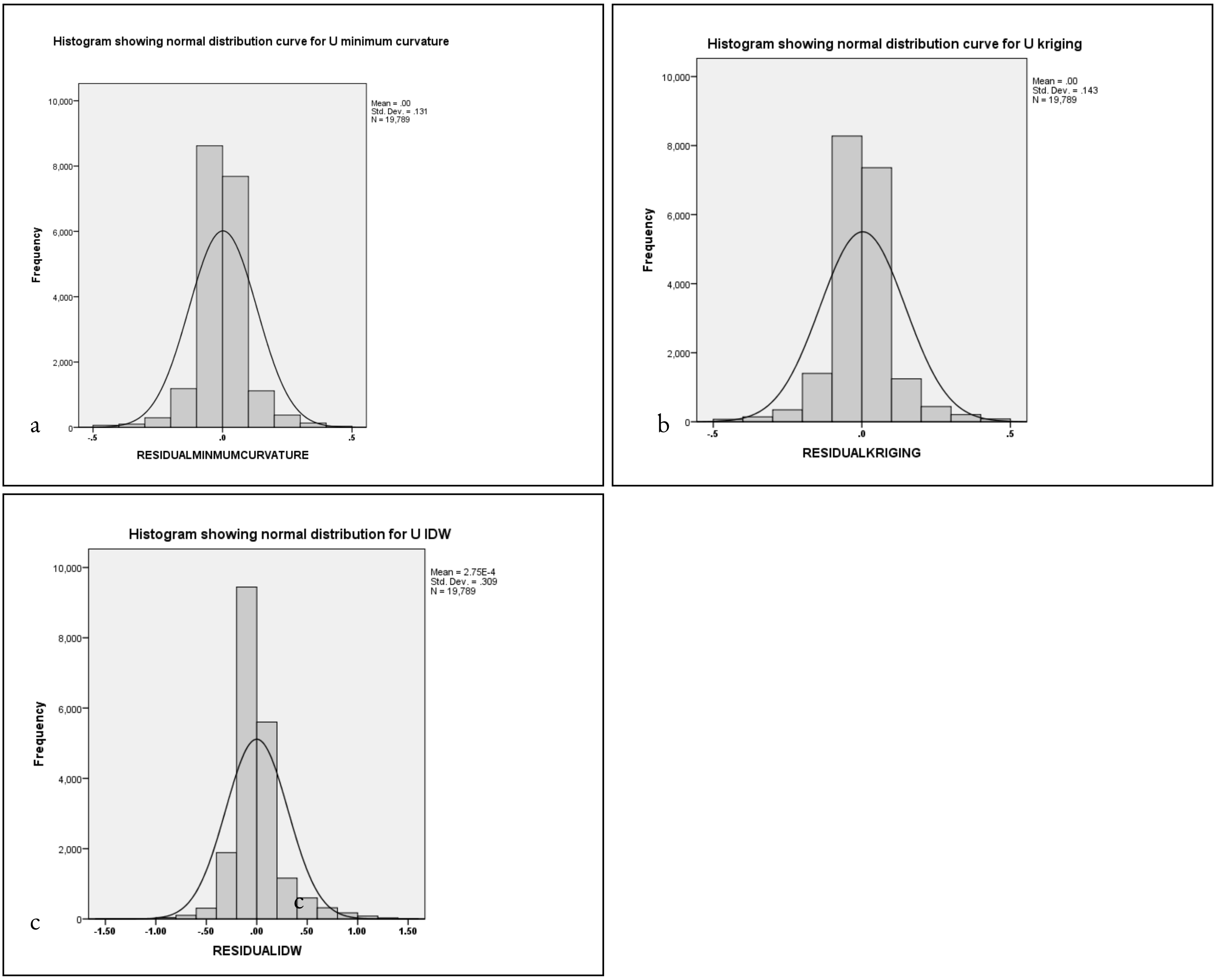

Figure 7-4 shows the results of the histograms for normal distribution curves for Uranium gridding data (a) Minimum Curvature, (b) Kriging and (c) IDW

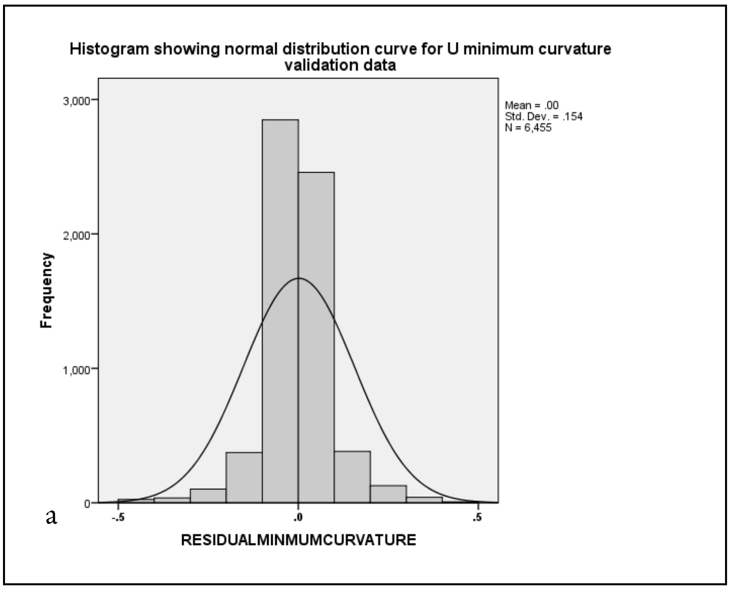

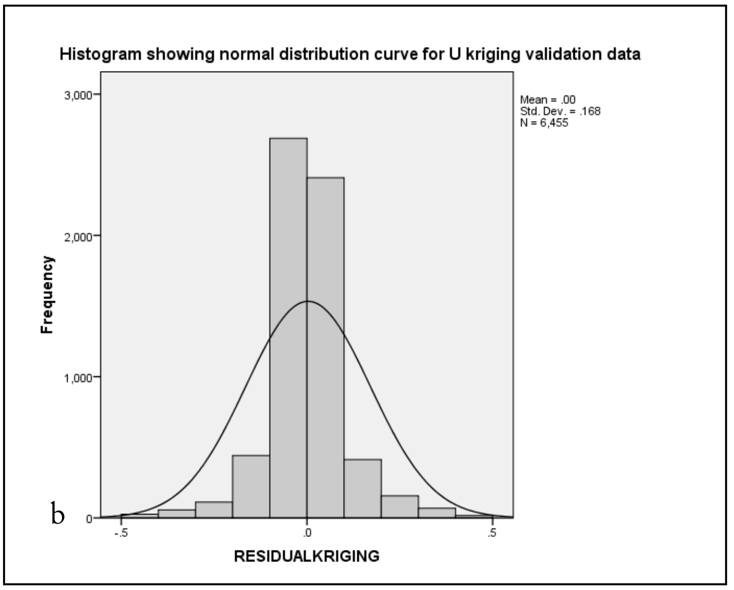

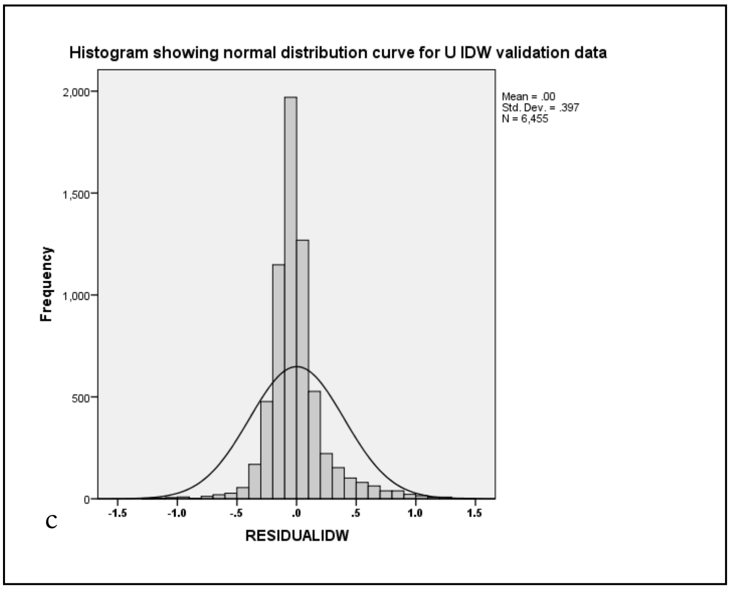

Validation data for uranium

rmse minimum curvature = 0.15

rmse kriging = 0.16

rmse idw = 0.38

Figure 7-5 shows the results of the histograms for normal distribution curves for uranium validation data (a) Minimum Curvature, (b) Kriging and (c) IDW

Total count

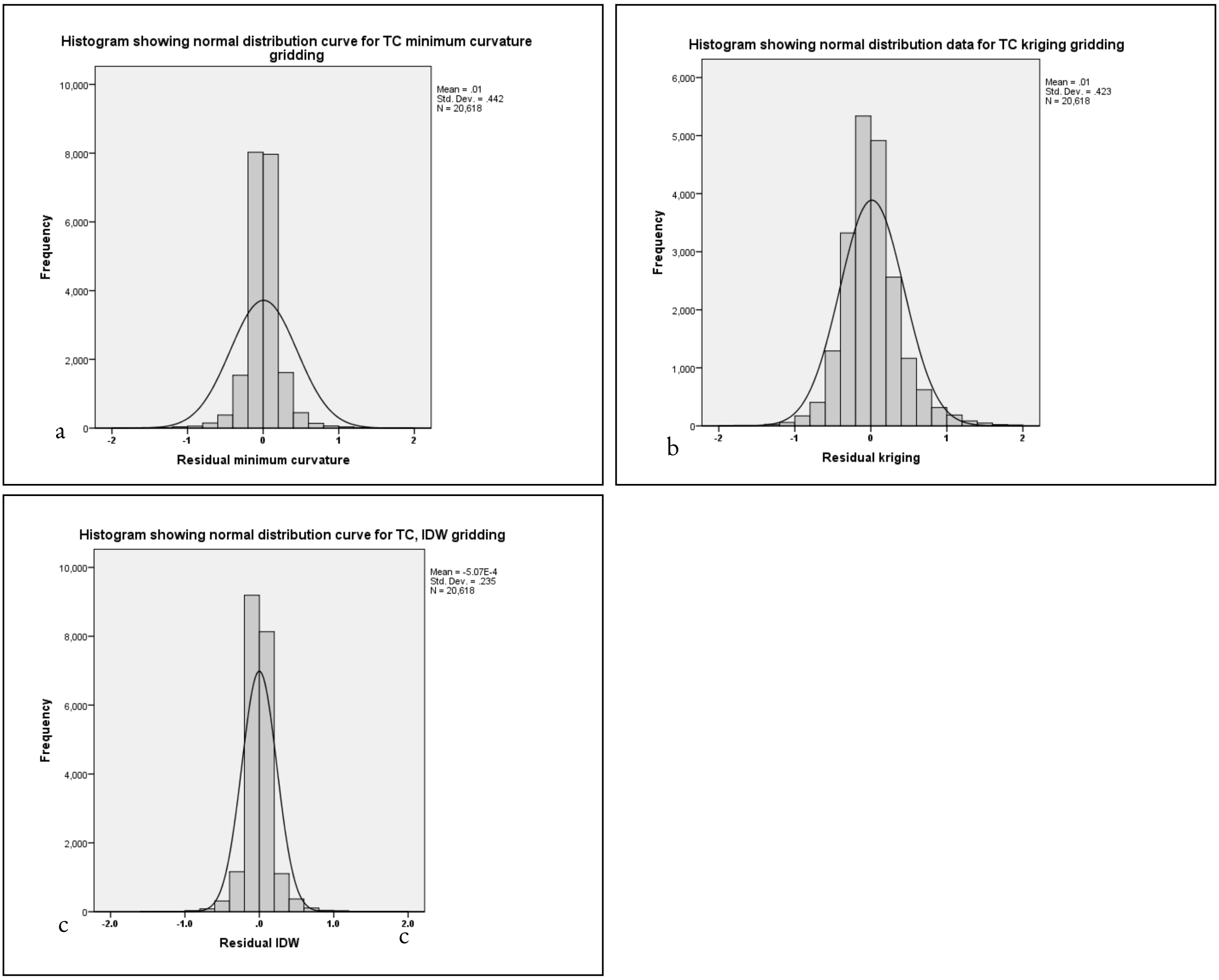

Figure 7-6 shows the results of the histograms for normal distribution curves for Total count (a) Minimum Curvature, (b) Kriging and (c) IDW

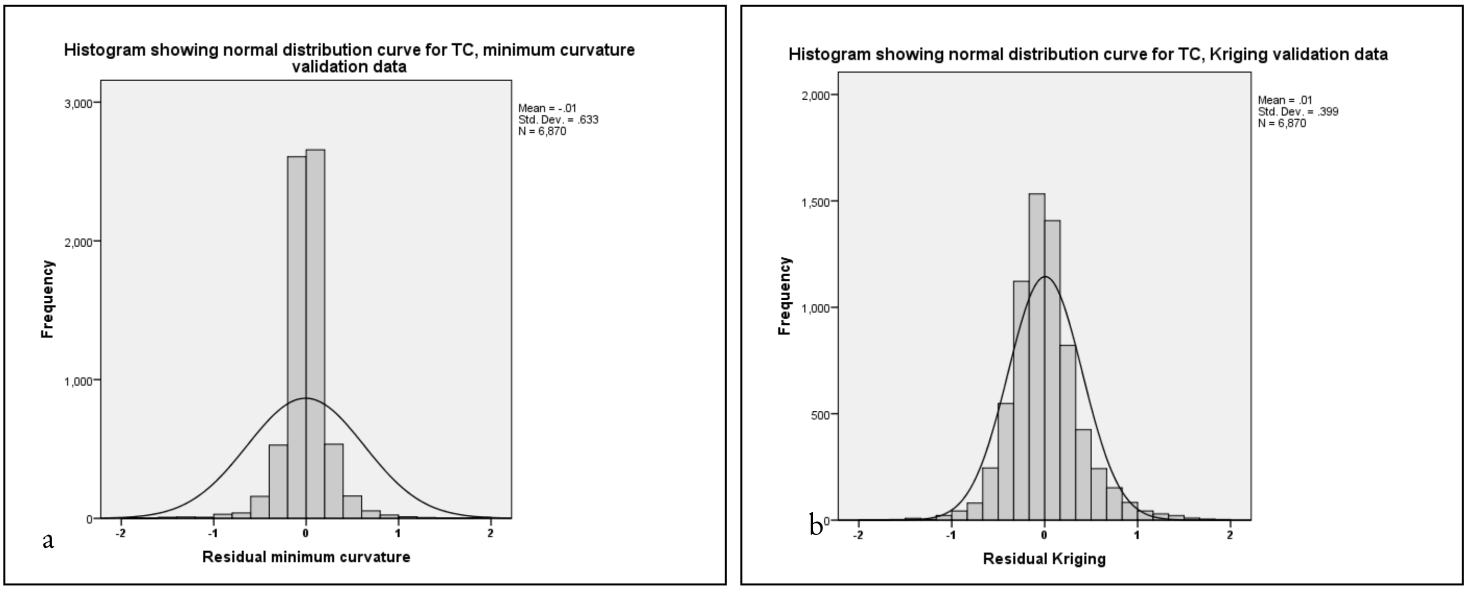

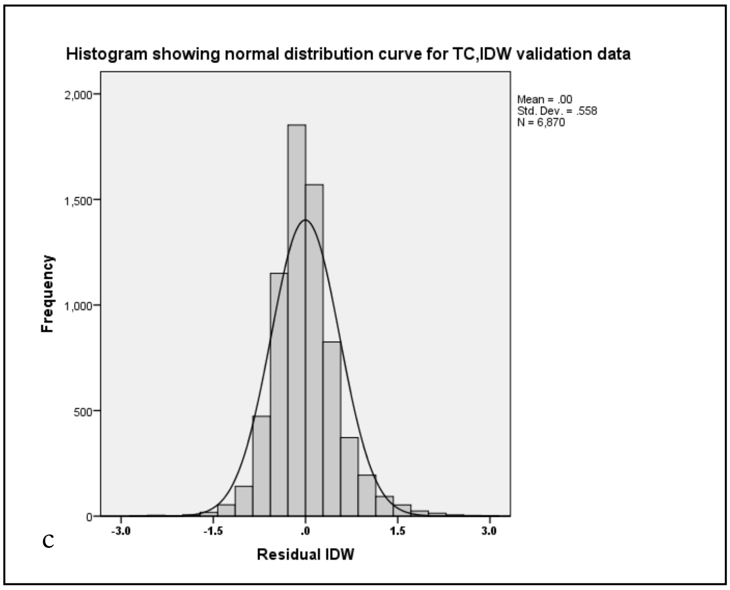

validation data for total count
rmse minimum curvature = 0.63
rmse krigging = 0.39
rmse idw = 0.56

Figure 7-7 shows the results of the histograms for normal distribution curves for Total count validation data (a) Minimum Curvature, (b) Kriging and (c) IDW

Total Magnetic Intensity

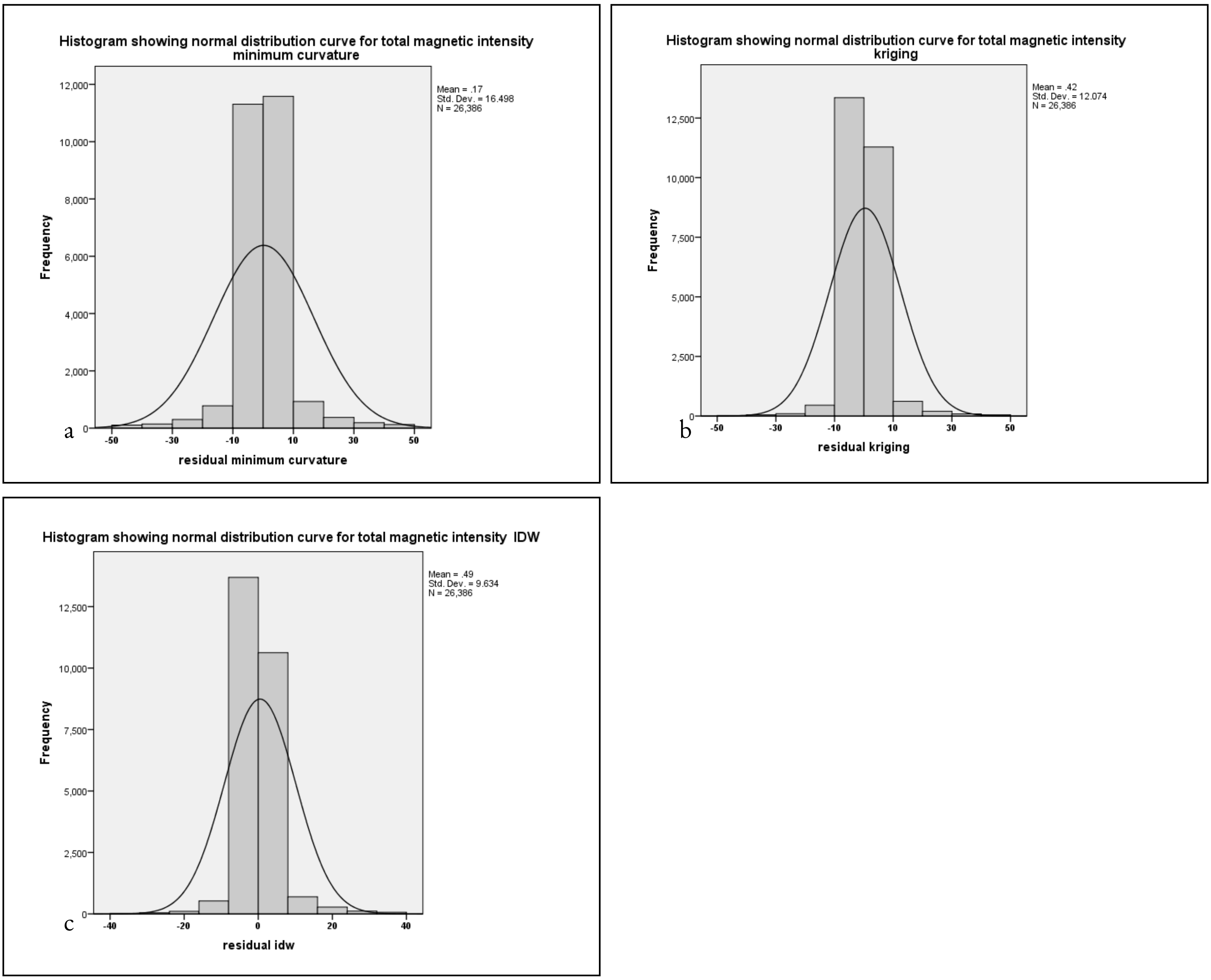

Figure7-8 shows the results of the histograms for normal distribution curves for Total magnetic Intensity(a) Minimum Curvature, (b) Kriging and (c) IDW

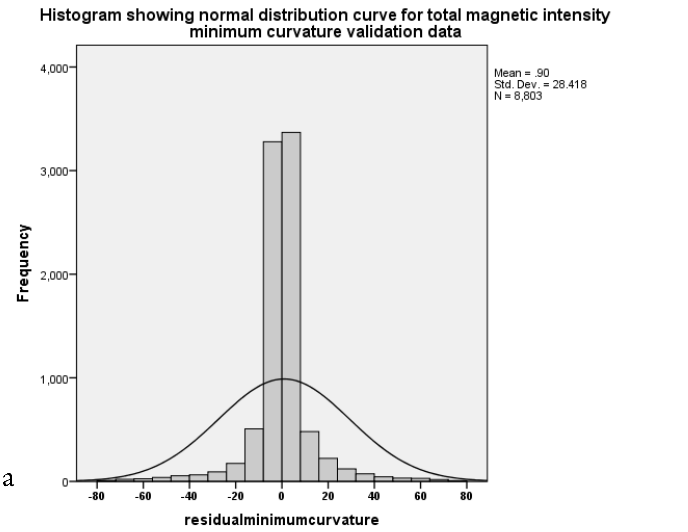

a

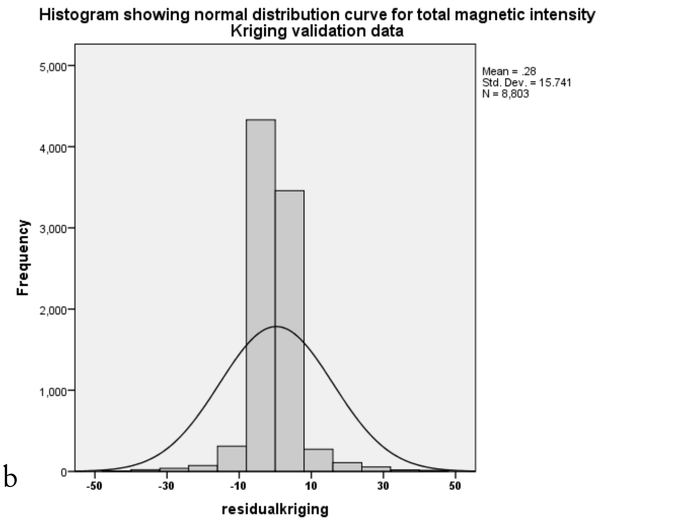

b

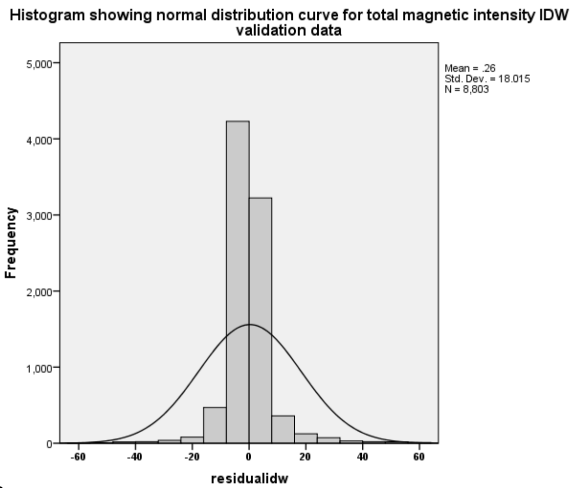

c

Validation data for total magnetic intensity

rmse minimum curvature = 28.43

rmse krigging = 15.74

rmse idw = 18.01

figure7-9 shows the results of the histograms for normal distribution curves for Total magnetic Intensity(a) Minimum Curvature, (b) Kriging and (c) IDW

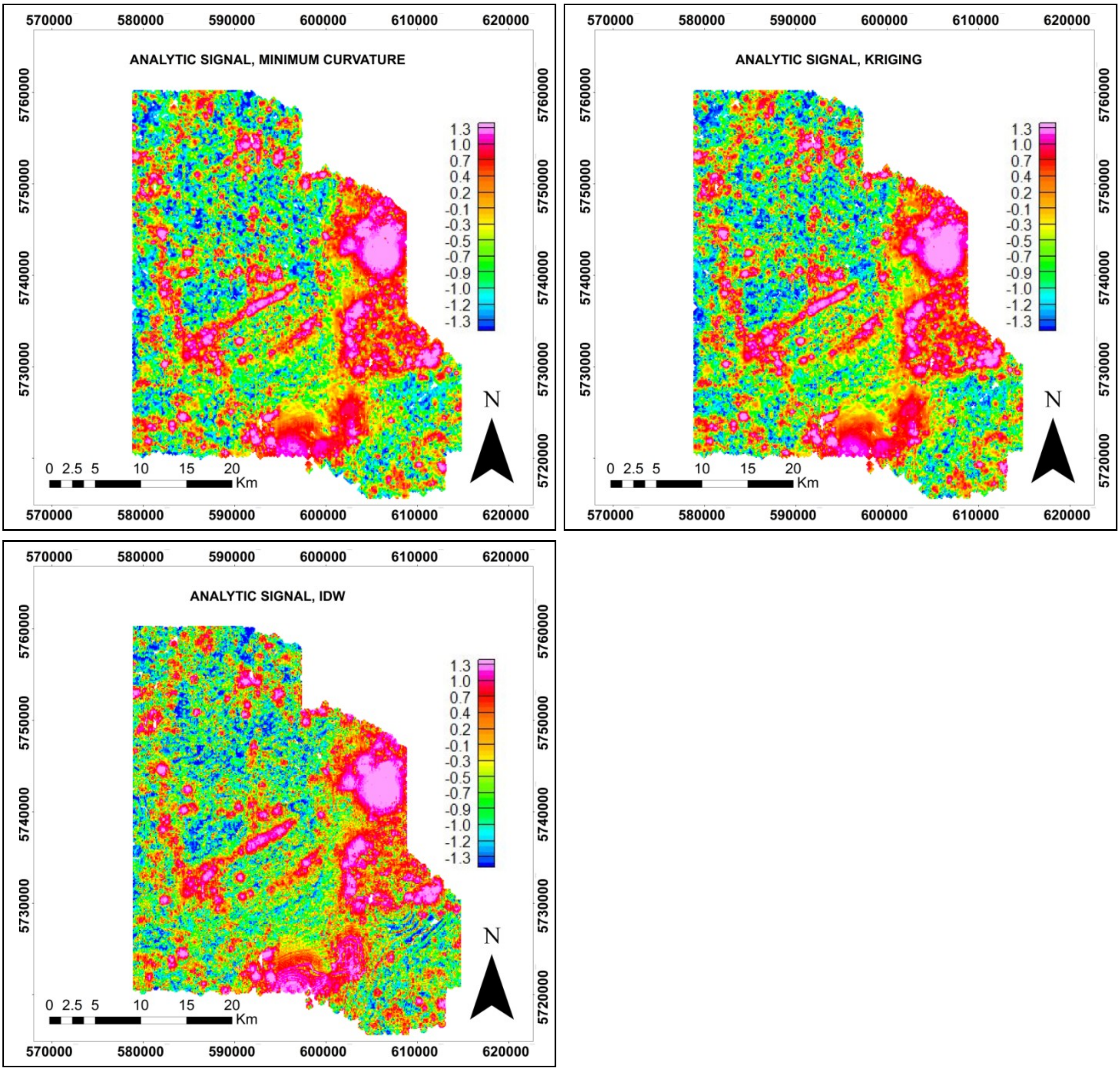

Figure 7-10 shows Analytic Signal grids for Minimum curvature, Kriging and IDW for Total magnetic Intensity (a) Minimum Curvature, (b) Kriging and (c) IDW. Kriging grid is crisp and sharp seconded by minimum curvature while IDW is a bit fuzzy.

7.4. Annex 3 showing landsat image, areas where training samples were taken and geological polygons overlain on unsupervised classified maps, this annex is linked to chapter 6

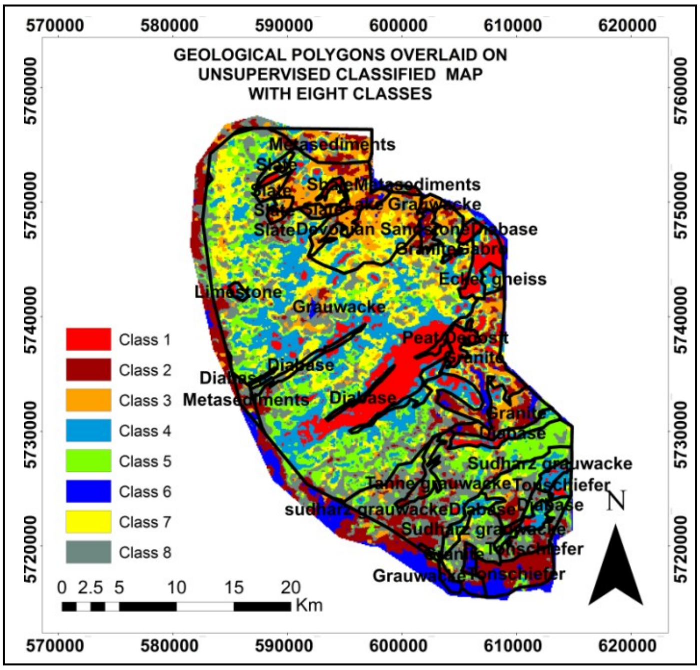

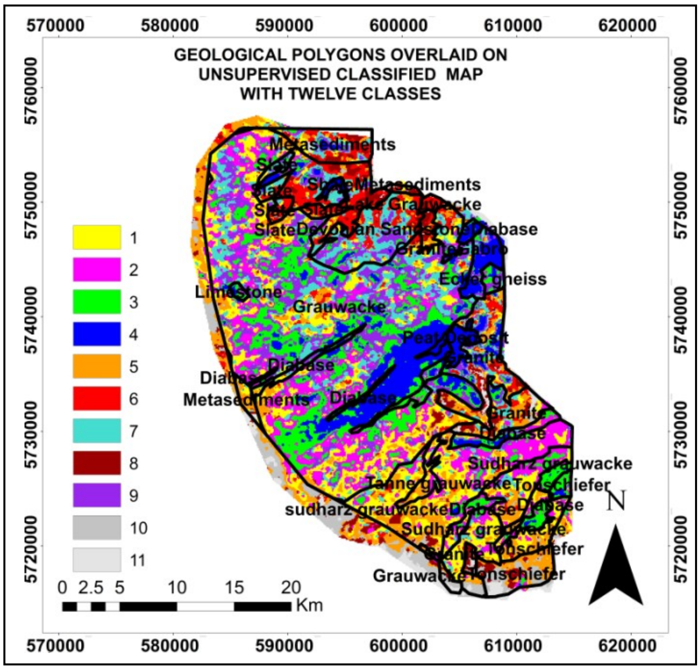

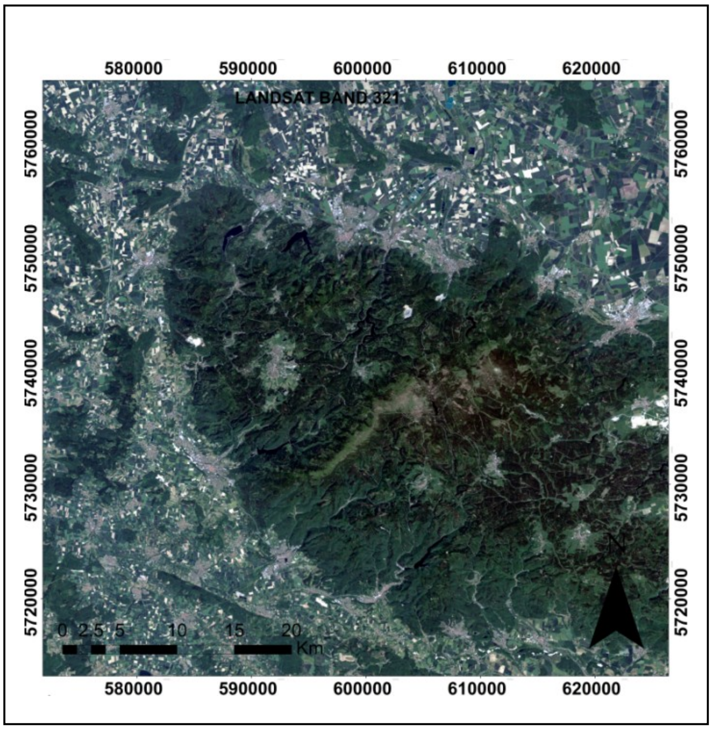

Landsat image band 321

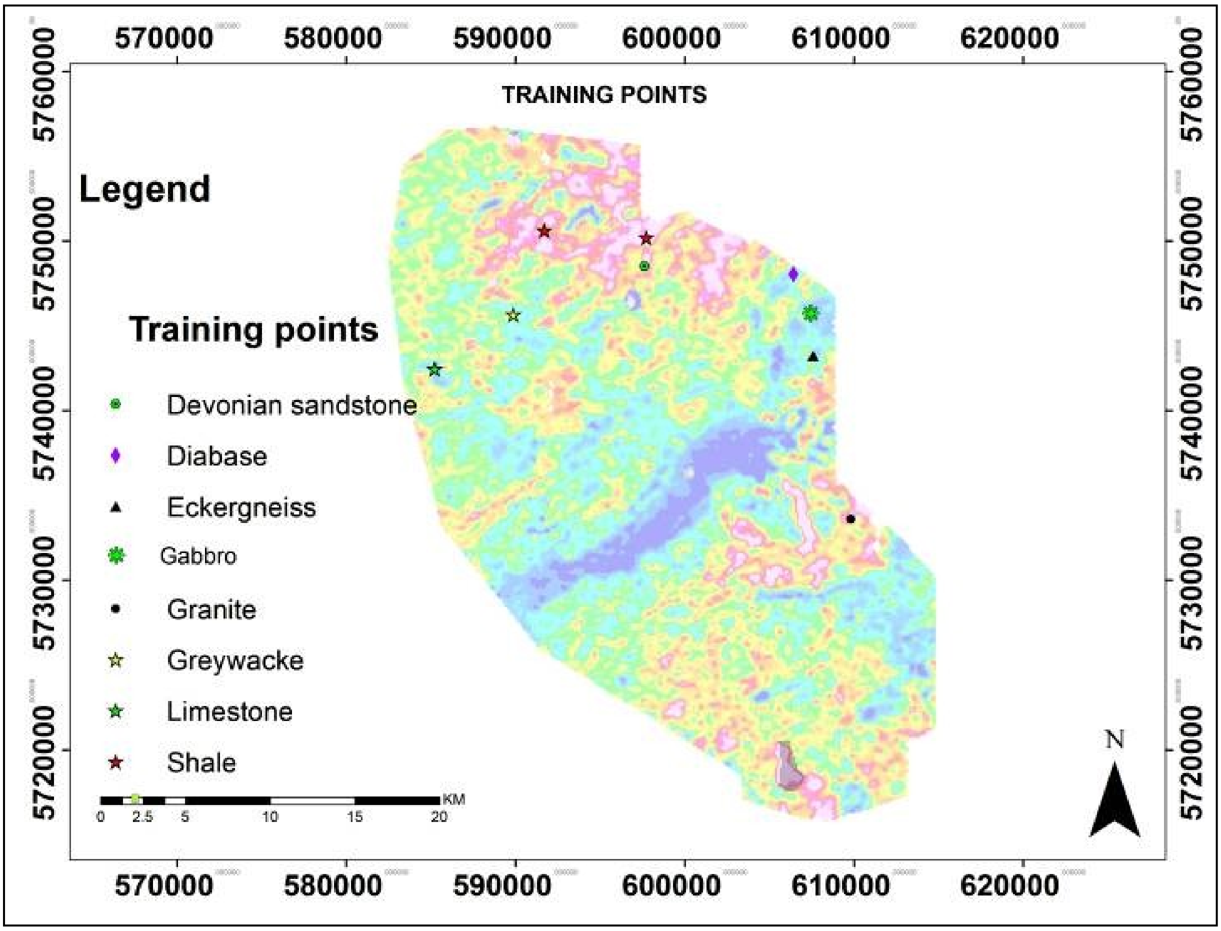

Training areas for supervised classification